MODELING AND CHARACTERIZATION OF A

FABRY PEROT PRESSURE SENSOR

by

SHRUTHIKA PRASANNA

Presented to the Faculty of the Graduate School of

The University of Texas at Arlington in Partial Fulfillment

of the Requirements

for the Degree of

MASTERS OF SCIENCE IN ELECTRICAL ENGINEERING

THE UNIVERSITY OF TEXAS AT ARLINGTON

August 2005

ACKNOWLEDGEMENTS

I wish to express my sincere gratitude to Dr. J C Chiao for giving me an opportunity for research under his guidance. He has been a source of inspiration to me. His timely guidance and never-ending encouragement has seen me through every step of this work.

I would like to thank Dr. B P Wang and Dr. W E Dillon for taking the time and interest in this research work. They have been instrumental in providing an insight to the aspects of modeling a device and simulation principles.

I am grateful to Smitha Malalur Nagaraj Rao and Praveen Pandojirao-Sunkojirao for the care with which they have reviewed this work and for conversations that helped me clarify my thinking during this research.

I would like to express my thanks to Shyam Venugopal and Vinayak Shamanna for supervising and helping me in finite element modeling and simulation on ANSYS.

My thanks to the members of the RF MEMS team at the University of Texas at Arlington for their help and support.

Not least, I thank my parents, my sister and my friends for believing in me and putting up with me during the course of this study.

July 20, 2005

ABSTRACT

MODELING AND CHARACTERIZATION OF A
FABRY PEROT PRESSURE SENSOR

Publication No. ______

Shruthika Prasanna, MS

The University of Texas at Arlington, 2005

Supervising Professor: J C Chiao

Fabry-Perot interferometers (FPIs) have been used as sensing elements for pressure transducers in many applications. Most of the current FPI pressure sensors measure amplitude changes of the reflected signals from a deformable diaphragm. A new technique to design an FPI pressure sensor has been proposed in this thesis. The proposed methodology aims to maximize the sensitivity by measuring frequency shifts and optimize the dimensions of the sensors for various materials and applications.

The sensor diaphragm is built directly on the end surface of an optical fiber with a sacrificial layer introducing the required FPI cavity height. The resulting sensor detects frequency shifts transduced by pressure variations deforming the diaphragm.

The sensor is modeled on two theories and a methodology is derived combining an iterative analysis between the mechanical characteristics and the optical performance to achieve optimal sensitivity. Applying this methodology, design parameters for different applications are extracted.

The practical issues of designing a fiber optic Fabry-Perot pressure sensor have been investigated. Structural modifications are introduced to optimize the dimensions without compromising sensitivity. A bossed diaphragm structure is proposed to eliminate the effects of optical scattering from the reflection surface. Different configurations of the bossed structures under conditions of diverse diaphragm supports have been studied. The optical performance and sensor dimension combination that yields in the maximum sensitivity has been achieved. The modeling-based methodology has been adopted to choose design parameters for different materials, catering to the requirements of small sensor dimensions over numerous different applications.

TABLE OF CONTENTS

ACKNOWLEDGEMENTS ii

ABSTRACT iii

TABLE OF CONTENTS v

LIST OF ILLUSTRATIONS viii

LIST OF TABLES xiv

Chapter

1. INTRODUCTION 1

1.1. Classification of pressure sensors 1

1.2. Motivation 3

2. DEFLECTION THEORIES AND THE FABRY PEROT CAVITY 5

2.1 Membrane Theory [15] 6

2.2 Plate Theories [16] 7

2.2.1 Thin plate with small deflection theory 7

2.2.2 Thin plate with large deflection theory 8

2.2.3 Thick plate theory 8

2.3 Thin plate theory with small deflection 8
2.4. Variation of deflection with radius and thickness of the diaphragm 14
2.5 Linking Fabry Perot performance to the applied Pressure 15
3. FEM AND SENSOR DESIGN 20
3.1 Finite Element Modeling 20
3.1.1 Advantages of FEM [23] 20
3.1.2 Disadvantages of FEM [23] 21
3.1.3 Steps for Finite Element Analysis [22, 23] 22
3.2. Design of Sensor 23
3.2.1 Assumptions for Design 23
3.2.2 Materials for the Sensor 24
3.3. An algorithm for the design 25
3.3.1 Thickness of the diaphragm 25
3.3.2 Radius of the diaphragm 28
3.3.3 Height of the cavity 28
4. DESIGN MODIFICATIONS 37
4.1 Modifying the sensor's structure 38
4.2 Optimizing the sensor dimensions 40
4.3 Comparison 43
4.4 Bossed membrane 47
4.5 Comparison - bossed membrane 55
5. CONCLUSION 57

Appendix

A. DESIGNING THE PRESSURE SENSOR USING ALUMINUM AS A MATERIAL 59

B. DESIGNING THE PRESSURE SENSOR USING NICKEL AS A MATERIAL 76

C. DESIGNING THE PRESSURE SENSOR USING SILICON NITRIDE AS A MATERIAL 91

REFERENCES 103

BIOGRAPHICAL INFORMATION 107

LIST OF ILLUSTRATIONS

Figure Page

1.1 Ideal curve and Sensitivity error [3] 2

2.1 Deflection mechanisms in membranes and plates [12] 5

2.2 Regions of plate and membrane behavior [13] 6

2.3 Deflection vs. Pressure for a 100µm Si_3N_4 diaphragm [15] 10

2.4 Deflection vs. Pressure for Si_3N_4 diaphragm verified using Ansys 11

2.5 Verification of results from Ansys for deflection vs. pressure for a Copper diaphragm 13

2.6 Dependence of deflection on radius and thickness of the diaphragm 14

2.7 Multiple reflections in a Fabry Perot cavity [17] 15

2.8 Fabry-Perot cavity mounted on an optical fiber [5] 16

2.9 Transmittance in a Fabry Perot cavity [18] 17

2.10 Free Spectral Range (FSR) [18] 18

3.1 Deflection vs. diaphragm radius for different thickness of diaphragm. 27

3.2 Low Pressure sensitivity of a Copper diaphragm of thickness 0.8µm 29

3.3 Low Pressure sensitivity of a Copper diaphragm of thickness 1µm 30

3.4 Low Pressure sensitivity of a Copper diaphragm of thickness 1.2µm 30

3.5 Low Pressure sensitivity of a Copper diaphragm of thickness 1.4µm 31

3.6 Low Pressure sensitivity of a Copper diaphragm of thickness 1.6µm 31

3.7 Low Pressure sensitivity of a Copper diaphragm of thickness 1.8µm 32

3.8 High Pressure sensitivity of a Copper diaphragm of thickness 0.8μm.............. 33

3.9 High Pressure sensitivity of a Copper diaphragm of thickness 1μm................. 33

3.10 High Pressure sensitivity of a Copper diaphragm of thickness 1.2μm............ 34

3.11 High Pressure sensitivity of a Copper diaphragm of thickness 1.4μm............ 34

3.12 High Pressure sensitivity of a Copper diaphragm of thickness 1.6μm............ 35

3.13 High Pressure sensitivity of a Copper diaphragm of thickness 1.8μm............ 35

4.1 Model of the sensor designed in Chapter 3 38

4.2 Four-pillar support for the pressure sensor.. 39

4.3 Two-pillar support for the pressure sensor.. 39

4.4 Comparison of the deflection observed for the three configurations of sensor support for a 1.6μm thickness, 50μm radius and 1μm height copper sensor... 40

4.5 Effect of increasing diaphragm thickness on a two-pillar support.................... 41

4.6 Effect of increasing diaphragm radius on a two-pillar support......................... 42

4.7 Deflection abnormality observed along the edges of a four pillar structure.. 43

4.8 Deflection abnormality observed along the edges of a two pillar structure.. 44

4.9 Deflection profile indicating non-flat diaphragm center.................................. 47

4.10 Embossed membrane structure for the pressure sensor.................................. 48

4.11 Bossed membrane structure on a hollow-cylinder support for a 1.6μm thickness, 50μm radius and 1μm height cavity 50

4.12 Bossed membrane on hollow-cylinder support - deflection profile. UZ indicates different pressures applied, UZ1<UZ2 and so on. 51

4.13 Bossed membrane on a four-pillar support structure for a 1.6μm thickness, 50μm radius and 1μm height cavity 52

4.14 Deflection profile of a bossed membrane on a four-pillar support structure. UZ indicates different pressures applied, UZ1<UZ2 and so on. 53

4.15 Two-pillar support with a bossed membrane. Dimensions of sensor – 35μm radius, 1.6μm thickness, 1μm cavity height, dimensions of the boss structure – 50μm in length (along x direction) and 20μm in width (perpendicular to x direction) and 7μm in height 54

4.16 Deflection profile for a bossed membrane on a two-pillar support. UZ indicates different pressures applied, UZ1< UZ2 and so on. UZ5 – cross is deflection profile along the support structure……………………………………55

A.1 Deflection vs. diaphragm Radius for different thickness of an Aluminum diaphragm.. 60

A.2 Low Pressure sensitivity of an Aluminum diaphragm of thickness 0.8μm.. 61

A.3 Low Pressure sensitivity of an Aluminum of diaphragm of thickness 1μm... 61

A.4 Low Pressure sensitivity of an Aluminum of diaphragm of thickness 1.2μm.. 62

A.5 Low Pressure sensitivity of an Aluminum diaphragm of thickness 1.4μm.. 62

A.6 Low Pressure sensitivity of an Aluminum diaphragm of thickness 1.6μm.. 63

A.7 Low Pressure sensitivity of an Aluminum diaphragm of thickness 1.8μm.. 63

A.8 Low Pressure sensitivity of an Aluminum diaphragm of thickness 2μm.......... 64

A.9 High Pressure sensitivity of an Aluminum diaphragm of thickness 0.8μm.. 65

A.10 High Pressure sensitivity of an Aluminum diaphragm of thickness 1μm... 65

A.11 High Pressure sensitivity of an Aluminum diaphragm of thickness 1.2μm.. 66

A.12 High Pressure sensitivity of an Aluminum diaphragm of thickness 1.4µm 66

A.13 High Pressure sensitivity of an Aluminum diaphragm of thickness 1.6µm 67

A.14 High Pressure sensitivity of an Aluminum diaphragm of thickness 1.8µm 67

A.15 High Pressure sensitivity of an Aluminum diaphragm of thickness 2µm 68

A.16 Bossed membrane structure on a hollow-cylinder support for a 1.8µm thickness, 50µm radius and 1µm height cavity 69

A.17 Bossed membrane on a hollow-cylinder support – deflection profile. UZ indicates different pressures applied, UZ1<UZ2 and so on 70

A.18 Bossed membrane on a four-pillar support structure for a 1.8µm thickness, 50µm radius and a 1µm cavity height 71

A.19 Deflection profile of a bossed membrane on a four-pillar support structure. UZ indicates different pressures applied, UZ1<UZ2 and so on 72

A.20 Two-pillar support structure with a bossed membrane. Dimensions of sensor – 35µm radius, 1.8µm thickness, 1µm cavity height, dimensions of the bossed structure – 50µm in length (along x direction) and 20µm in width (perpendicular to x direction) and 9.6µm in height 73

A.21 Deflection profile for a bossed membrane on a two-pillar support structure. UZ indicates different pressures applied, UZ1<UZ2 and so on. UZ5 – cross is deflection profile along the support structure. 74

B.1 Deflection vs. diaphragm Radius for different thickness of a Nickel diaphragm. 77

B.2 Low Pressure sensitivity of a Nickel diaphragm of thickness 0.8µm 78

B.3 Low Pressure sensitivity of a Nickel diaphragm of thickness 1µm 78

B.4 Low Pressure sensitivity of a Nickel diaphragm of thickness 1.2µm 79

B.5 Low Pressure sensitivity of a Nickel diaphragm of thickness 1.4µm 79

B.6 Low Pressure sensitivity of a Nickel diaphragm of thickness 1.6μm 80

B.7 High Pressure sensitivity of a Nickel diaphragm of thickness 0.8μm 81

B.8 High Pressure sensitivity of a Nickel diaphragm of thickness 1μm 81

B.9 High Pressure sensitivity of a Nickel diaphragm of thickness 1.2μm 82

B.10 High Pressure sensitivity of a Nickel diaphragm of thickness 1.4μm 82

B.11 High Pressure sensitivity of a Nickel diaphragm of thickness 1.6μm 83

B.12 Bossed membrane structure on a hollow-cylinder support for a 1.4μm thickness, 50μm radius and 1μm height cavity 84

B.13 Bossed membrane on a hollow-cylinder support – deflection profile. UZ indicates different pressures applied, UZ1<UZ2 and so on.. 85

B.14 Bossed membrane on a four-pillar support structure for a 1.4μm thickness, 50μm radius and 1μm height cavity 86

B.15 Deflection profile of a bossed membrane on a four-pillar support structure, UZ indicates different pressures applied, UZ1<UZ2 and so on............ 87

B.16 Two-pillar support structure with a bossed membrane.Dimensions of sensor – 40μm radius, 1.4μm thickness, 1μm cavity height, dimensions of the bossed structure – 50μm in length (along x direction) and 30μm in width (perpendicular to x direction) and 5μm in height...................................... 88

B.17 Deflection profile for a bossed membrane on a two-pillar support structure, UZ indicates different pressures applied, UZ1<UZ2 and so on. UZ5 –cross is deflection profile along the support structure 89

C.1 Deflection vs. diaphragm Radius for different thickness of a Silicon Nitride diaphragm.. 92

C.2 Low Pressure sensitivity of a Silicon Nitride diaphragm of thickness 0.8μm.. 93

C.3 Low Pressure sensitivity of a Silicon Nitride diaphragm of thickness 1μm.. 93

C.4 Low Pressure sensitivity of a Silicon Nitride diaphragm of thickness 1.2μm 94

C.5 High Pressure sensitivity of a Silicon Nitride diaphragm of thickness 0.8μm 94

C.6 High Pressure sensitivity of a Silicon Nitride diaphragm of thickness 1μm 95

C.7 High Pressure sensitivity of a Silicon Nitride diaphragm of thickness 1.2μm 95

C.8 Bossed membrane structure on a hollow-cylinder support for a 1μm thickness, 40μm radius and 1μm height cavity 96

C.9 Bossed membrane on a hollow-cylinder support – deflection profile. UZ indicates different pressures applied, UZ1<UZ2 and so on 97

C.10 Bossed membrane on a four-pillar support structure for a 1μm thickness, 40μm radius and 1μm height cavity 98

C.11 Deflection profile of a bossed membrane on a four-pillar support structure. UZ indicates different pressures applied, UZ1<UZ2 and so on 99

C.12 Two-pillar support structure with a bossed membrane. Dimensions of sensor – 35μm radius, 1μm thickness, 1μm cavity height, dimensions of thebossed structure – 50μm in length (along x direction) and 30μm in width (perpendicular to x direction) and 3μm in height 100

C.13 Deflection profile for a bossed membrane on a two-pillar support structure, UZ indicates different pressures applied, UZ1<UZ2 and so on. UZ5 – cross is deflection profile along the support structure 101

LIST OF TABLES

Table Page

1.1Performance parameters for a pressure sensor [3]……………………………….1

2.1 Material properties for Si_3N_4 11

2.2 Material properties for pure Copper 12

3.1 Properties of materials used for sensor fabrication 25

3.2 Max deflection for different thickness for linear range of operation 26

3.3 Maximum radius conforming to the one-fifth rule 27

3.4 Design parameters for different materials 36

4.1 Comparison of deflection behavior of three types of diaphragm
support structures…………………………………………………………....45

4.2 Comparison of deflection profile of a bossed membrane clamped onto
the different support structures……………………………………………...56

5.1 Overview of different materials used for the sensor, their dimensions,
operating range and the sensitivity…………………………………………… 57

A.1 One-fifth rule applied to Aluminum diaphragms……………………………..60

A.2 Summary of the Sensor and Boss structure for a sensor made of
Aluminum………………………………………………………………….. 75

B.1 One-fifth rule applied to Nickel Diaphragms…………………………………77

B.2 Summary of the Sensor and Boss structure for a sensor made of
Nickel………………………………………………………………………..90

C.1 One-fifth rule applied to Silicon Nitride diaphragms……………………………92

C.2 Summary of Sensor and Boss structure for a sensor made of
Silicon Nitride………………………………………………………………. 102

CHAPTER 1

INTRODUCTION

1.1 Classification of pressure sensors

MEMS pressure sensors have been developed for a variety of automotive, biomedical and industrial applications. Automotive applications include pressure sensors for engine manifolds, fuel lines, exhaust gases, tires, seats and other uses. Biomedical applications that have been proposed or developed include implantable devices for measuring ocular, cranial or bowel pressure and devices built into catheters that can assist in procedures such as angioplasty. Many industrial applications related to monitoring manufacturing processes exist [1].

The parameters that decide the performance of a given pressure sensor are mainly its sensitivity, dynamic range, linearity and resolution (table 1.1).

Table 1.1 Performance parameters for a pressure sensor [2].

Performance parameter	Definition
Sensitivity	Ratio of the output signal change to the change in pressure
Dynamic range	Total range of the sensor from minimum to maximum
Linearity	Extent to which the actual measured curve of a sensor departs from the ideal curve
Resolution	Smallest detectable incremental change of input parameter that can be detected in the output signal. Can be expressed either as a proportion of the reading (or the full-scale reading) or in absolute terms (fig 1.1).

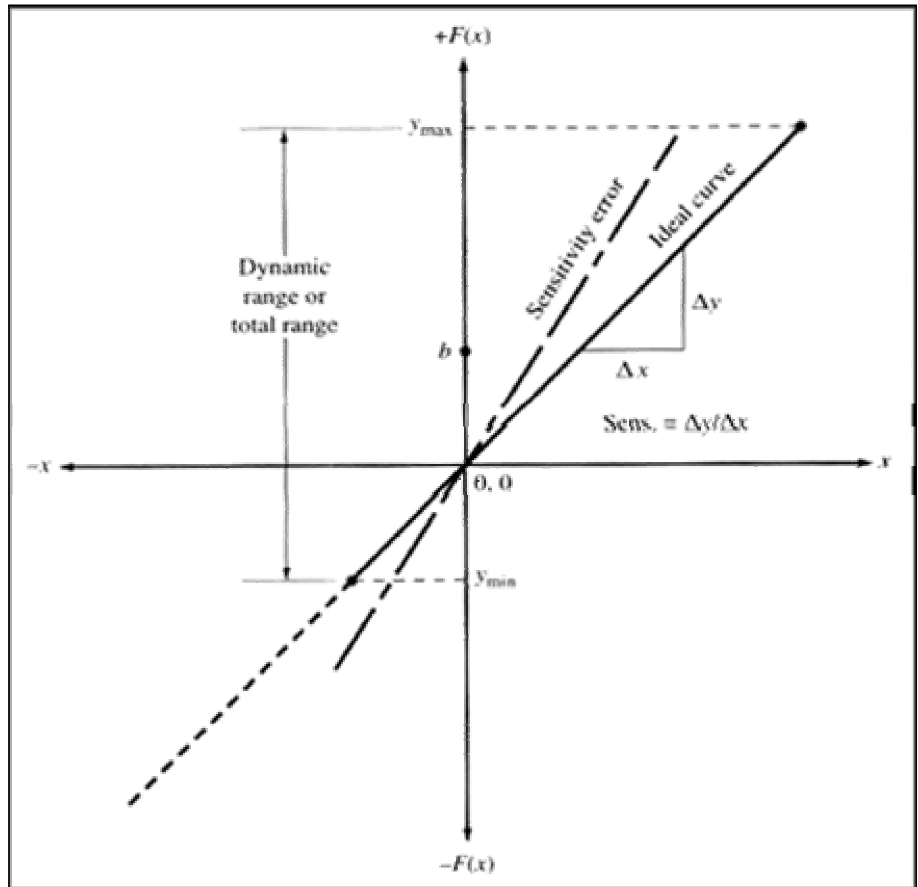

Figure 1.1 Ideal curve and Sensitivity error [3].

There are different configurations used to build the sensing element in pressure sensors like flexible elements, tubes, coils, diaphragms etc. Diaphragms are commonly used because they require less space and because the motion (or force) they produce is sufficient for operating electronic transducers. They also are available in a wide range of materials.

The output measured from a pressure sensor can be any of the following types –

a) Measuring stress produced on a diaphragm – Piezoresistive pick-off.

b) Measuring the displacement of the diaphragm – Capacitive pick-off.

c) Measuring the change in effective spring constant of a beam – Resonant beam pick-off.

d) Measuring a change in phase or optical intensity of incident light – Optical pick-off.

Pressure sensors with optical pick-off are most popular due to their small size and light weight, immunity to electromagnetic interference and harsh environments, absence of electrical contacts, ease in remote operation and simple integration methods with other devices.

Optical pick-off or Fiber Optic pressure sensors either detect a change in the intensity of the reflected light or detect a change in the phase of the reflected light. The former are classified as Intensity based sensors and the latter as Interferometric sensors. There are different types of interferometers, the Mach-Zehnder interferometer, the Michelson interferometer, the Sagnac interferometer and the Fabry-Perot interferometer (FPI). A number of literatures can be found for these interferometers, their working and applications [4 - 7]. The focus of this thesis is the FPI based pressure sensor. Before the design details for this sensor are described, it is necessary to understand the motivation behind designing this sensor when a wide range of pressure sensors are already available for commercial purposes.

1.2 Motivation

The inherent advantages of fiber optic pressure sensors have resulted in the replacement of other types of pressure sensors at an exponential rate. Commercial sensors have achieved goals of small size and high performance [8]. Yet, there exists an

ever-growing demand for smaller and smaller sensors in every field of application [9]. Different techniques of fabrication and design methodologies have been proposed to achieve a small size sensor for conventional pressure sensors based on bulk silicon [10, 11].

The diaphragm of the sensor proposed in this thesis is fabricated directly onto the cross section of the end surface of the optical fiber. This ensures a high sensitivity for the sensor. A sacrificial layer is used to provide the required height of the cavity between the sensor diaphragm and the fiber end surface. The sensor now works like an interferometer detecting a change in frequency for a change in ambient pressure.

The absence of a modeling technique for this type of a device makes it difficult to choose the sensor dimensions and design parameters to achieve high sensitivity. Thus, this thesis aims to develop a step-by-step modeling approach for an FPI based pressure sensor, which will result in a set of sensor dimensions and design parameters for best sensitivity.

CHAPTER 2

DEFLECTION THEORIES AND THE FABRY PEROT CAVITY

Membranes and Plates are often used interchangeably without concern regarding the implications when circular diaphragms have been modeled. The fact that the analysis is not the same for the two, forces one to define and enlist the differences between a membrane and a plate. In the broad sense, a membrane is used for a diaphragm that can sustain only tensile stresses and a plate is a diaphragm that can sustain both tensile and bending stresses. In the limiting case of a very thin plate, the bending stresses become insignificant as compared to the tensile stresses, so that the plate in essence behaves like a membrane [12]. In such cases, the terms plate and membrane can be used interchangeably.

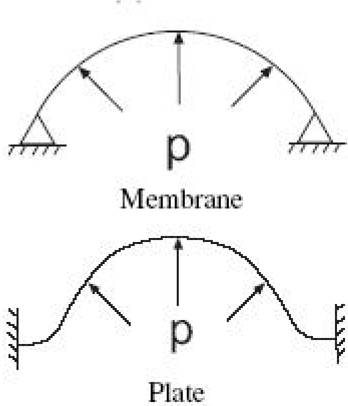

Figure 2.1 Deflection mechanisms in membranes and plates [12].

The following sections will explain the plate and membrane theories in detail and the behavior of our sensor will be approximated to one of them.

2.1 Membrane Theory [13]

The deflection behavior of a membrane under external pressure can be either linear or non-linear in nature depending on the nature of two-dimension less parameters - α, a function of pre-stretch and film thickness and γ, a function of the load and film thickness.

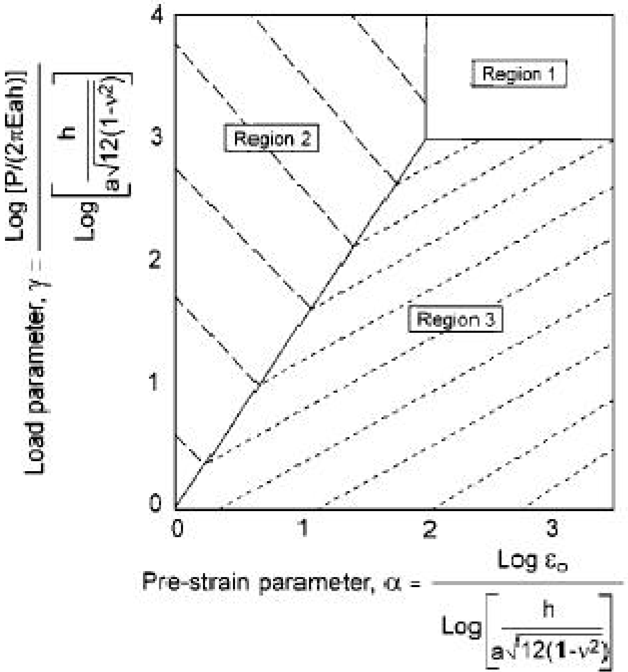

Figure 2.2 Regions of plate and membrane behavior [13].

The parameter space delineating between regions of plate behavior (region 1), linear or pre-stretched membrane behavior (region 2) and nonlinear membrane behavior (region 3) is illustrated in figure 2.2. Increase in the pre-strain parameter (ε_o) or load parameter (P) corresponds to a decrease in α and γ respectively.

In region 2, the membrane pre-stretching is large and membrane stretching predominates the bending and linear results are obtained. This corresponds to the scenario where the membrane prestrain is comparable to the bending stiffness and the loads are small enough to avoid large deflections. In region 3, the membrane pre-stretching is negligible and membrane stretching predominates bending. This corresponds to the situation where either the membrane thickness is very small or the loads are large resulting in large deflections.

On a more general note, in region 2 the magnitude of deflection is said to be linear with pressure, $y \propto P$ and in region 3 the magnitude of deflection is related to the cube-root of pressure, $y \propto P^{1/3}$. A more detailed explanation of the plate behavior corresponding to region 1 is provided in section 2.2.

2.2 Plate Theories [14]

The bending properties of a plate depend greatly on the thickness as compared to other dimensions. There are three theories that describe the behavior of plates under conditions of deflection – Thin plate with small deflection theory, thin plate with large deflection theory and Thick plate theory.

2.2.1 Thin plate with small deflection theory

This is applicable to plates when the observed deflection is comparable to the thickness of the plate. This theory is developed on the assumptions that there is no deformation in the middle plane of the plate, the points lying initially on the normal-to-the-middle plane of the plate remain on the normal-to-the-middle surface of the plate after bending and the normal stresses in the direction transverse to the plate can be

neglected. Under these assumptions the stress components are all expressed as a function of the deflection.

2.2.2 *Thin plate with large deflection theory*

In many cases it has been observed that strains develop in the middle plane of a plate under deflection. These strains are negligible if the bending is small in comparison with the thickness of the plate. For deflections that are not small, these stresses must be accounted for in the derivation of the differential equation of the plate. In this way non-linear solutions are obtained and solution of the problem becomes more complicated.

2.2.3 *Thick plate theory*

The above two theories become invalid in case of plates with large thickness subjected to highly concentrated loads. In such cases the theory of thick plates is applied. This theory considers the problem of the plate as a three-dimensional problem of elasticity which makes the solution highly complicated.

The proposed sensor in this thesis has been chosen to comply with the plate deflection theory since the diaphragm has to tolerate both bending and tensile stresses under the influence of external pressure. What needs to be verified is whether the thin plate or the thick plate deflection theory needs to be chosen.

2.3 Thin plate theory with small deflection

The thin plate theory is popularly known as the *Classical Plate theory*. The *small* transverse (out-of-plane) displacement w of a *thin* plate is described by equation 2.1,

$$\nabla^2 D \nabla^2 w = p \qquad (2.3.1)$$

Where, p is the distributed load (force per unit area) acting in the same direction as z (and w), and D is the bending/flexural rigidity of the plate defined as follows,

$$D = \frac{Eh^3}{12(1-v^2)} \tag{2.3.2}$$

E is the Young's modulus of the plate material, v is the Poisson's ratio of the plate material, and h is the thickness of the plate. If the bending rigidity D is constant throughout the plate, the plate equation can be simplified to,

$$\nabla^4 w = \frac{p}{D} \tag{2.3.3}$$

Where ∇^4 is called the Bi-harmonic Differential factor.

The plate is clamped along its edges ensuring only one direction bending (bending along the z direction). Solving equation 2.3.3 for w, with constraints for a clamped plate we get,

$$w(r) = \frac{pr_0^4}{64D}\left[1-\left(\frac{r}{r_0}\right)^2\right]^2 \tag{2.3.4}$$

Where r_o is the center of the plate and r is the distance of the applied load from the center. If $r = r_o$, equation becomes,

$$w_{max} = w(r=0) = \frac{pr_0^4}{64D} \tag{2.3.5}$$

Or

$$w(0) = \frac{3(1-v^2)Pa^2}{16Eh^3} \tag{2.3.6}$$

The variation of the deflection at the center is a function of radius and thickness of the diaphragm and the pressure applied. Thus for a plate made of a given material of fixed dimensions the deflection under pressure is proportional to the applied pressure. The constant of proportionality differs for different materials and different dimensions.

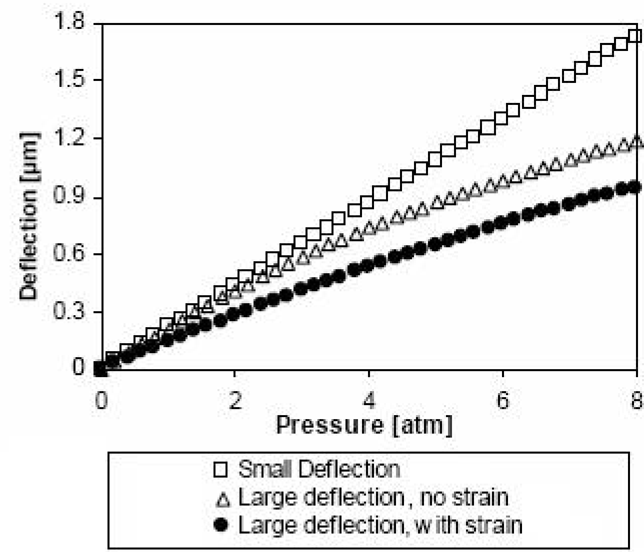

Figure 2.3 Deflection vs. Pressure for a 100µm Si_3N_4 diaphragm [15].

Deflection theory for both thick and thin plates has been analyzed [15]. The considered plate was of radius 50µm and made up of Silicon Nitride, with a plate thickness of 1.2µm. Figure 2.3 represents the relation between deflection and pressure when plate is subjected to a small deflection and a large deflection under no strain and strain conditions. The linearity in relationship between deflection and pressure for small deflection can be easily observed in the figure.

For verification purposes the results obtained by the ANSYS simulation of the Silicon Nitride plate were plotted and compared against the theoretical values obtained

by using equation 2.3.6 (fig. 2.4). The material properties for Silicon Nitride are tabulated in Table 2.1.

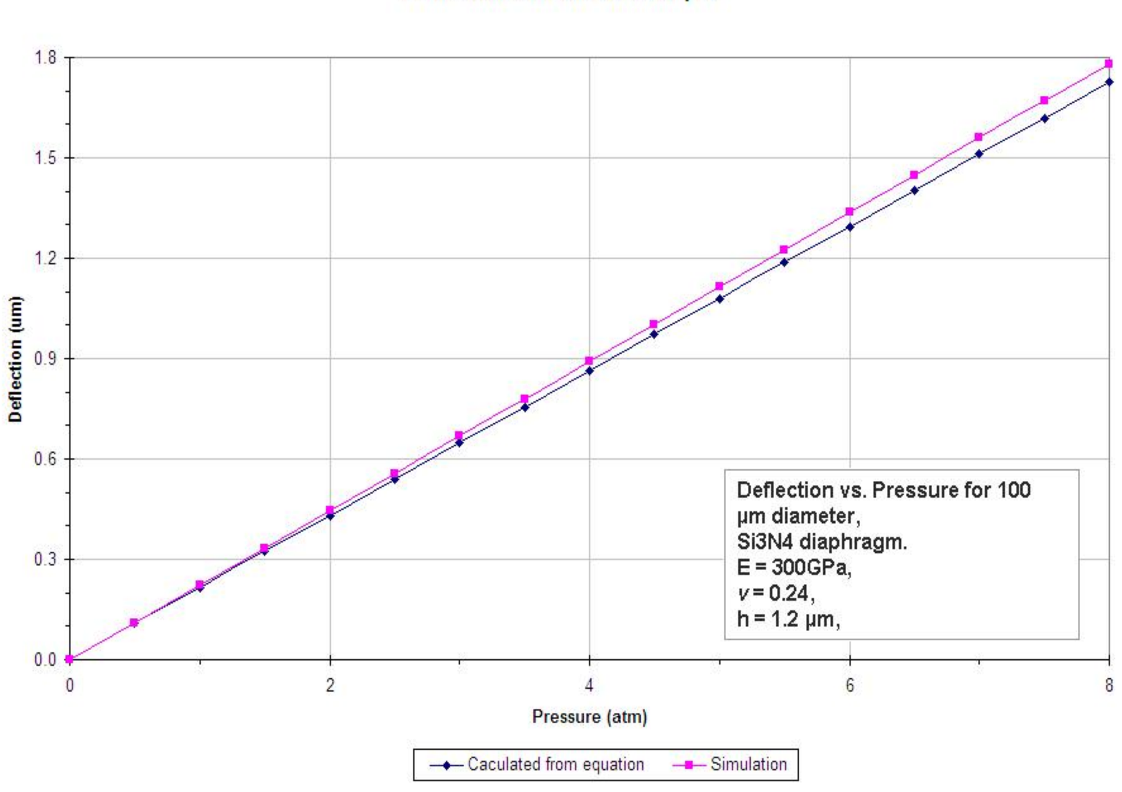

Figure 2.4 Deflection vs. Pressure for Si_3N_4 diaphragm verified using Ansys.

Table 2.1 Material properties for Si_3N_4.

Property	Symbol	Value
Young's Modulus	E	300GPa
Poisson's Ratio	v	0.24
Thickness of the diaphragm	h	1.2µm
Radius of the diaphragm	r_o	50µm

In the same manner, the plate deflection with respect to pressure was plotted for a plate made of copper. The material properties and dimensions of the copper plate are listed in Table 2.2.

Table 2.2 Material properties for pure Copper.

Property	Symbol	Value
Young's Modulus	E	130GPa
Poisson's Ratio	V	0.34
Thickness of the diaphragm	h	2μm
Radius of the diaphragm	r_o	25μm

The plot of deflection versus pressure for a copper plate is depicted in figure 2.5. The results obtained from Ansys simulation are being compared with the results obtained from calculation using the formula.

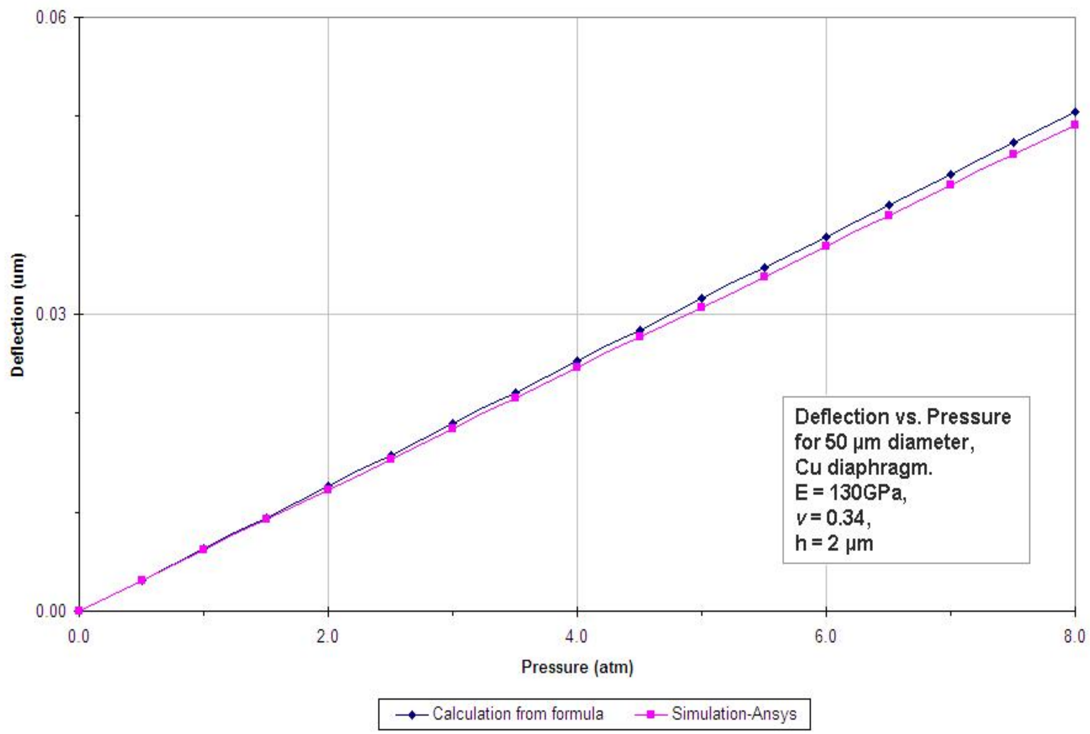

Figure 2.5 Verification of results from Ansys for deflection vs. pressure for a Copper diaphragm.

It can be clearly seen from figure 2.5 that the extent of deflection remains proportional to the applied pressure. This leads to the conclusion that the thin plate theory with small deflection would be the best modeling theory for the diaphragm of the sensor. Close observation of figures 2.4 and 2.5 reveals that as the pressure increases the value of deflection obtained through ANSYS simulation deviates from the value of deflection obtained numerically. This is attributed to the fact that the simulation underestimates the actual deflection for higher pressures due to stiffness factors associated with the material model [16].

2.4 Variation of deflection with radius and thickness of the diaphragm

Equation 2.3.6 clearly demonstrates the dependence of extent of deflection on the on the amount of pressure applied for Thin plate theory. Section 2.3 illustrates this dependence graphically for two materials viz. Silicon Nitride and Copper.

The dependence of plate deflection on the thickness and radius of the plate is important to understand especially from the point of view of designing a sensor using such a configuration. Figure 2.6 illustrates this dependence.

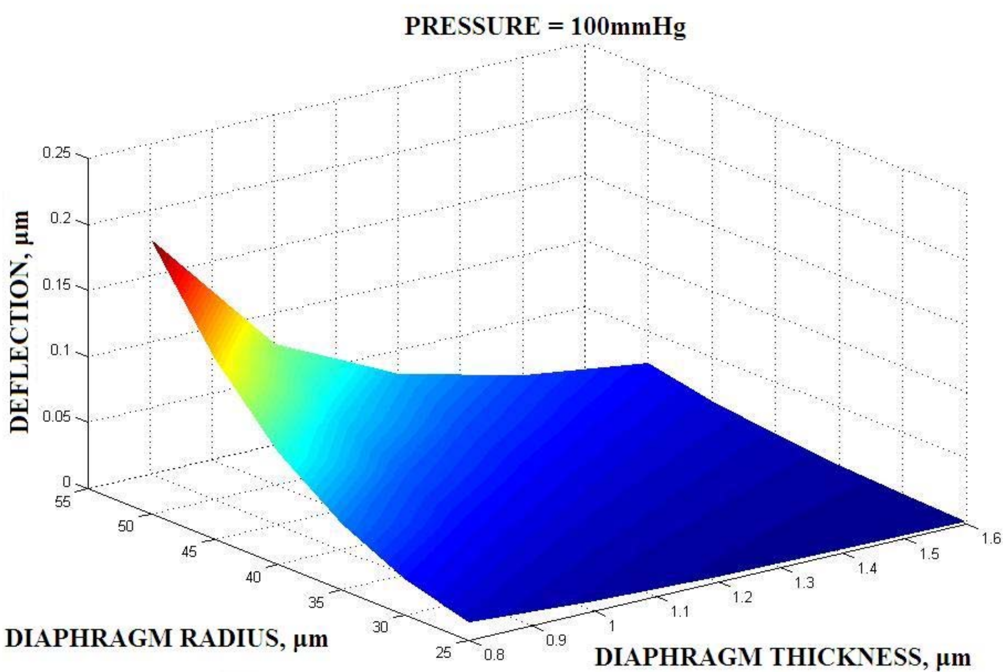

Figure 2.6 Dependence of deflection on radius and thickness of the diaphragm.

Some important observations from figure 2.6 can be summarized as follows.

a) Given constant pressure and same plate material, for a constant radius the deflection increases/decreases with increase in thickness of the plate. This can be attributed to the fact that plate resistance increases as plate becomes thicker.

b) Given constant pressure and same plate material, for a constant thickness the deflection increases as the radius of the diaphragm increases. This can be attributed to the fact that plate flexibility increases as the plate becomes larger in area.

For a sensor with high sensitivity to changes in pressure, the diaphragm must be both flexible and thick enough to withstand large variations in pressures. It is important to investigate the optical performance before the design methodology to achieve these goals is laid down.

2.5 Linking Fabry Perot performance to the applied Pressure

A Fabry perot interferometer consists of two partially transmitting mirrors precisely aligned to form a reflective cavity. Incident light enters the cavity and undergoes multiple reflections between the mirrors so that the light interferes with itself many times [17].

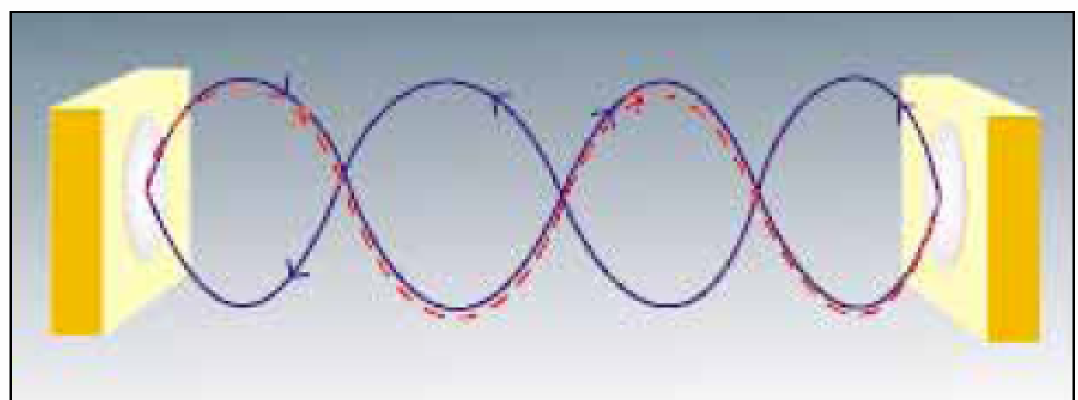

Figure 2.7 Multiple reflections in a Fabry Perot cavity [17].

Constructive interference occurs when the frequency of light is a multiple of the cavity height, figure 2.7. One end of this cavity sits on the optical fiber and the other

end acts as the interface to the outer environment. This end can be modeled as a diaphragm and the deformation of the diaphragm induced by external pressure varies the cavity length of the interferometer, figure 2.8.

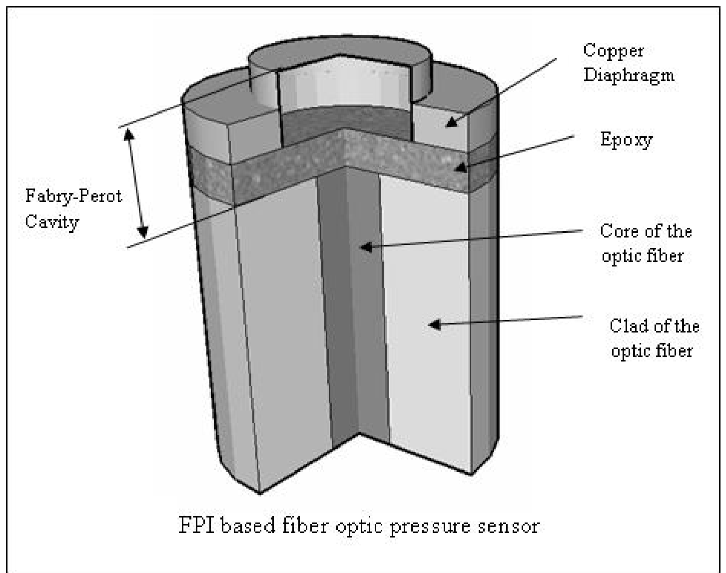

Figure 2.8 Fabry-Perot cavity mounted on an optical fiber [5].

A detailed mathematical analysis of the working of the fabry-perot interferometer has been presented in [5]. Summarizing the equations for the interferometer, the transmitted intensity is given by [18],

$$I = \frac{I_0}{(1 - R_{eff})^2 + 4R_{eff}\sin^2(kL)} \qquad (2.5.1)$$

Where,

k –wave number

I_o – Intensity of light entering the cavity

R_{eff} – Effective Reflectivity of the two mirrors present at the ends of the cavity and is dependent on the reflectivity of the diaphragm (copper as shown in figure 2.8), R_1 and the reflectivity of the optical coating/glue on the fiber, R_2. R is thus calculated as [19],

$$R_{eff} = \frac{(\sqrt{R_1} - \sqrt{R_2})^2 + 4\sqrt{R_1 R_2}\sin^2(\delta/2)}{(1-\sqrt{R_1 R_2})^2 + 4\sqrt{R_1 R_2}\sin^2(\delta/2)} \tag{2.5.2}$$

And,

$$\delta/2 = \frac{2\pi nd}{\lambda}\cos\theta \tag{2.5.3}$$

Where,

n - Refractive index of media (air = 1)

d - Distance between reflecting surfaces (= L, under no pressure)

λ - Wavelength of light used

θ - Beam incidence angle (assumed = 0)

For $R_1 = R_2 = R$, the expression for reflectivity is approximated to,

$$R_{eff} = \frac{4R}{(1+R)^2} \tag{2.5.4}$$

The transmission spectrum of the FPI for different reflectivity is plotted in figure 2.9.

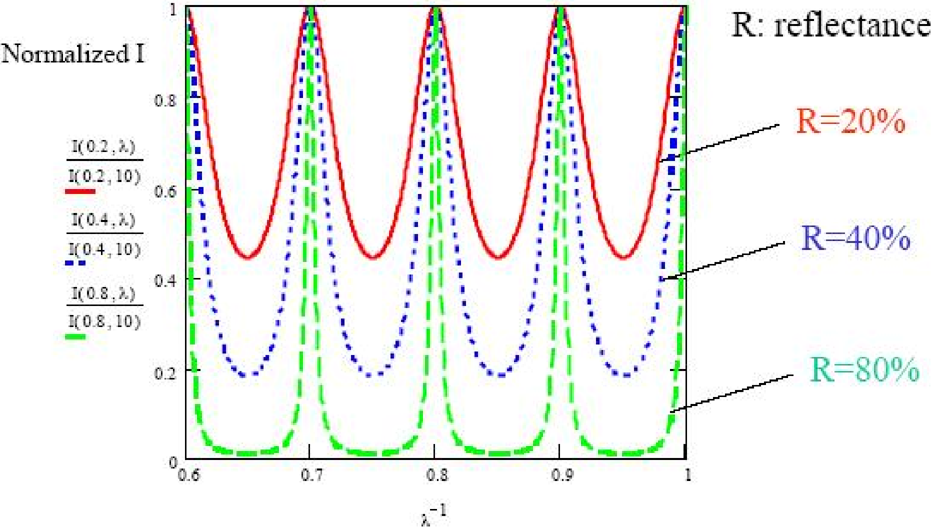

Figure 2.9 Transmittance in a Fabry-Perot cavity [18].

The free spectral range, fig 2.10., of an FPI is defined as the distance (in frequency space) between adjacent transmission peaks. The free spectral range is a function of the cavity height for an FPI and is expressed as [18],

$$f_{FSR} = \frac{c}{2nL} \tag{2.5.5}$$

Where,

c – Speed of light in vacuum or air,

n – Refractive index of the cavity (in most cases = 1, refractive index of air),

L – Height of the FPI cavity

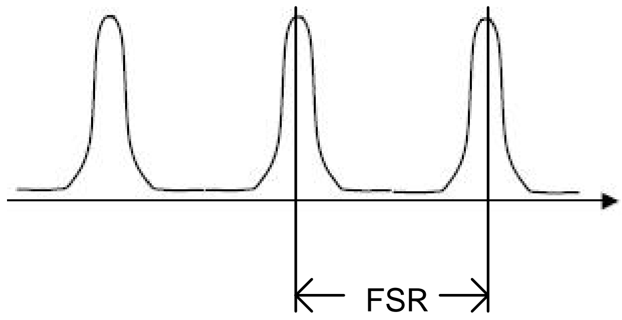

Figure 2.10 Free Spectral Range (FSR) [18].

The height of the cavity varies with change in applied pressure on the FPI. This change in height is due to the induced deflection on the diaphragm. The deflection of a membrane is modeled by the equation for thin-plate deflection, explained in section 2.3. Therefore, the height of the cavity now translates to an effective height which is related to the deflection as,

$$L_{eff} = L - w(0) \tag{2.5.6}$$

The equation for FSR now changes to,

$$f_{FSR}(P) = \frac{c}{2nL_{eff}} \tag{2.5.7}$$

The change in length of the cavity hence translates to a shift in the frequency spectrum of the FPI. Tracing this shift would provide an approximation regarding the amount of pressure applied on the diaphragm.

Another parameter used to quantify the FPI performance is sensitivity, which is defined as the change in optical phase, or frequency shift as in this case, with respect to the change in pressure and is expressed as [5],

$$\frac{\Delta f_{FSR}}{\Delta P} = \frac{\Delta f_{FSR}}{\Delta l}\frac{\Delta l}{\Delta P} = \frac{4\pi n}{\lambda}\frac{3(1-\mu^2)a^4}{16Eh^3} \tag{2.5.8}$$

Equation 2.5.8 maps the change in cavity height due to pressure to the sensitivity of the sensor. Also, equation 2.5.8 clearly illustrates that the sensitivity of an FPI is dependent on the height of the cavity, and the radius of the diaphragm, if the wavelength of laser and material properties is held constant. Also, in order to increase the sensitivity, the diaphragm thickness should be thin so as to maximize load deflection responses. But this may result in large deflections and non-linear effects might creep in, which are not desirable.

Therefore, it is important to characterize the relationship between diaphragm thickness, diaphragm height, radius, deflection and sensitivity, both analytically and experimentally in order to establish the design guidelines for Fabry Perot pressure sensor. The analytical approach has been presented in chapter 3 and 4.

CHAPTER 3

FEM AND SENSOR DESIGN

3.1 Finite Element Modeling

Modeling and simulation of MEMS devices is of vital importance to develop innovative products. The Finite Element Method (FEM) is a numerical solution of field problems. FEM cuts a structure into several elements and reconnects them at the 'node' of each element. This reconnection is called meshing. The structure is subjected to various constraints and loads which generates a number of simultaneous equations. The equations are solved using boundary equations determined from the constraints and loads. The end result is a convergence value obtained after solving the equations [20].

3.1.1 Advantages of FEM [21]

Finite Element Modeling is popular for the following reasons.

a) It can readily handle very complex geometry. FEM divides the problem into smaller elements, solves each element independently and then, converges them to one solution that ultimately describes the structure in question. A mathematical model on the other hand will work on the whole structure at once, thus increasing the level of complexity of the analysis.

b) FEM handles a wide variety of engineering problems – Solid mechanics, Dynamics, Heat Problems, Fluids, Electrostatic and Electromagnetic problems.

c) Complex constraints on the structure can be handled with ease using FEM. In the case of indeterminate structures complex loading can be a tough task with mathematical modeling and can involve a large number of non-linear equations and unknowns.

d) FEM also handles complex loading. Loads can be applied on nodes or on individual elements of a structure. Loading can be time or frequency dependent.

3.1.2 Disadvantages of FEM [21]

Apart from the inherent advantages that FEM displays, it is also equally popular for the disadvantages associated with this method.

a) FEM does not produce a general closed-form solution, therefore, making it difficult to observe the response to changes in various parameters.

b) An FEM model is said to be approximate as the method works with interpolation formulas.

c) FEM depends a lot on user inputs and thus any mistakes made by the user can be fatal.

d) Producing a good quality mesh is a major hurdle in FEM. The mesh should be fine enough for good detail where information is needed, but not too fine, or the analysis will require considerable time and space in the computer.

e) Proper computer equipment, training on FEA, a finer mesh, nonlinear analysis (large displacement and material plasticity), and more thorough post-processing of results is required to eliminate failures from this analysis.

Despite the disadvantages FEM is widely used for the sheer fact that many mathematical model assumptions have been corrected/eliminated based on the analysis. The results and modeling carried out with FEM is also found to be closer to the actual model than the mathematical equations that represent it [24]. ANSYS has been the most widely used tool for finite element modeling.

3.1.3 Steps for Finite Element Analysis [21, 22]

Finite element analysis setup on Ansys can be described as a three step process:

a) **Preprocessing:** Or defining the problem.

   i. Define keypoints/lines/areas/volumes of the structure.

   ii. Defining the type of element that would be used to model the structure. This varies from lines, solids to shell structures.

   iii. Define material/geometric properties like Young's Modulus, Poisson's ratio etc.

   iv. Mesh lines/areas/volumes of the structure. The density of the mesh will depend on whether the analysis is a one-dimensional or two-dimensional or axisymmetric or three-dimensional in nature.

b) **Solution:** In this step loads are assigned, constraints are applied and the resulting equations are solved. The external loads can be applied as a surface load or a body load on the structure. The constraints are used to restrict either translational or rotational motion of the structure. The set of equations resulting from these loads and constraints are solved.

c) **Postprocessing:** The results obtained need to be processed further in order gain an understanding of the behavior of the structure. In this stage the following data can be obtained:

i. Lists of nodal displacements

ii. Element forces and moments

iii. Deflection plots

iv. Stress contour diagrams

3.2 Design of Sensor

3.2.1 Assumptions for Design

The following assumptions have been made to facilitate choosing accurate dimensions for the sensor.

a) The sensor is said to be operated such that the response satisfies small deflection theory i.e. deflection is proportional to the applied pressure.

b) The fiber on which the sensor will be mounted is single mode. Therefore, core diameter = 10µm and cladding diameter is = 125 µm.

c) The minimum diameter of the diaphragm of the sensor is chosen to be 50µm. This will ensure that the portion of the diaphragm that corresponds to the spot size will remain flat under deflection [6].

d) The maximum diameter is restricted by the diameter of the cladding of the single mode fiber.

e) The light exiting from the fiber is assumed to be perpendicular to the surface of the fiber, therefore eliminating any reflectivity losses due to dispersion of light in the cavity.

f) The fiber face is assumed to have a reflectivity of 90%.

g) The diaphragm thickness is assumed to be large enough to ensure a perfect mirror like behavior having a reflectivity of 100%.

h) The walls of the fabry perot cavity of the sensor are made of the same material as the diaphragm. This facilitates removing material non-linearities during modeling.

3.2.2 Materials for the Sensor

Four materials, Copper, Nickel, Aluminum and Silicon Nitride, have been considered for studying the behavior of the sensor. The choice of Aluminum is attributed to the fact that it is cheap and easy to work with. Aluminum is also more flexible than Copper. Copper and Nickel have similar physical properties but Nickel is less brittle, more flexible and has good optical properties making it suitable for applications involving high reflectivity [25]. Copper on the other hand is immune to magnetic interference. Silicon Nitride, though brittle, is a strong material and can be used in high temperature applications structures made of Silicon Nitride also have higher longetivity [24]. The material properties for these materials have been tabulated in table 3.1.

Table 3.1 Properties of materials used for sensor fabrication.

Material Property	Copper	Nickel	Aluminum	Silicon Nitride
Young's Modulus (E)	130GPa	200GPa	70GPa	310GPa
Poisson's ratio (μ)	0.34	0.31	0.35	0.27

3.3 An algorithm for the design

The design of the sensor involves three important variables –

a) Radius of the diaphragm

b) Thickness of the diaphragm

c) Height of the cavity

Though all the three variables influence the deflection characteristics of the diaphragm, modeling becomes simpler when one of these variables is held constant and the other two are changed. For example, keeping the cavity height constant, the radius and thickness of the sensor is changed.

The following sub-sections illustrate the design methodology using Copper as the material. The same methodology is applicable to the other materials.

3.3.1 Thickness of the diaphragm

The thickness of the sensor can be chosen such that the deflection behavior remains in the linear range (small-deflection) of the analysis. One rule of thumb that has been followed is that for a given value of thickness, the maximum deflection observed does not exceed one-fifth the thickness value [14, 23, 26]. For ease this rule will be

referred to as the *one-fifth rule* in this thesis. A range of thickness spanning from 0.8µm to 1.4µm were simulated. For linear behavior the maximum value of deflection according to the one-fifth rule is tabulated in table 3.2. For each of these thicknesses the deflection of the diaphragm was noted for different radii.

Table 3.2 Max deflection for different thickness for linear range of operation.

Thickness	Max deflection allowed using $1/5^{th}$ rule
0.8µm	0.16µm
1µm	0.2µm
1.2µm	0.24µm
1.4µm	0.28µm
1.6um	0.32µm

The sensor structure is modeled on Ansys. The sensor diaphragm is assigned the material properties of Copper (Young's Modulus and Poisson's Ratio). The height of the cavity is fixed, the diaphragm radius is fixed and the diaphragm thickness is varied. A pressure range from 0 to 1000mmHg in steps of 200mmHg is applied on the diaphragm. The maximum deflection occurs when the maximum pressure of 1000mmHg is applied on the sensor (figure 3.1).

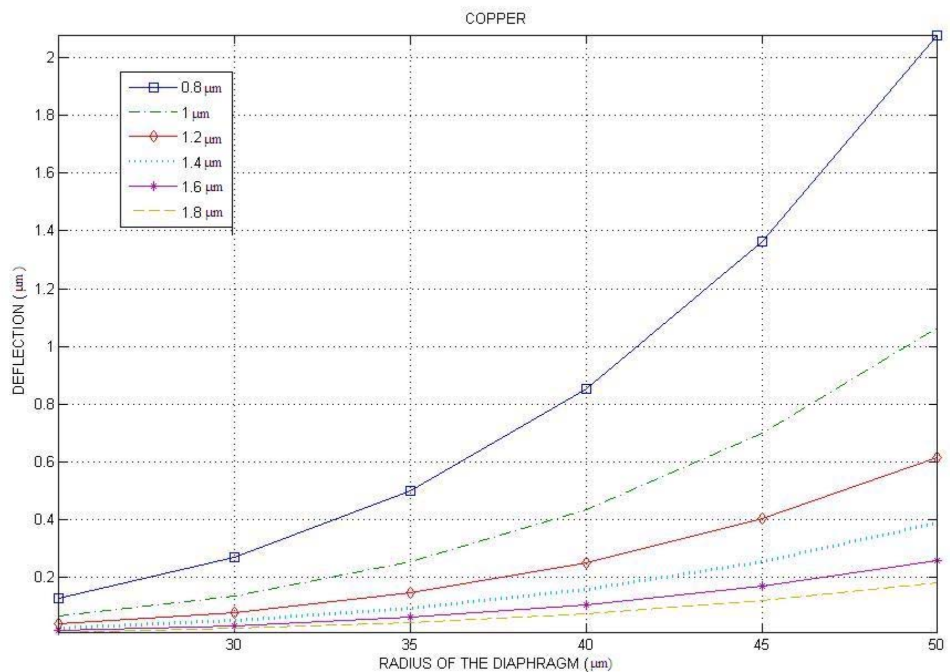

Figure 3.1 Deflection vs. diaphragm radius for different thickness of diaphragm.

The maximum radius of the copper diaphragm that satisfies the one-fifth rule for each value of thickness is listed in table 3.3.

Table 3.3 Maximum radius conforming to the one-fifth rule.

Thickness (µm)	Maximum deflection (µm)	Radius satisfying one-fifth rule (µm)
0.8	0.16	25
1	0.2	30
1.2	0.24	35
1.4	0.28	45
1.6	0.32	50
1.8	0.36	50

A change in thickness of the diaphragm can change the extent of deflection from less than 1% to as high as 10% of the initial value. This large range of changes may force a sensor working under perfect linear conditions to exhibit non-linear behavior. Therefore, while fabricating the sensor, high precision control for thickness of the diaphragm is necessary.

3.3.2 Radius of the diaphragm

Keeping the material properties and the stiffness of the diaphragm constant, it is the radius of the diaphragm that controls the extent of deflection that the sensor experiences under given conditions of external pressure. A slight change in the radius does not show a large change in the deflection characteristics of the sensor. Although the radius of the sensor does not need critical control while fabrication, a change in the radius while fabrication can change the linear behavior of the sensor to non-linear.

One way of choosing the radius is to choose a thickness for the sensor and according to table 3.3, choose the radius that conforms to the one-fifth rule. The table also shows that for a diaphragm thickness of 1.4μm, any radius less than 45μm will satisfy the criteria for one-fifth rule. Therefore, slight changes in radius while fabrication would not significantly alter the performance of the sensor. But this method cannot be used as an absolute rule due to reasons that will become obvious in the following section.

3.3.3 Height of the cavity

A popular figure of merit for an FPI is the sensitivity of the sensor (equation 2.5.8). This is because the sensitivity depends not only on the dimensions of the sensor

but also on the height of the cavity. The accuracy of the dimensions picked in sections 3.3.1 and 3.3.2 can only be verified by combining all of the design variables and observing the sensitivity of the pressure sensor. It is important to verify that the crude elimination used for diaphragm dimensions, i.e. the one-fifth rule, is valid before observing the sensitivity for the regions proposed to have a linear response.

Figures 3.2 to 3.7 show a variation of the sensitivity for a sensor made of Copper under conditions of low pressure change. Also illustrated on the plots is the maximum value of cavity height and radius of the diaphragm corresponding to the one-fifth rule. For a given radius, the diaphragm displays highest sensitivity for a height of 1μm in all the cases.

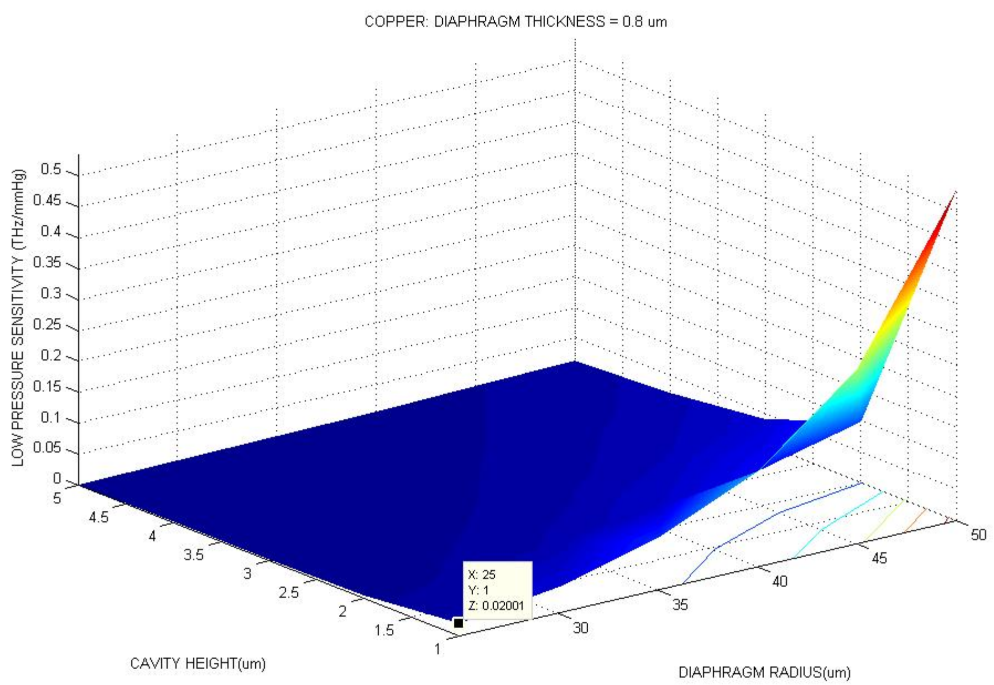

Figure 3.2 Low Pressure sensitivity of a Copper diaphragm of thickness 0.8μm.

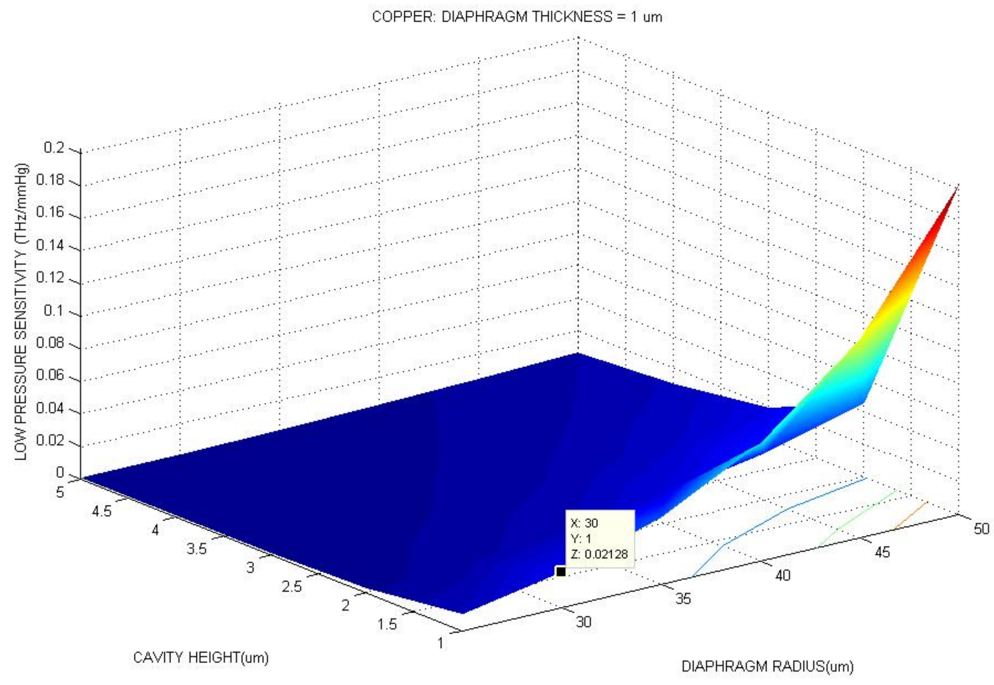

Figure 3.3 Low Pressure sensitivity of a Copper diaphragm of thickness 1µm.

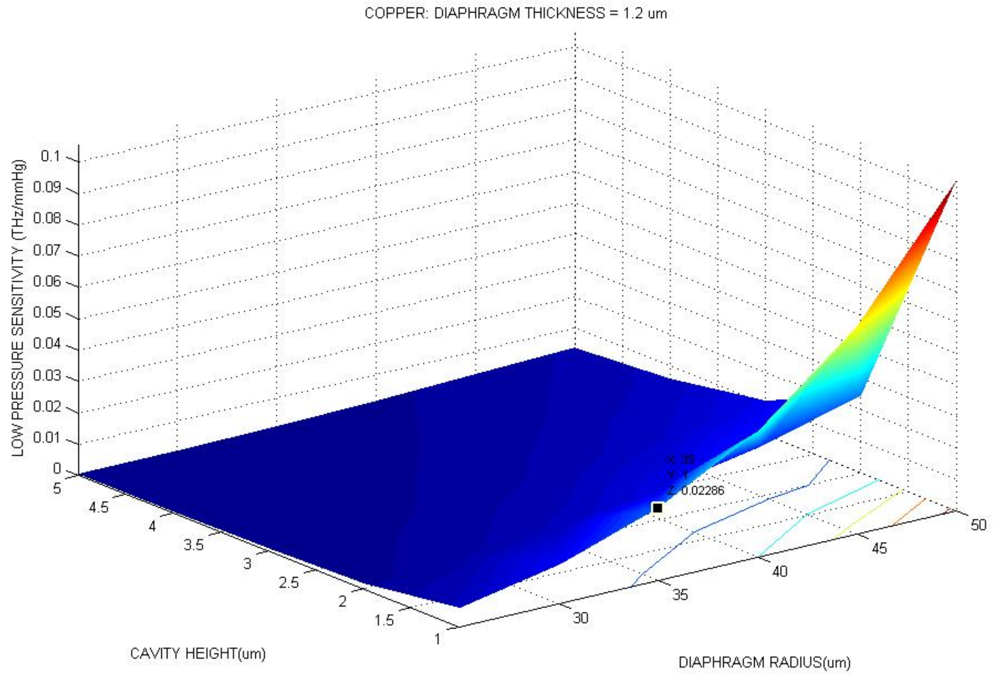

Figure 3.4 Low Pressure sensitivity of a Copper diaphragm of thickness 1.2µm.

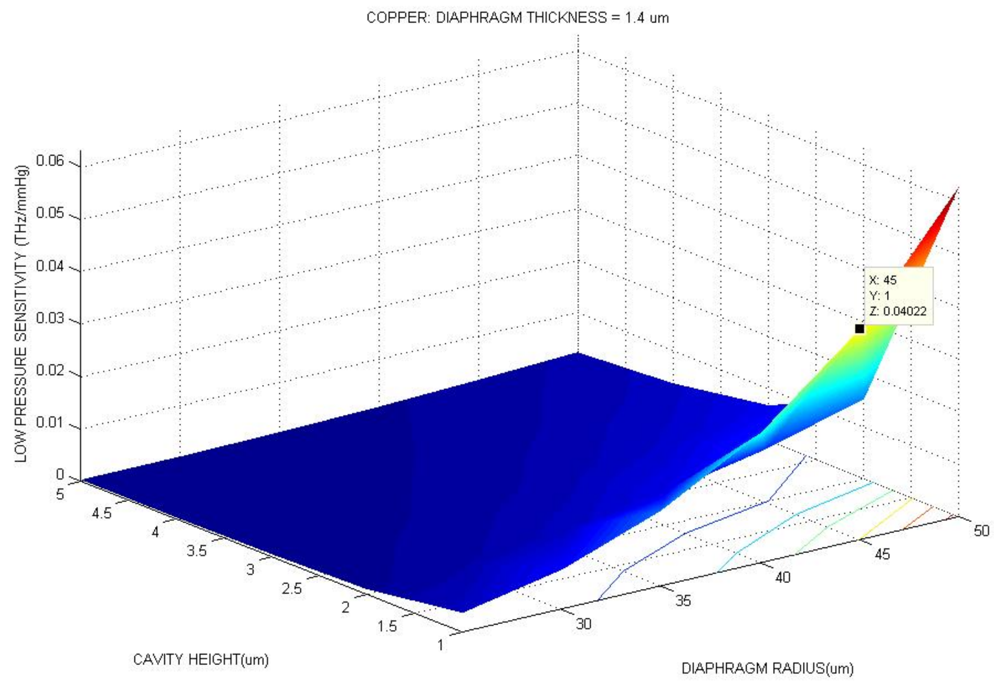

Figure 3.5 Low Pressure sensitivity of a Copper diaphragm of thickness 1.4μm.

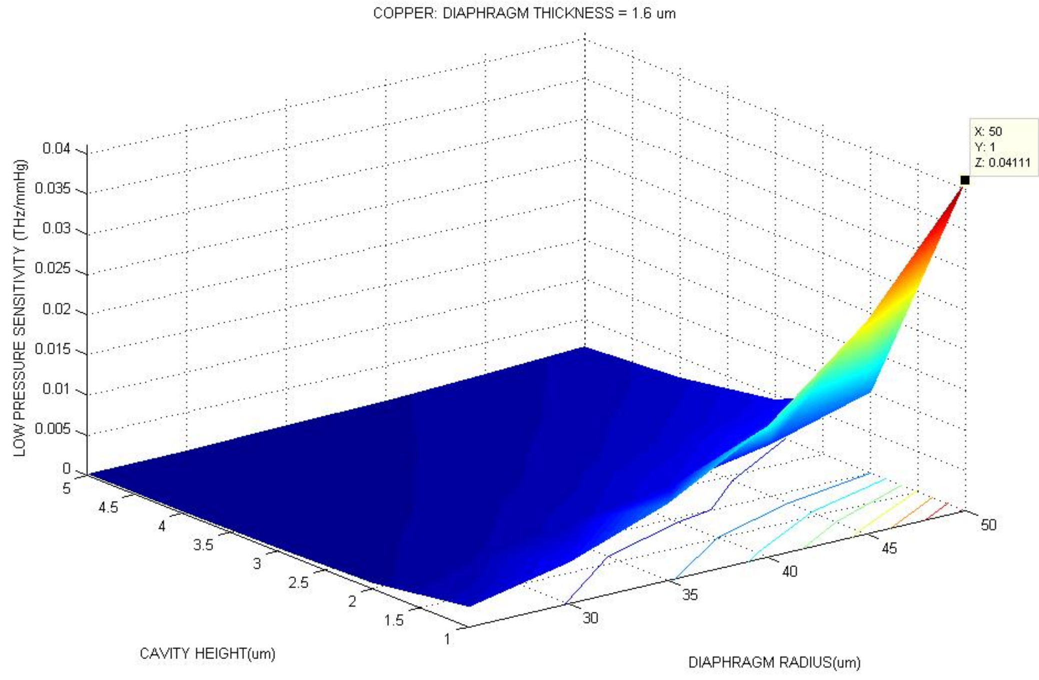

Figure 3.6 Low Pressure sensitivity of a Copper diaphragm of thickness 1.6μm.

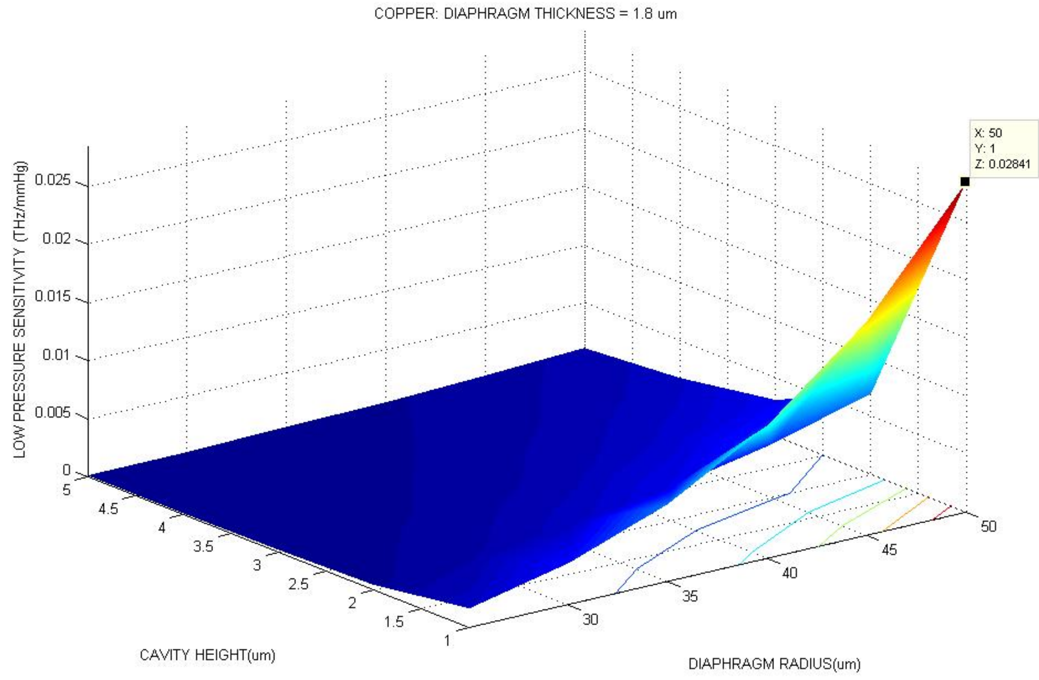

Figure 3.7 Low Pressure sensitivity of a Copper diaphragm of thickness 1.8μm.

Under conditions of high pressure the sensitivity is plotted for the different values of thickness (figures 3.8 – 3.13).

It can be seen that for diaphragm thickness of less than 1μm, the sensitivity of the diaphragm tends to a large negative value for a cavity height of 1μm and radius between 40-50μm, indicating the presence of some kind of non-linearity. A closer observation at the deflection at high pressure observed for the dimensions in question indicates that the diaphragm does not follow the one-fifth rule at these points. For thicknesses of 1.2μm and above this non-linearity is absent. This verifies that the dimensions excluded using the one-fifth rule can be used as a dimension elimination tool. A similar observation can be made for a sensor made of Aluminum, Nickel and Silicon Nitride illustrated in Appendices A, B and C respectively.

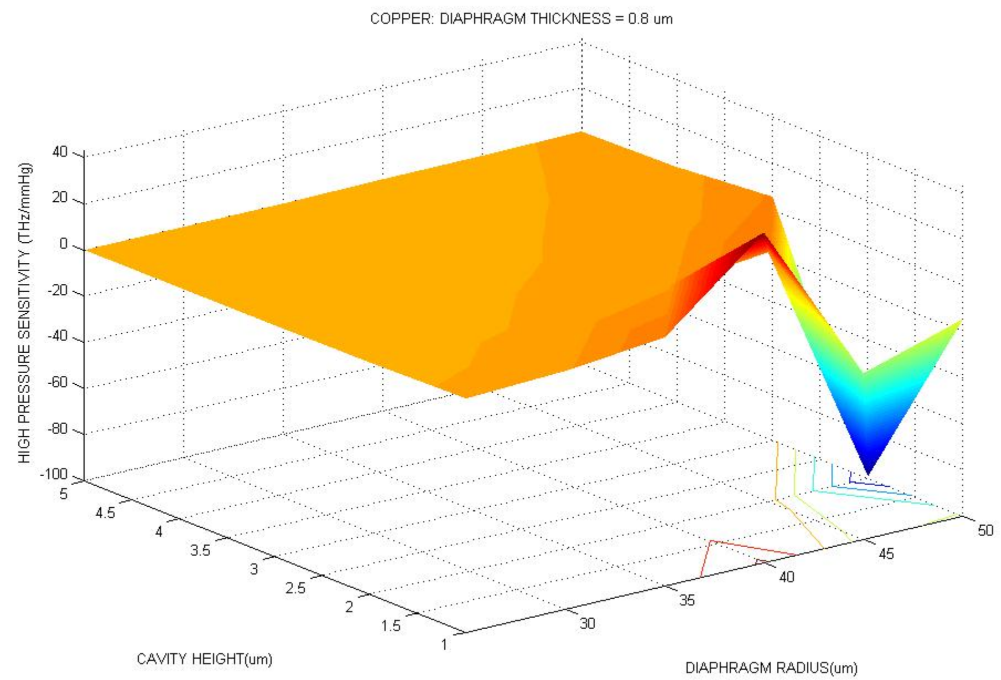

Figure 3.8 High Pressure sensitivity of a Copper diaphragm of thickness 0.8µm.

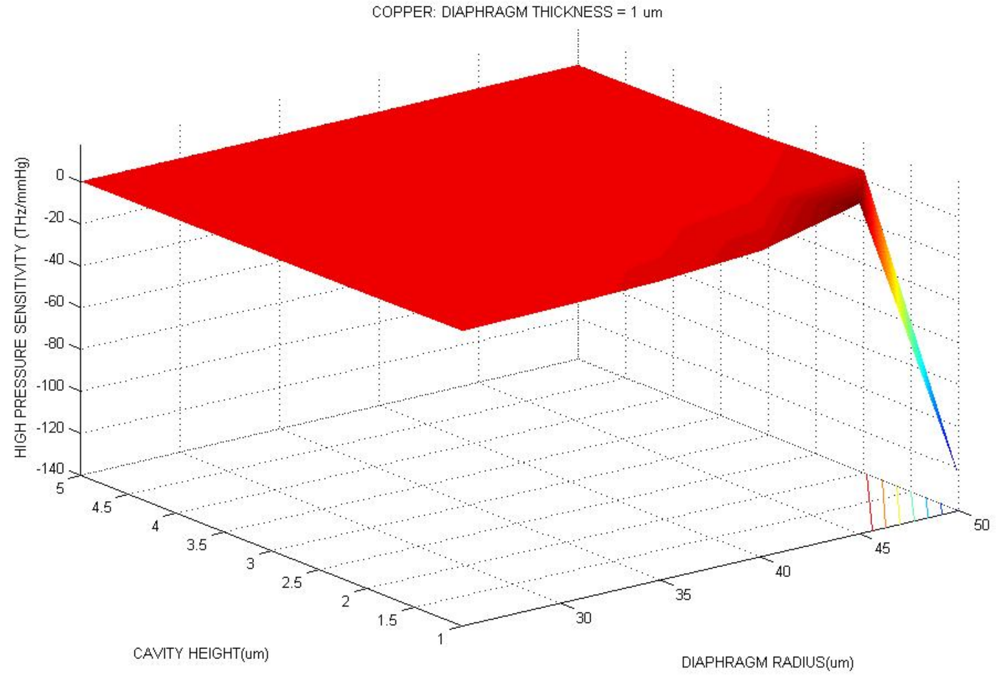

Figure 3.9 High Pressure sensitivity of a Copper diaphragm of thickness 1µm.

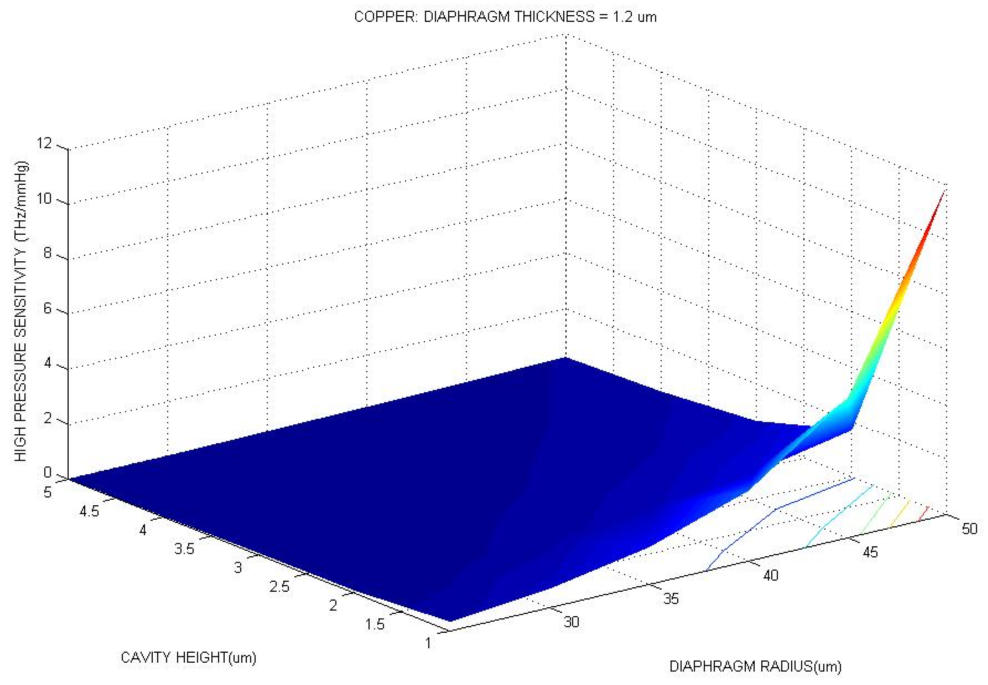

Figure 3.10 High Pressure sensitivity of a Copper diaphragm of thickness 1.2μm.

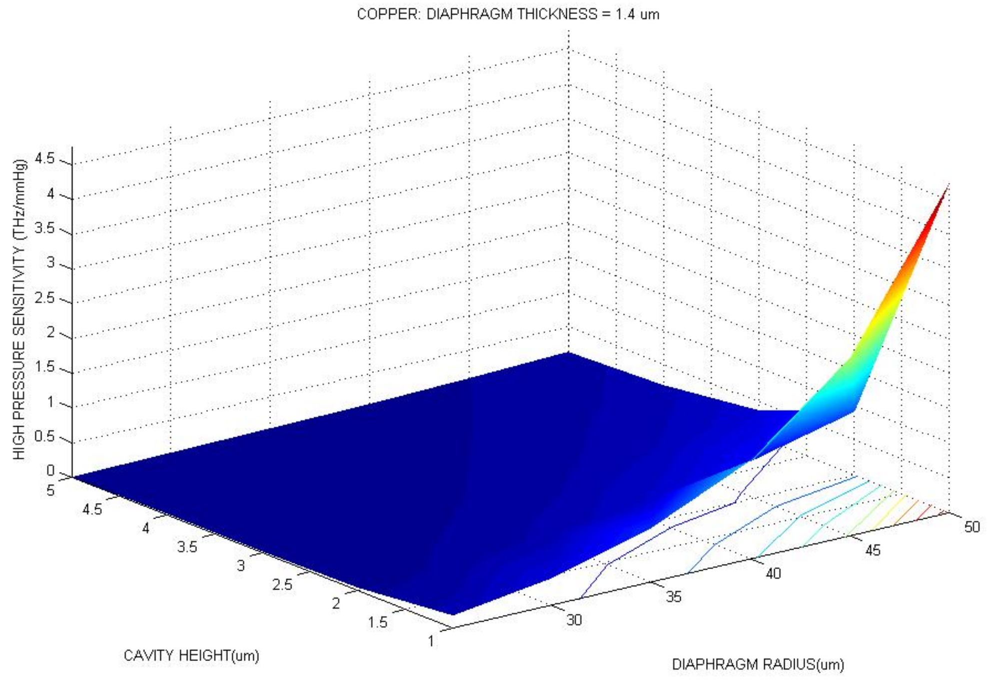

Figure 3.11 High Pressure sensitivity of a Copper diaphragm of thickness 1.4μm.

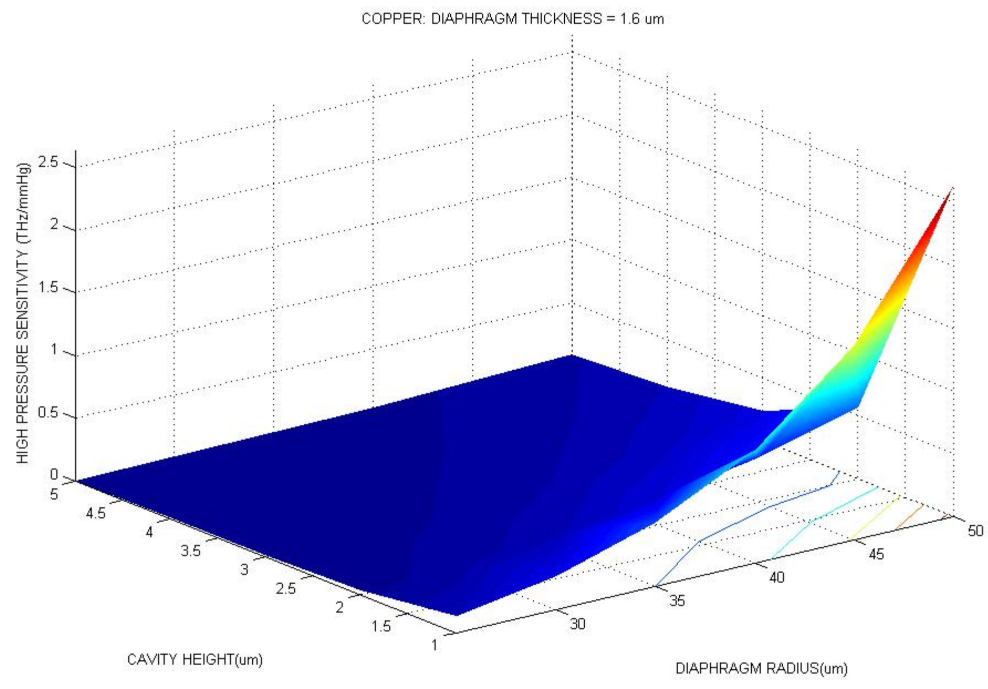

Figure 3.12 High Pressure sensitivity of a Copper diaphragm of thickness 1.6μm.

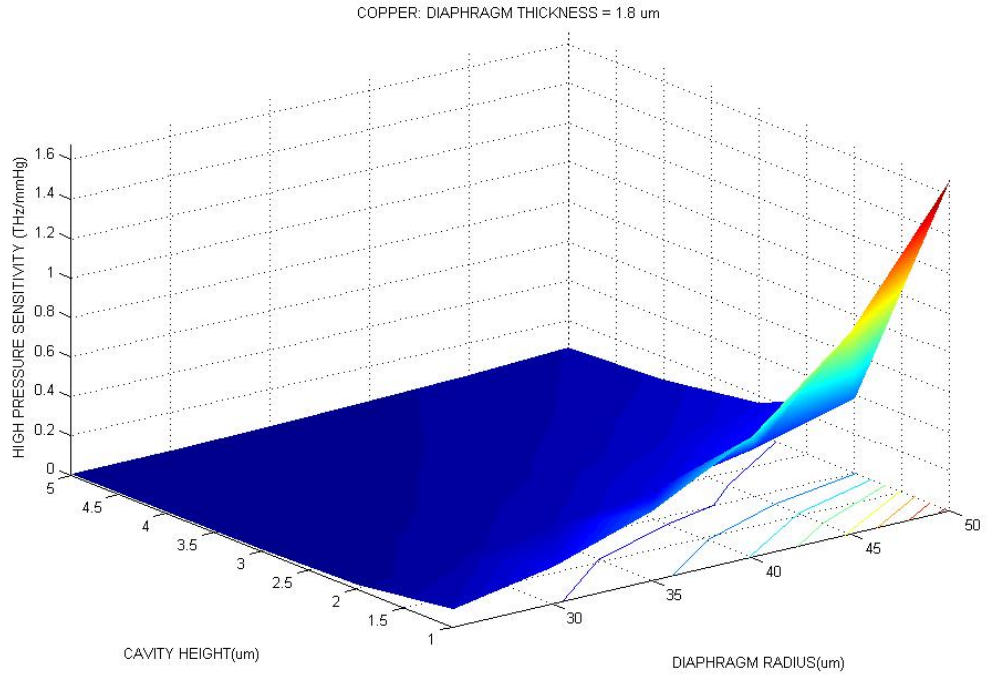

Figure 3.13 High Pressure sensitivity of a Copper diaphragm of thickness 1.8μm.

The value of sensitivity, as observed in figures 3.2-3.7, corresponding to the one-fifth rule limit first increases, reaches a maximum value and then decreases. This leads us to conclude that dimensions of the sensor that results in the maximum sensitivity at 1μm height must be chosen. For a copper diaphragm, this corresponds to a diaphragm radius of 50μm, diaphragm thickness of 1.6μm. The sensitivity value for these dimensions is 41.11GHz/atm.

The same methodology is adopted when the material of the sensor is replaced with Aluminum, Nickel or Silicon Nitride. Table 3.4 lists the sensor design parameters and the sensitivity for these materials along with Copper.

Table 3.4 Design parameters for different materials.

MATERIAL	**THICKNESS (μm)**	**RADIUS (μm)**	**HEIGHT (μm)**	**MAX SENSITIVITY (THz/Pa)**
COPPER	1.6	50	1	0.04111
ALUMINUM[1]	1.8	50	1	0.05408
NICKEL[2]	1.4	50	1	0.04075
SILICON[3] NITRIDE	1	40	1	0.02989

[1] See Appendix A
[2] See Appendix B
[3] See Appendix C

CHAPTER 4

DESIGN MODIFICATIONS

The dimensions chosen for the proposed sensor at the end of Chapter 3 conforms to the design criteria and sensitivity range. The question that needs to be asked at this point is whether the sensitivity of the sensor can be increased further without compromising the linear region of operation. There are four variables in the design of this sensor –

a) Thickness of the diaphragm – This variable cannot be modified as the one-fifth rule depends on it. Changing the thickness would only alter the maximum radius that satisfies the one-fifth rule.

b) Radius of the diaphragm – Changes made to the radius of the sensor may affect the sensitivity. Section 4.2 investigates this further before a conclusion is stated.

c) Height of the cavity – The height chosen so far, viz. 1μm, exhibits the best sensitivity response. This variable should not be changed.

d) Support structure for the diaphragm – The support structure onto which the diaphragm has been clamped is a hollow-cylinder. Further investigations are required (section 4.1) to see if this structure can be modified and what implications would this modification have on the sensitivity.

4.1 Modifying the sensor's structure

The sensor designed in chapter 3 has a structure as illustrated in figure 4.1. The sensing element, or diaphragm, is mounted on a solid structure that clamps it in place. If the ambient environment of the sensor is maintained constant by external packaging, the support structure for the diaphragm can be modified.

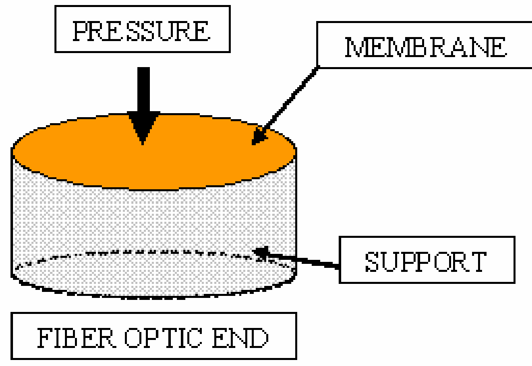

Figure 4.1 Model of the sensor designed in Chapter 3.

One form of modification proposed would be to change the solid structure from a hollow-cylinder to four pillars. The pillars are of equal height and cross-section and are placed equidistant from the center of the diaphragm. There is no overhang of the diaphragm on the pillars (figure 4.2). This sensor structure is now tested for deflection characteristics for the same range of external pressure.

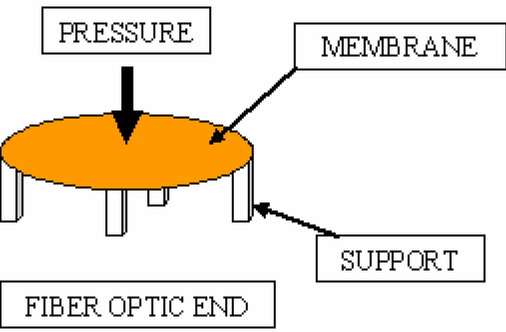

Figure 4.2 Four-pillar support for the pressure sensor.

Another modification to the structure is to reduce the four pillars to two pillars and observe the behavior of the sensor (figure 4.3). Again, the range of pressure applied remains the same.

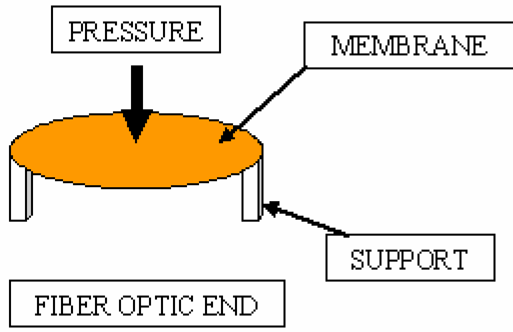

Figure 4.3 Two-pillar support for the pressure sensor.

Figure 4.4 compares the deflection characteristics of the three different sensor configurations – hollow-cylinder, four-pillar and two-pillar. The difference in the extent of deflection observed between the hollow-cylinder and four-pillar is not as prominent as the difference observed between the hollow-cylinder and two-pillar structures. The

presence of the kink (irregularity) on the deflection characteristics for four-pillar and two-pillar indicates the deviation of the deflection characteristics into the non-linear deflection regime.

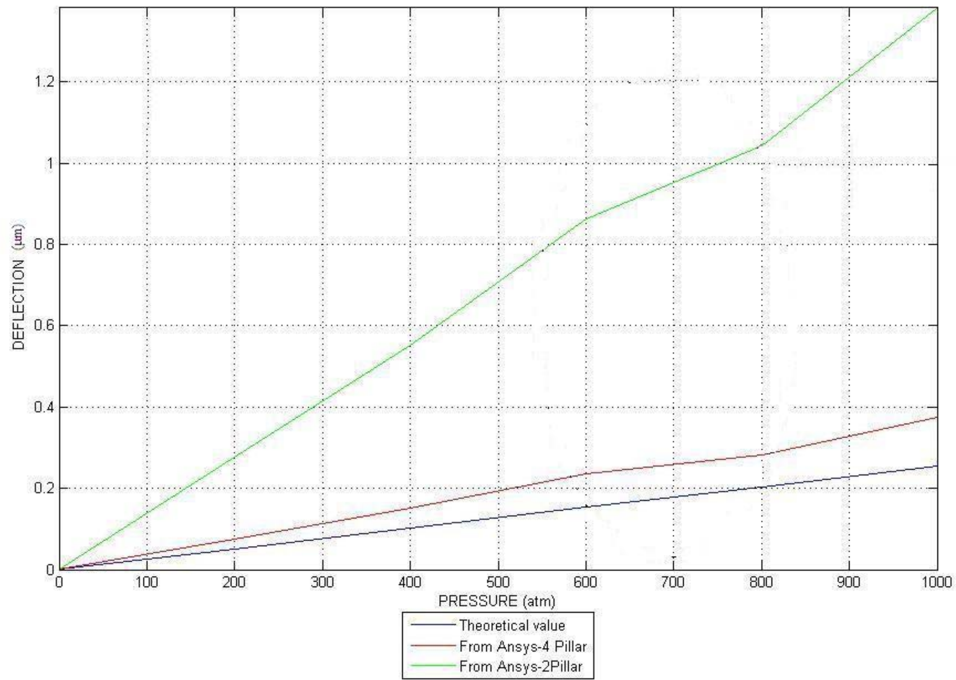

Figure 4.4 Comparison of the deflection observed for the three configurations of sensor support for a 1.6μm thickness, 50μm radius and 1μm height copper sensor.

4.2 Optimizing the sensor dimensions

It is evident from figure 4.4 that the deflection characteristics can change from linear regime to non-linear regime when a two-pillar or four-pillar structure replaces the hollow-cylinder structure. The only solution to make the four-pillar and two-pillar structures to behave linearly is to modify the dimensions of the diaphragm. Changing the height of the cavity does not have any effect on the deflection characteristics.

Therefore, there are two ways of modifying the diaphragm – change the radius of the diaphragm or change the thickness of the diaphragm.

Decreasing the thickness of the diaphragm would only increase its tendency to follow non-linear behavior. Also, the radius of the diaphragm is in the range of the maximum radius that the sensor can have. Therefore, either the diaphragm thickness must be increased (figure 4.5) or the diaphragm radius must be decreased (figure 4.6).

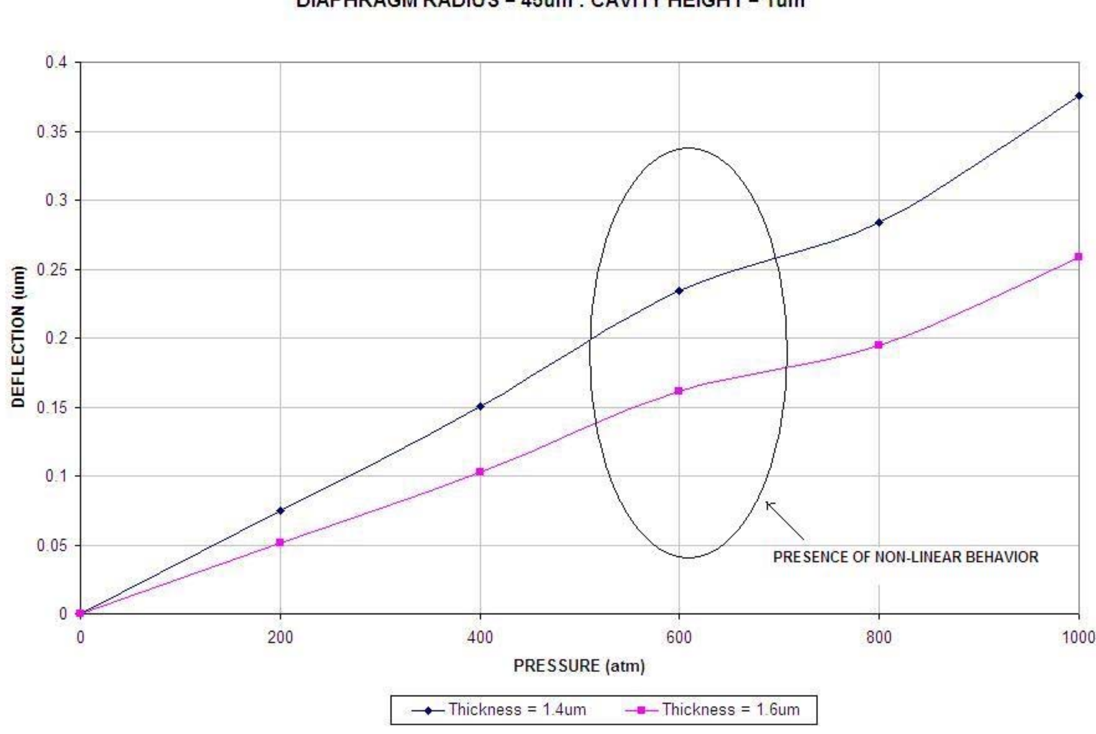

Figure 4.5 Effect of increasing diaphragm thickness on a two-pillar support.

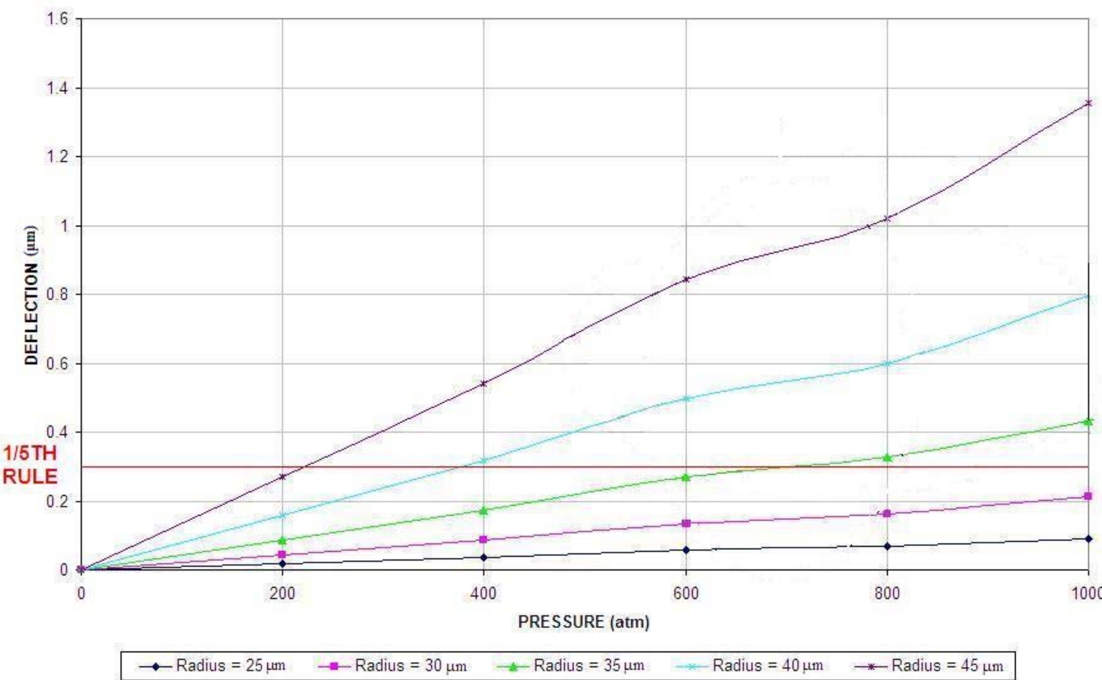

Figure 4.6 Effect of increasing diaphragm radius on a two-pillar support.

Increasing the thickness of the diaphragm, by 0.2µm, results in a decrease in deflection by approximately 10-20%. Decreasing the diaphragm radius, by 5µm, results in a decrease in deflection by 5-10% approximately. Although increasing the thickness would help achieve linear behavior for a two-pillar structure sensor, it is not desirable as the diaphragm may turn out to be much stiffer at lower pressures, effecting the sensitivity of the sensor. Also, change in the thickness affects the one-fifth rule. Thus, the radius of the diaphragm should be reduced till linear behavior is observed.

For a 1.4µm thickness diaphragm the maximum deflection allowed using the 'one-fifth' rule is 0.28µm. A 30µm radius with a 2 pillar support satisfies this criterion. Thus the radius of the hollow-cylinder structure of 45µm gets reduced to a 30µm two-pillar structure.

4.3 Comparison

Introducing a two-pillar structure resulted in a marked decrease in the dimensions of the diaphragm as seen in section 4.2. But, this leads to some abnormal behavior under the influence of external pressure.

For a four pillar structure, although the bending at the center of the diaphragm remains almost flat, the edges experience some irregularities in bending (figure 4.7).

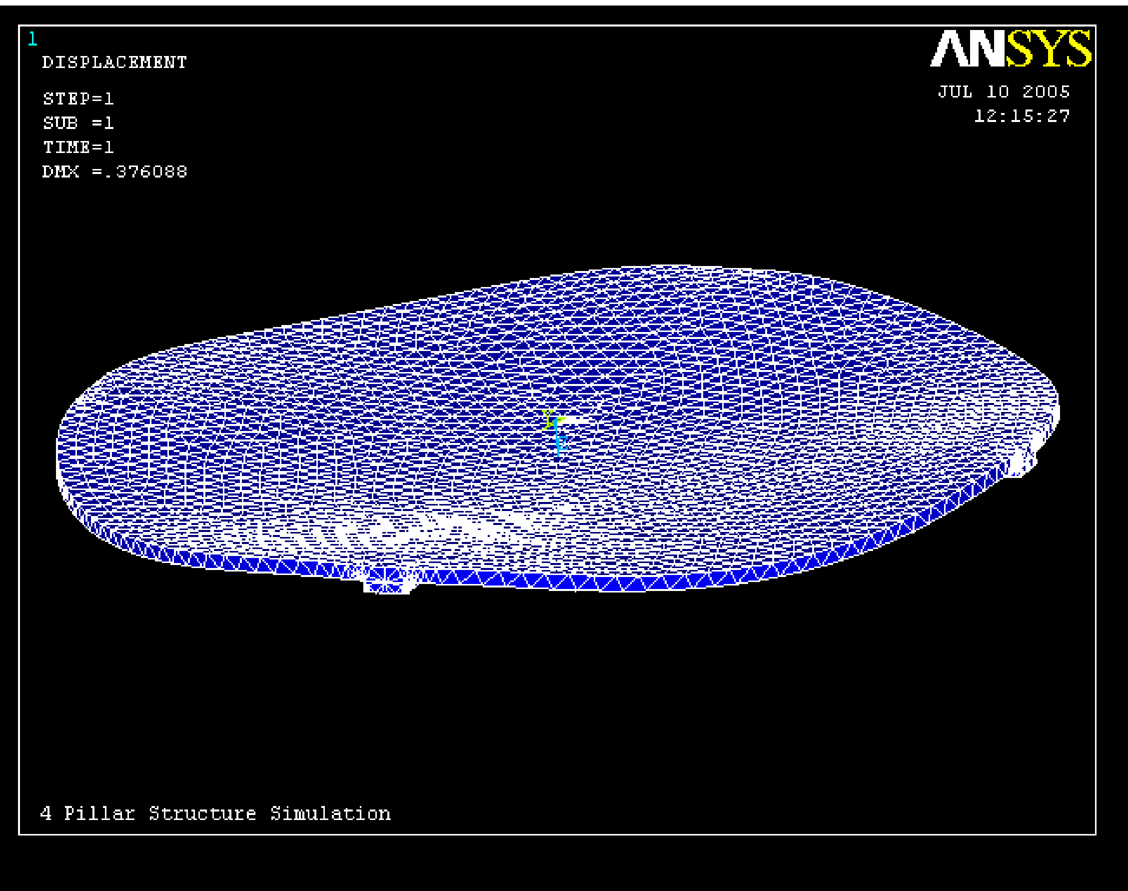

Figure 4.7 Deflection abnormality observed along the edges of a four-pillar structure.

In case of a two-pillar structure this effect becomes more pronounced at the edges (figure 4.8). Also, the diaphragm undergoes more deflection at the edges than at the center, which is undesirable. The curvature of the diaphragm is no longer flat and this can introduce errors in the detector end.

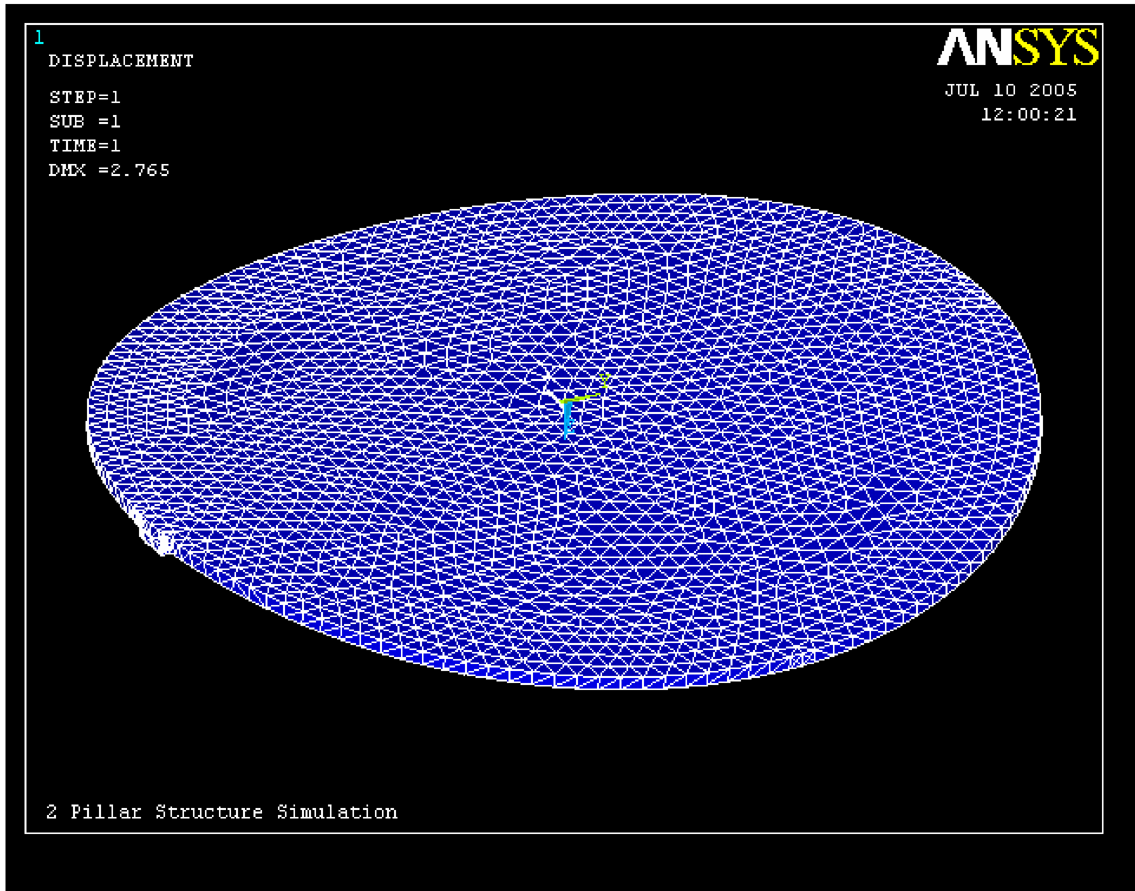

Figure 4.8 Deflection abnormality observed along the edges of a two-pillar structure.

A brief comparison between the different support configurations for the sensor's diaphragm has been made in table 4.1.

Table 4.1 Comparison of deflection behavior of three types of diaphragm support structures.

Support structure type	Deflection behavior	Contour plot showing regions of maximum deflection
Hollow-Cylinder support	Extent of deflection is proportional to the applied pressure	NODAL SOLUTION STEP=1 SUB =1 TIME=1 UZ (AVG) RSYS=0 DMX =.252381 SMN =-.706E-03 SMX =.252381 ANSYS JUL 4 2005 11:15:39 -.706E-03 .027415 .055535 .083656 .111777 .139898 .168019 .196139 .22426 .252381 3D Sensor Simulation
Four-pillar support	Extent of deflection is 1-1/2 times the deflection observed in a hollow-cylinder support.	NODAL SOLUTION STEP=1 SUB =1 TIME=1 UZ (AVG) RSYS=0 DMX =.376088 SMN =-.00535 SMX =.376088 ANSYS JUL 4 2005 11:43:20 -.00535 .037032 .079414 .121796 .164178 .20656 .248942 .291324 .333706 .376088 4 Pillar Structure Simulation

Table 4.1 – *Continued*

Two-pillar support	Extent of deflection is 5-10 times greater than a cylindrical support structure. The behavior can be approximated to that of a simply supported diaphragm.	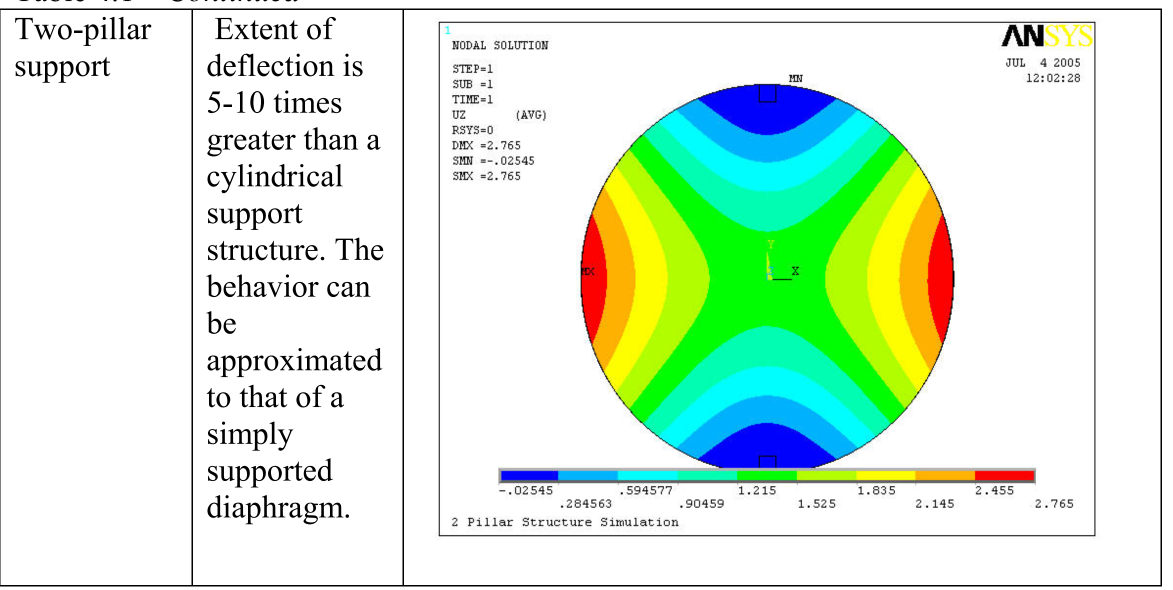

The contour diagrams indicate clearly the regions of maximum (red) deflection and minimum (blue) deflection. The presence of irregularities in bending can be clearly observed in the four-pillar and two-pillar structure.

Although the diaphragms appear to be flat at the center, a closer look at the deflection profile would provide a clearer picture of the performance characteristics. The deflection profile indicates the nature of the curvature of the diaphragm at its center. It is measured along the diameter of the diaphragm and the diameter is chosen such that no support structures lie on it (exception of the hollow-cylinder).

The deflection profile of the sensor diaphragm for all three supports does not remain flat, but exhibits a curvature (fig 4.9). This is contrary to the assumption made before formulating the design methodology. Reflection of light from such a surface could result in scattering of light and will affect the sensitivity. This introduces bending losses in the detector. Such a loss may interfere in clearly distinguishing the change in

pressure at the sensor end, i.e. reduced sensitivity. The sensor, therefore, has to be modified to obtain a flat deflection profile at the center of the diaphragm and maximum possible sensitivity.

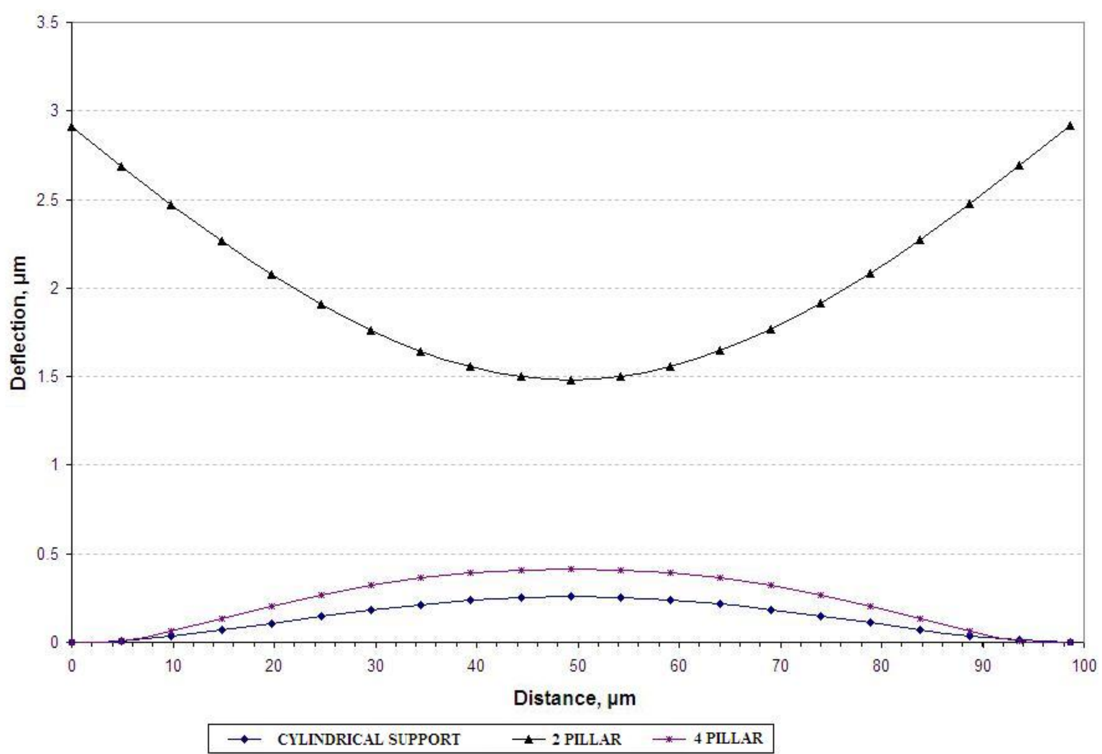

Figure 4.9 Deflection profile indicating non-flat diaphragm center.

4.4 Bossed membrane

A bossed membrane structure consists of a diaphragm with an additional structure fabricated at the center of the diaphragm [27, 28]. The center structure need not be cylindrical in shape and can vary depending on the type of deflection profile desired. For a circular diaphragm on a hollow-cylinder support the shape of the boss structure is a solid cylinder. This kind of a structure ensures low bending loss as it keeps the center of the diaphragm flat, under the application of an external pressure. Figure 4.10 illustrates the bossed membrane on a solid cylinder support.

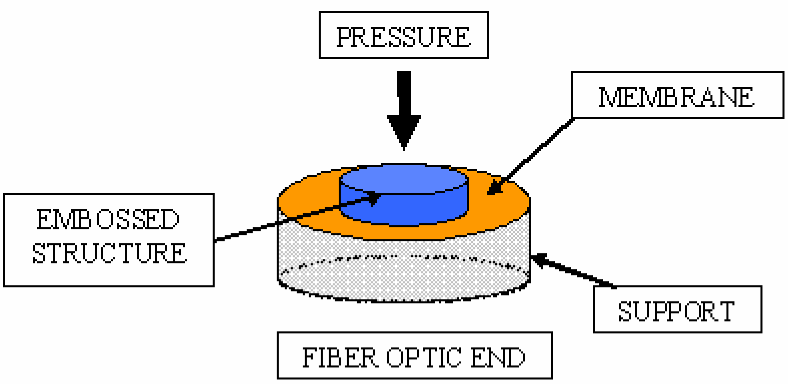

Figure 4.10 Embossed membrane structure for the pressure sensor.

The deflection experienced by the bossed membrane shown in figure 4.9 can be modeled as [29, 30],

$$w = A_p \left(\frac{P\left(\frac{d_m}{2}\right)^4}{E(t_m)^3} \right) \qquad (4.4.1)$$

Where

d_m, radius of the membrane

t_m, thickness of the membrane

P, pressure applied

E, Young's modulus

A_p, Stiffness coefficient given by,

$$A_p = \frac{3(1-v^2)}{16}\left[1 - \frac{(d_b)^4}{(d_m)^4} - 4\frac{(d_b)^2}{(d_m)^2}\log(d_m / d_b)\right] \qquad (4.4.2)$$

With d_b representing the diameter of the boss structure.

The term d_b/d_m is called the solidity ratio and is responsible for the stiffness introduced by the boss structure. Under thin plate deflection (no shear and bending stresses), the thickness of the boss structure must be atleast six times the thickness of the membrane ($t_b \geq 6\ t_m$) and the diameter of the boss must be one-third the diameter of the membrane ($d_b = 1/3\ d_m$).

For the best sensitivity response, a Copper diaphragm of 50µm radius and thickness of 1.6µm was chosen (chapter 3). Therefore the bossed structure must have a radius of 15µm and a thickness of atleast 9.6µm (figure 4.11). The deflection profile of the structure is shown in figure 4.12. The operating range of the sensor is the diameter span over which the diaphragm remains. The spot size at a height of 1µm for a single mode fiber is approximately equal to its core diameter, i.e. 9.5µm.

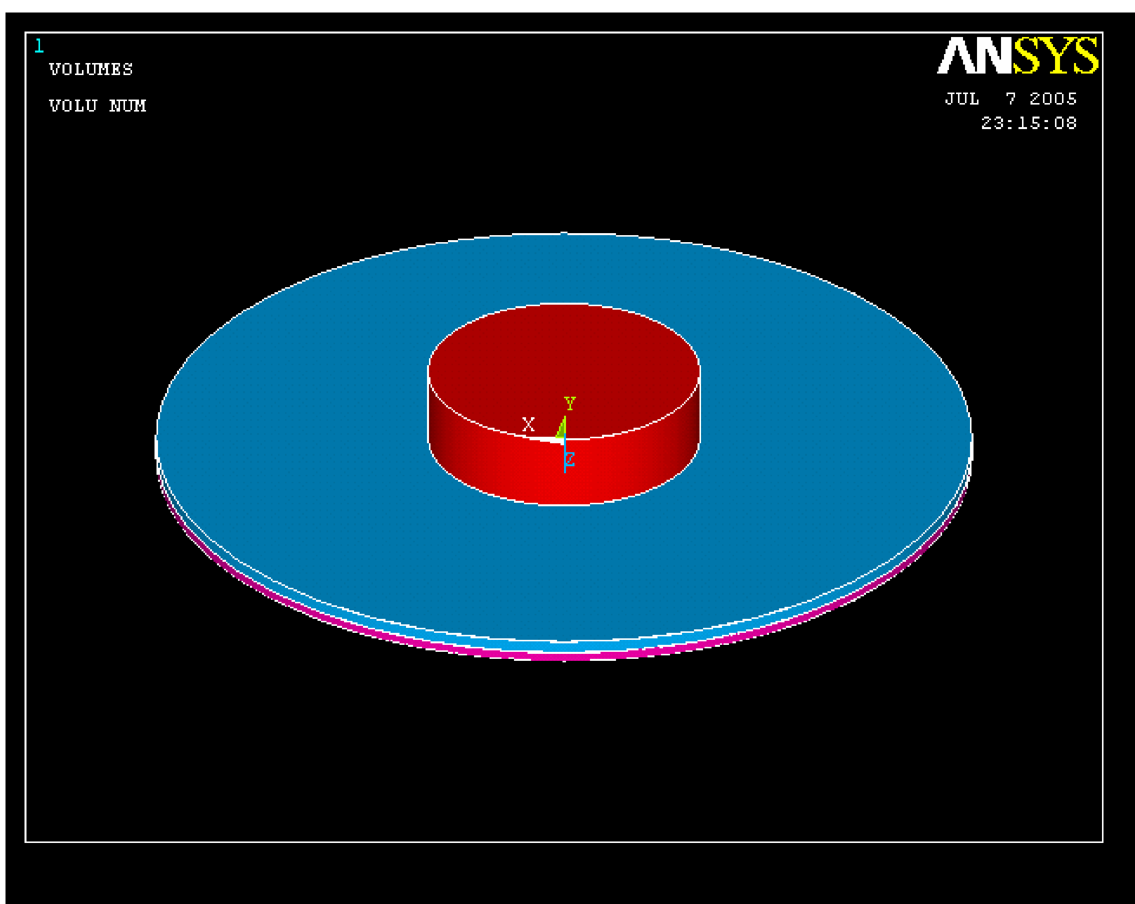

Figure 4.11 Bossed membrane structure on a hollow-cylinder support for a 1.6μm thickness, 50μm radius and 1μm height cavity.

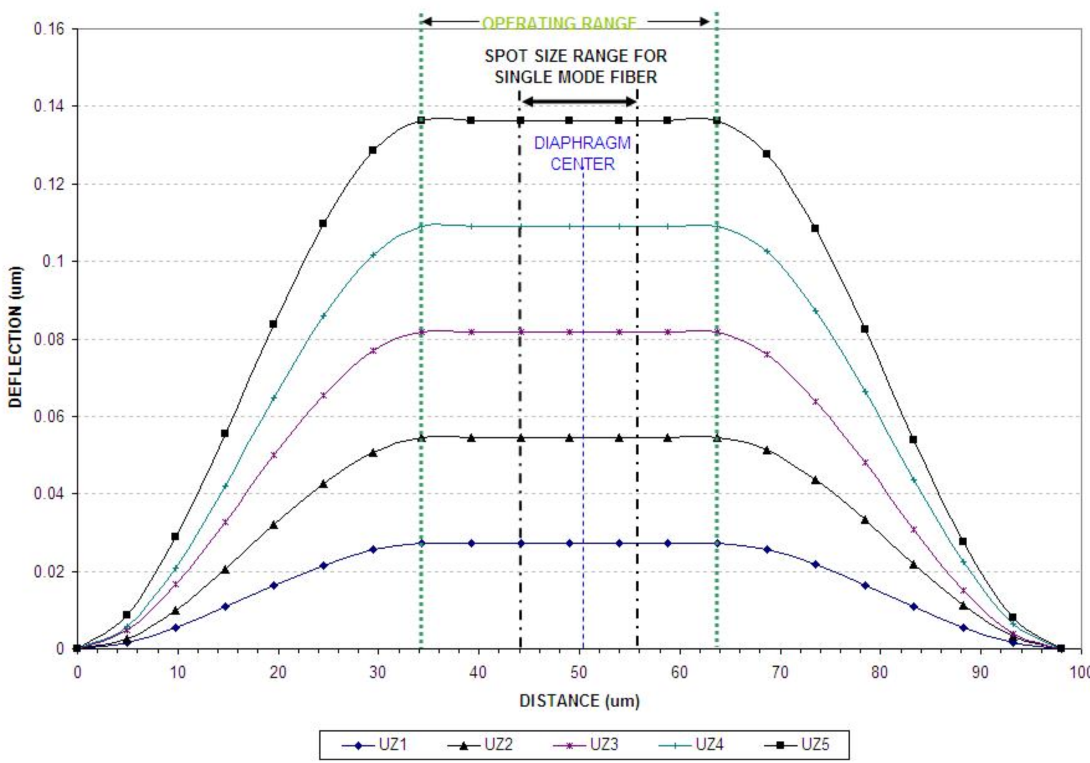

Figure 4.12 Bossed membrane on hollow-cylinder support - deflection profile. UZ indicates different pressures applied, UZ1<UZ2 and so on.

Although the bossed membrane structure exhibits a perfectly flat deflection profile, the extent of deflection reduces by atleast ten times, thereby reducing sensitivity. The operating range of this membrane is more than the spot size for the single mode fiber. Though this will reduce bending losses, it reduces the sensitivity due to low deflection.

The sensor is now replaced by a four-pillar structure with a bossed membrane. The embossed structure dimensions are manipulated such that area of maximum deflection has a diameter more than the spot size of a single mode fiber (10μm). To get the best sensitivity the radius of the membrane can be varied from 30μm to 45μm. The

structure of the boss on a four-pillar support is shown in figure 4.13. Note the shape of the boss structure is chosen such that it is not along the same direction as the pillars.

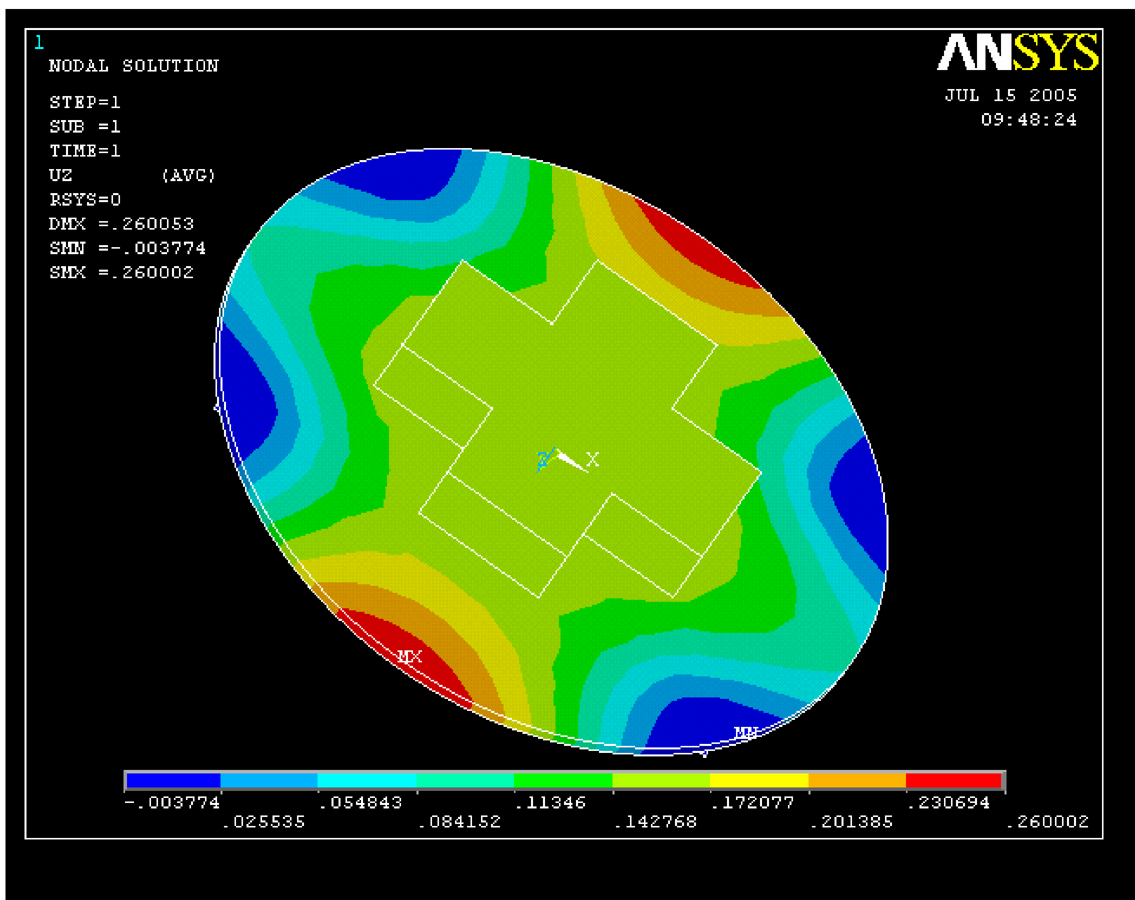

Figure 4.13 Bossed membrane on a four-pillar support structure for a 1.6μm thickness, 50μm radius and 1μm height cavity.

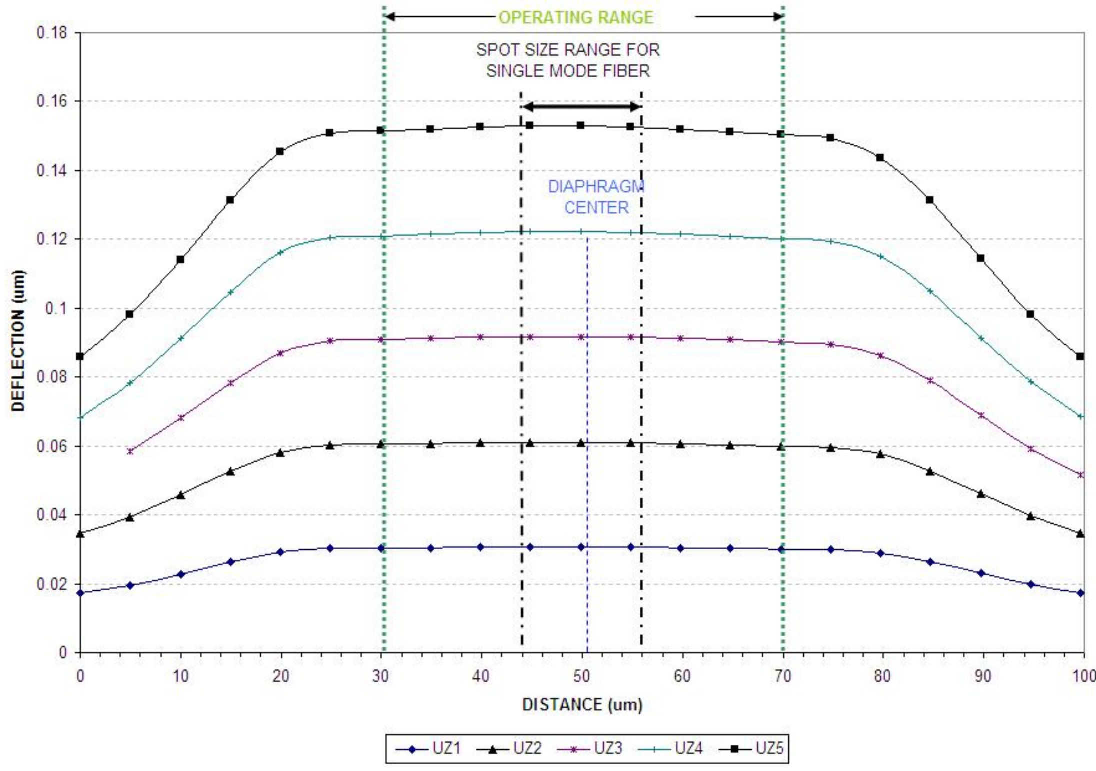

Figure 4.14 Deflection profile of a bossed membrane on a four-pillar support structure. UZ indicates different pressures applied, UZ1<UZ2 and so on.

From the deflection profile, figure 4.13, it is clear that the sensor diaphragm exhibits a flat deflection profile like the solid support. There is no dramatic improvement over the solid structure as far as the extent of deflection is concerned. The operating region is still greater than the spot size range of the single mode fiber 10µm. This structure will therefore experience no bending losses but will not yield a very high sensitivity as the deflection is not very large.

The four-pillar support in the sensor is now replaced by a two-pillar support. The design parameters for the boss remain the same as that for a four-pillar structure, i.e. maximum deflection has to cover an area of diameter greater than 10µm.

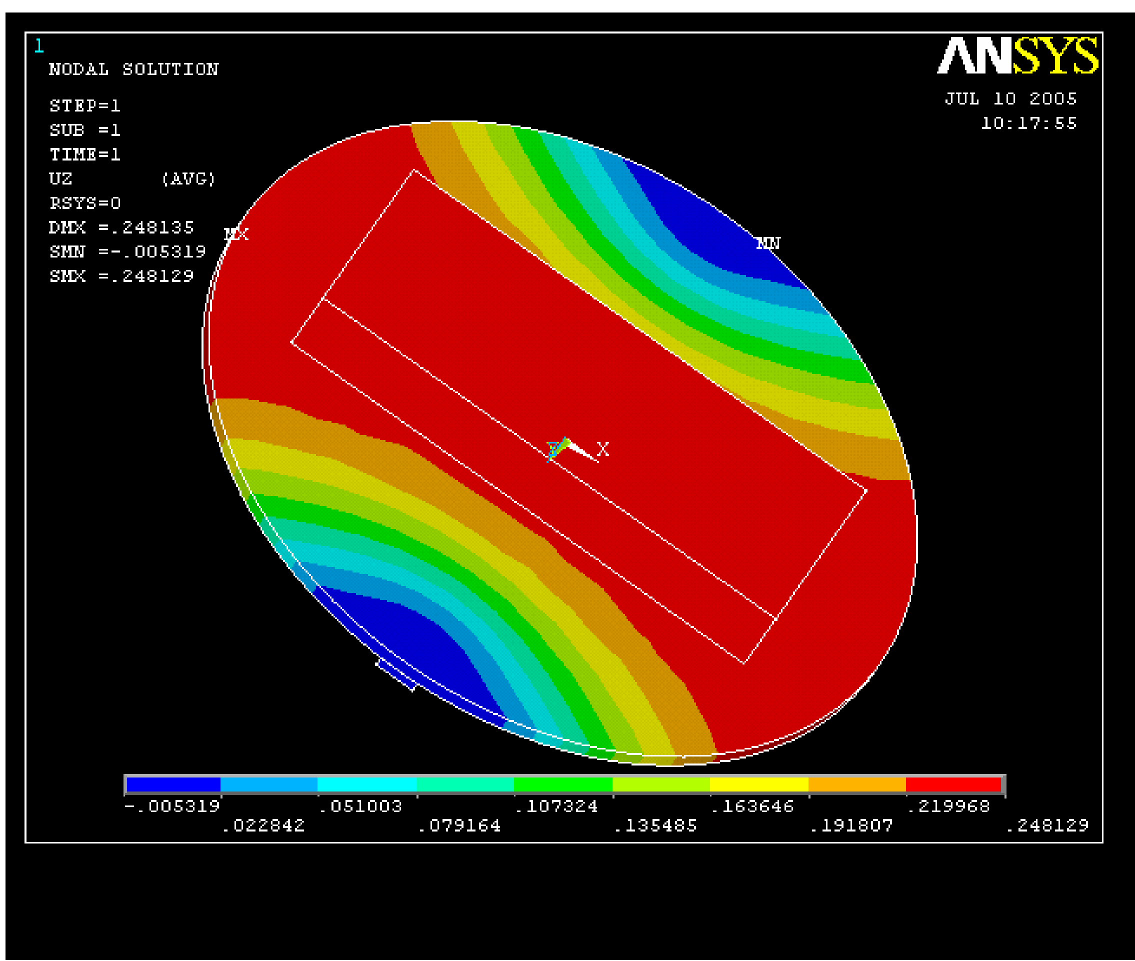

Figure 4.15 Two-pillar support with a bossed membrane. Dimensions of sensor – 35μm radius, 1.6μm thickness, 1μm cavity height, dimensions of the boss structure – 50μm in length (along x direction) and 20μm in width (perpendicular to x direction) and 7μm in height.

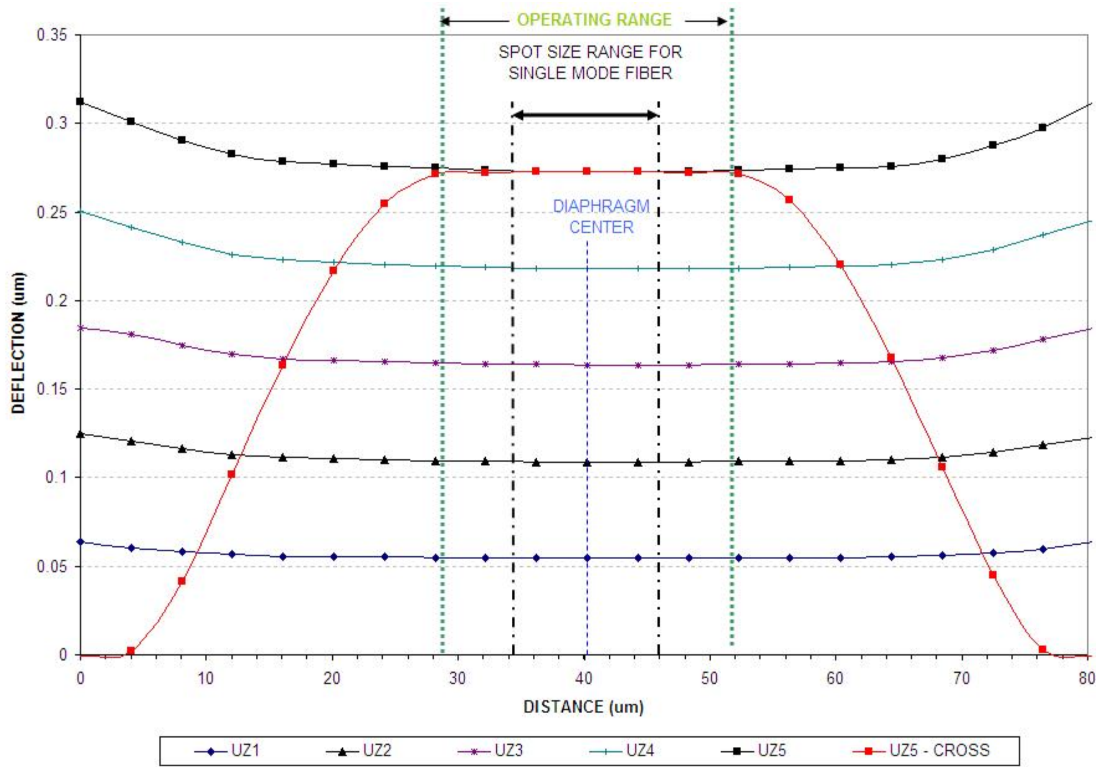

Figure 4.16 Deflection profile for a bossed membrane on a two-pillar support. UZ indicates different pressures applied, UZ1< UZ2 and so on. UZ5 – cross is the deflection profile along the support structure.

The bossed membrane on a two-pillar support for the dimensions indicated in figure 4.15 shows a flat deflection profile (figure 4.16) for different pressures. Also one must note here that the dimensions of the sensor have been reduced. This is due to the fact that the sensor behaves in a non-linear fashion for dimensions exceeding those mentioned in fig 4.16. The change of dimension may not be required in other materials. The magnitude of deflection is also large and is comparable in magnitude with the sensitivity of a diaphragm on hollow-cylinder support without a boss.

4.5 Comparison - bossed membrane

Table 4.2 summarizes the three bossed membrane sensors discussed in this section.

Table 4.2 Comparison of deflection profile of a bossed membrane clamped onto the different support structures.

Type of support	Best dimensions	Deflection profile of diaphragm
Hollow-cylinder	Sensor: Diaphragm Radius – 45µm Diaphragm Thickness – 1.6µm Cavity height – 1µm Emboss: Shape: Solid cylinder Radius – 15µm Thickness – 8.4µm	1. Remains flat but the operating range is more than the desired spot size 2. Magnitude of deflection is small 3. Sensitivity is low
Four-pillar	Sensor: Diaphragm Radius – 45µm Diaphragm Thickness – 1.6µm Cavity height – 1µm Emboss: Shape: two cuboids at right angles to each other Length – 50µm Width – 20µm Thickness – 8.4µm	1. Remains flat with operating range more than the desired spot size 2. Magnitude of deflection is small 3. Sensitivity is low
Two-pillar	Sensor: Diaphragm Radius – 45µm Diaphragm Thickness – 1.6µm Cavity height – 1µm Emboss: Shape: One cuboid at the center of diaphragm Length – 50µm Width – 20µm Thickness – 7µm	1. Remains flat with operating range is more than the desired spot size 2. Magnitude of deflection is large 3. Sensitivity is high 4. Diaphragm dimensions may reduce depending on the type of material used.

CHAPTER 5

CONCLUSION

A design methodology for an FPI based pressure sensor has been proposed. Design modifications proposed for the sensor resulted in a smaller sensor dimension and optimized sensitivity. The proposed sensor in this thesis has been designed for toxic gas environments where electrical sensing can prove hazardous. Depending on the pressure range, following the methodology would result in optimum dimensions with best sensitivity. Table 5.1 provides an overview of the different materials used for the sensor, their dimensions, operating range and the sensitivity for pressures ranging from 0-1000mmHg.

Table 5.1 Overview of different materials used for the sensor, their dimensions, operating range and the sensitivity.

Material	Operating Range	Sensitivity (GHz/mmHg)	Dimensions	
			Sensor	Emboss:
ALUMINUM	20µm radius	54.08	Diaphragm radius – 35µm Diaphragm thickness – 1.8µm Cavity height – 1µm	Shape: one cuboids at the center of the diaphragm Length – 50µm Width – 20µm Thickness – 9.6µm

Table 5.1 - *Continued*

COPPER	20µm radius	41.11	Diaphragm Radius –50µm Diaphragm thickness – 1.6µm Cavity height – 1µm	Shape: One cuboid at the center of the diaphragm Length – 50µm Width – 20µm Thickness – 7µm
NICKEL	30µm radius	40.75	Diaphragm radius – 40µm Diaphragm thickness – 1.4µm Cavity height – 1µm	Emboss: Shape: one cuboid at the center of the diaphragm Length – 50µm Width – 30µm Thickness – 5µm
SILICON NITRIDE	30µm radius	58.29	Diaphragm radius – 40µm Diaphragm thickness – 1µm Cavity height – 1µm	Emboss: Shape: one cuboid at the center of the diaphragm Length – 50µm Width – 30µm Thickness – 5µm

APPENDIX A

DESIGNING THE PRESSURE SENSOR USING ALUMINUM AS A MATERIAL

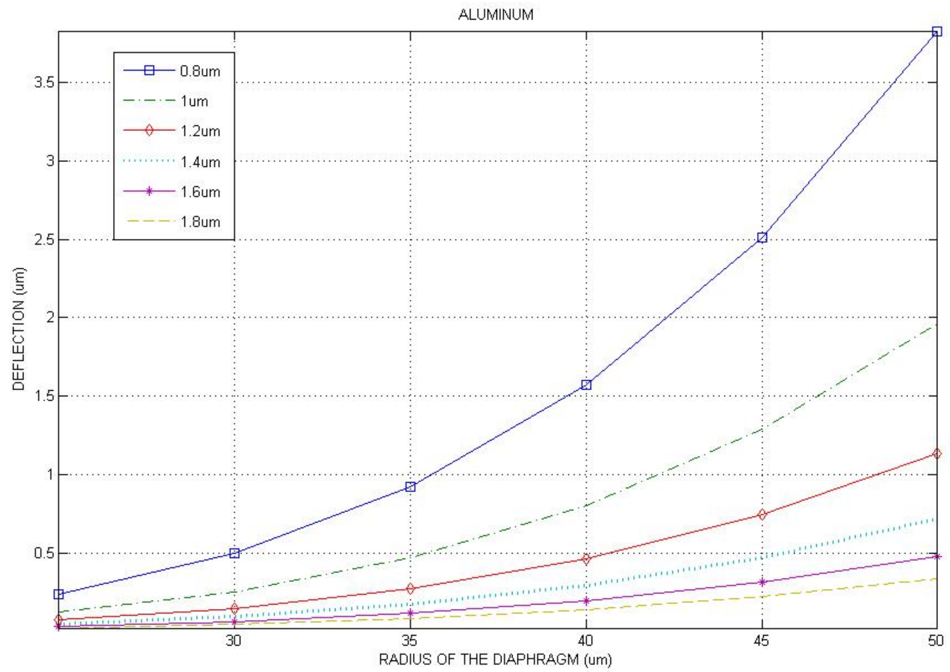

Figure A. 1 Deflection vs. diaphragm radius for different thickness of an Aluminum diaphragm.

Table A.2 One-fifth rule applied to Aluminum diaphragms.

Thickness (µm)	Maximum deflection (µm)	Radius satisfying one-fifth rule (µm)
0.8	0.16	25 (Pressure cannot exceed 800 mmHg)
1	0.2	25
1.2	0.24	30
1.4	0.28	35
1.6	0.32	45
1.8	0.36	50
2	0.4	50

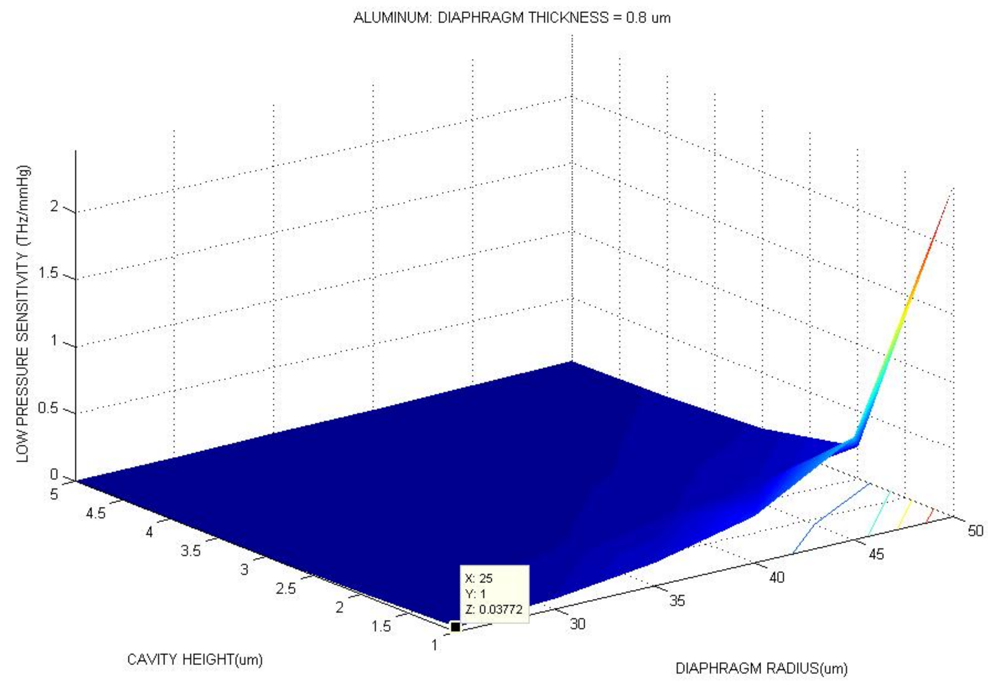

Figure A. 2 Low Pressure sensitivity of an Aluminum diaphragm of thickness 0.8μm.

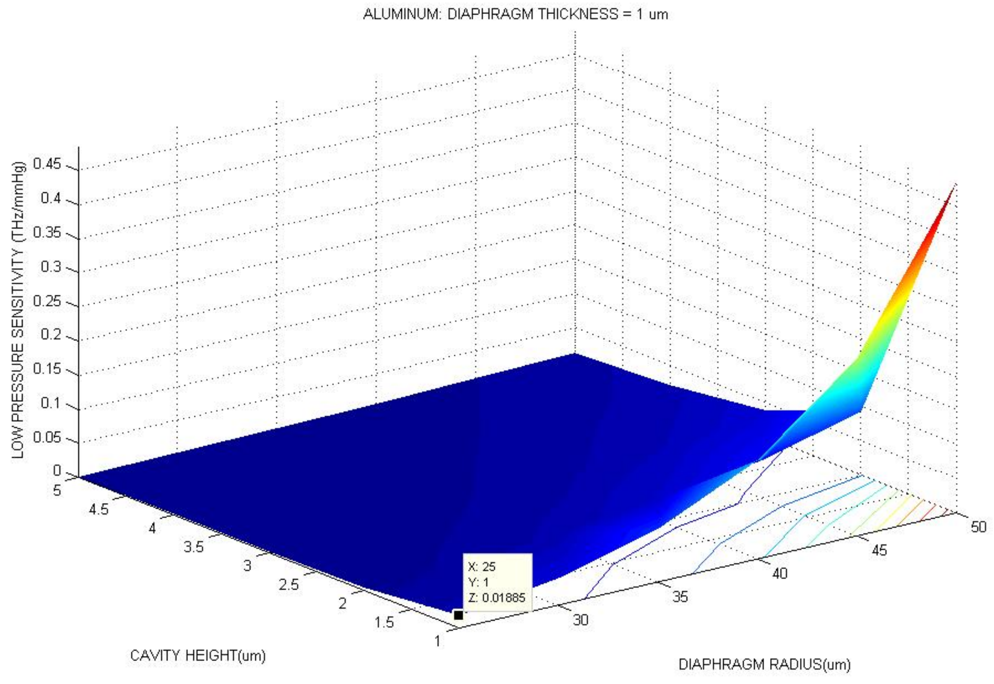

Figure A. 3 Low Pressure sensitivity of an Aluminum diaphragm of thickness 1μm.

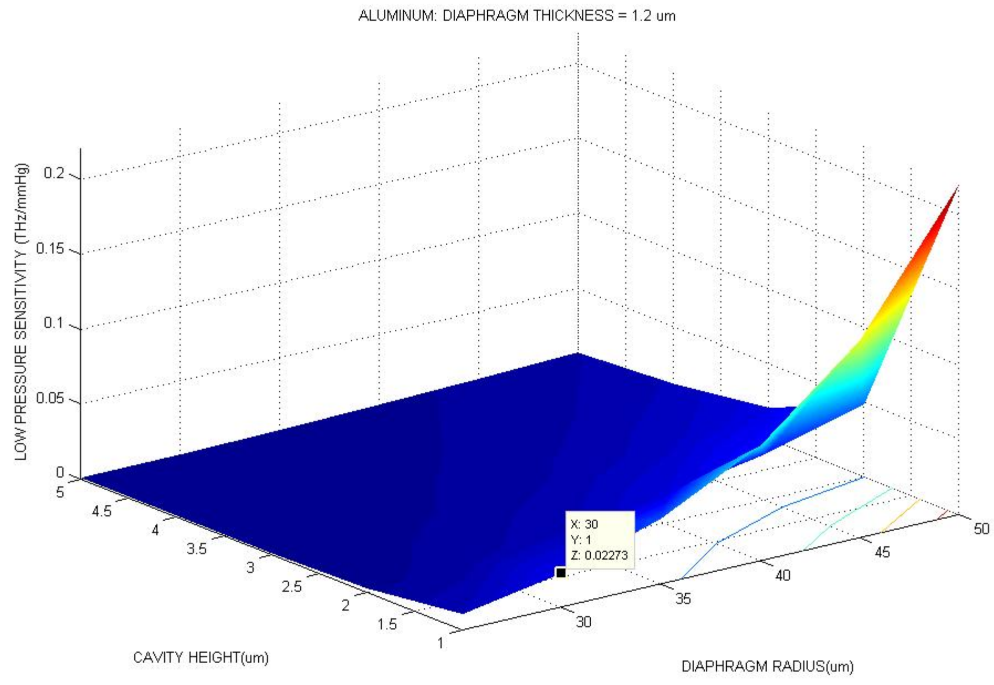

Figure A. 4 Low Pressure sensitivity of an Aluminum diaphragm of thickness 1.2μm.

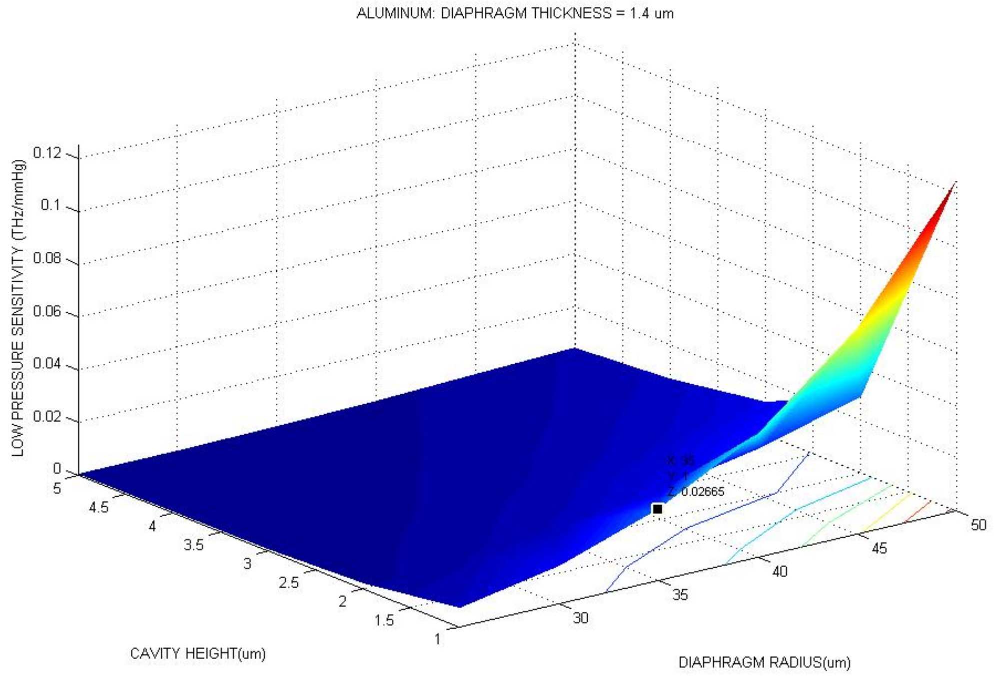

Figure A. 5 Low Pressure sensitivity of an Aluminum diaphragm of thickness 1.4μm.

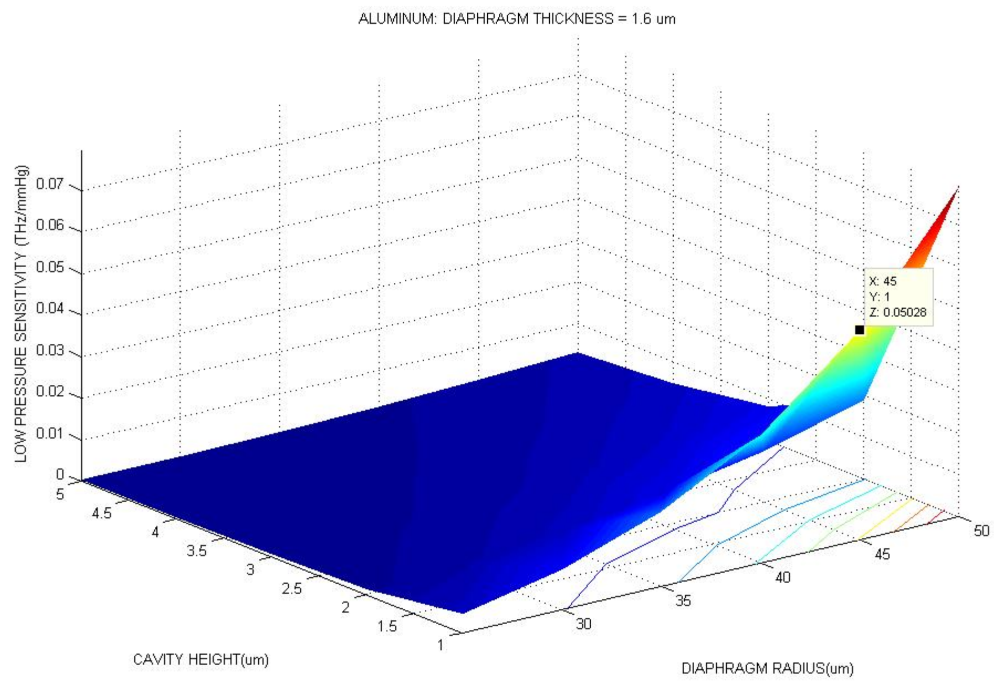

Figure A. 6 Low Pressure sensitivity of an Aluminum diaphragm of thickness 1.6μm.

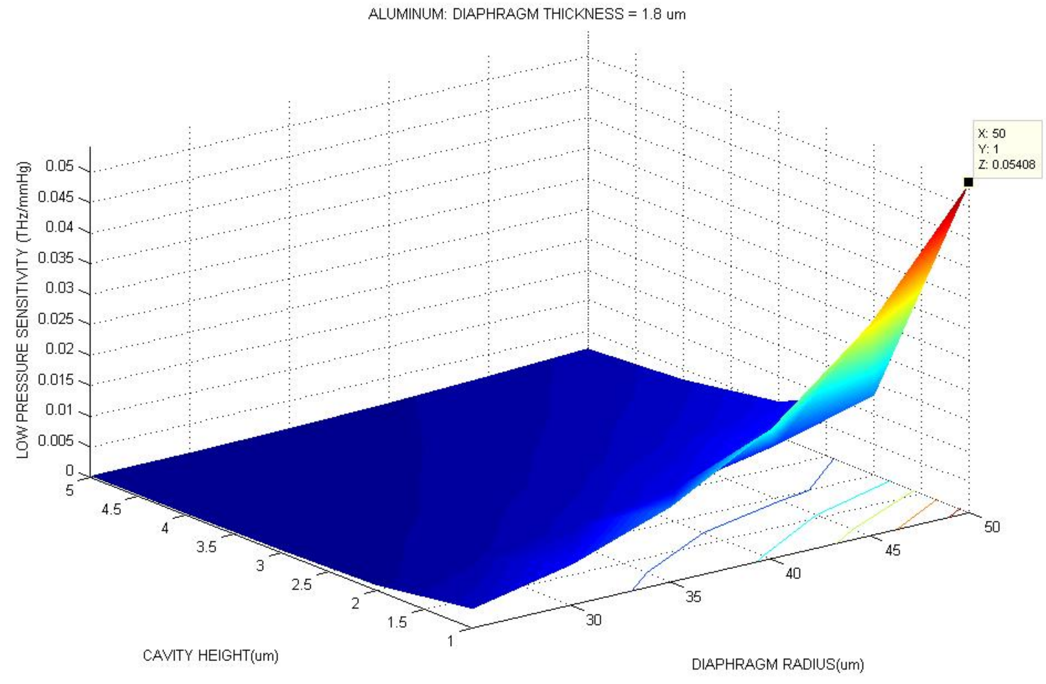

Figure A. 7 Low Pressure sensitivity of an Aluminum diaphragm of thickness 1.8μm.

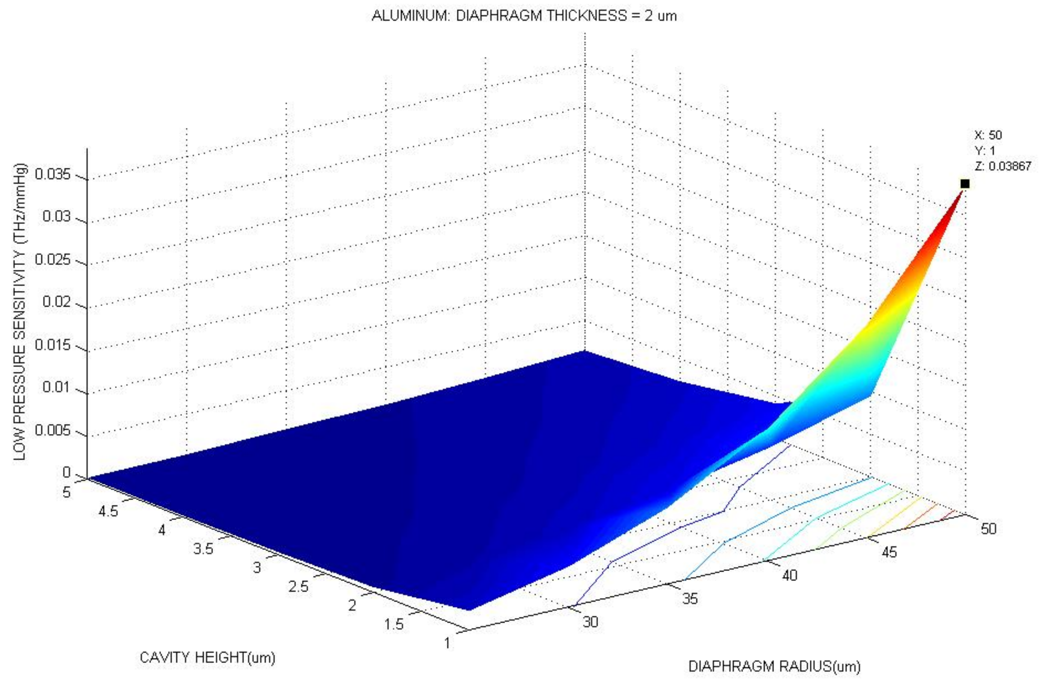

Figure A. 8 Low Pressure sensitivity of an Aluminum diaphragm of thickness 2μm.

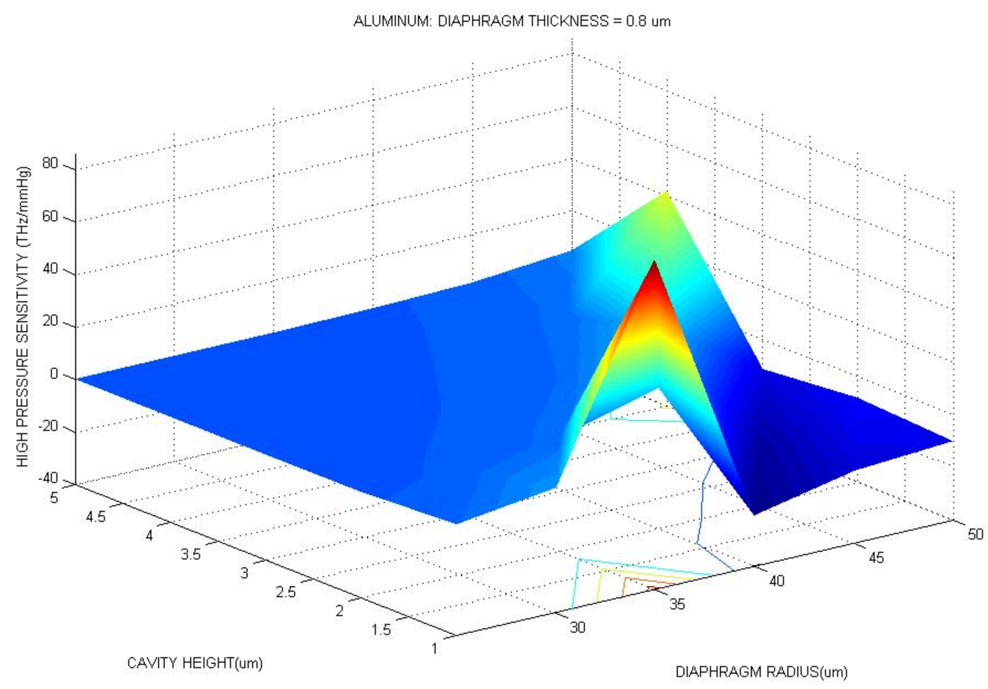

Figure A. 9 High Pressure sensitivity of an Aluminum diaphragm of thickness 0.8μm.

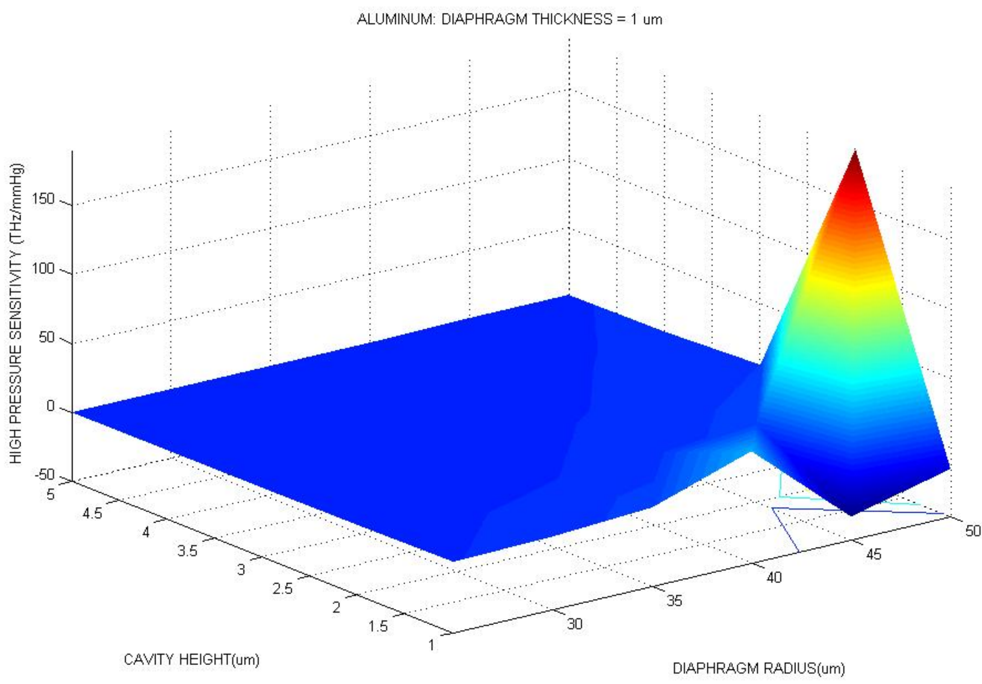

Figure A. 10 High Pressure sensitivity of an Aluminum diaphragm of thickness 1μm.

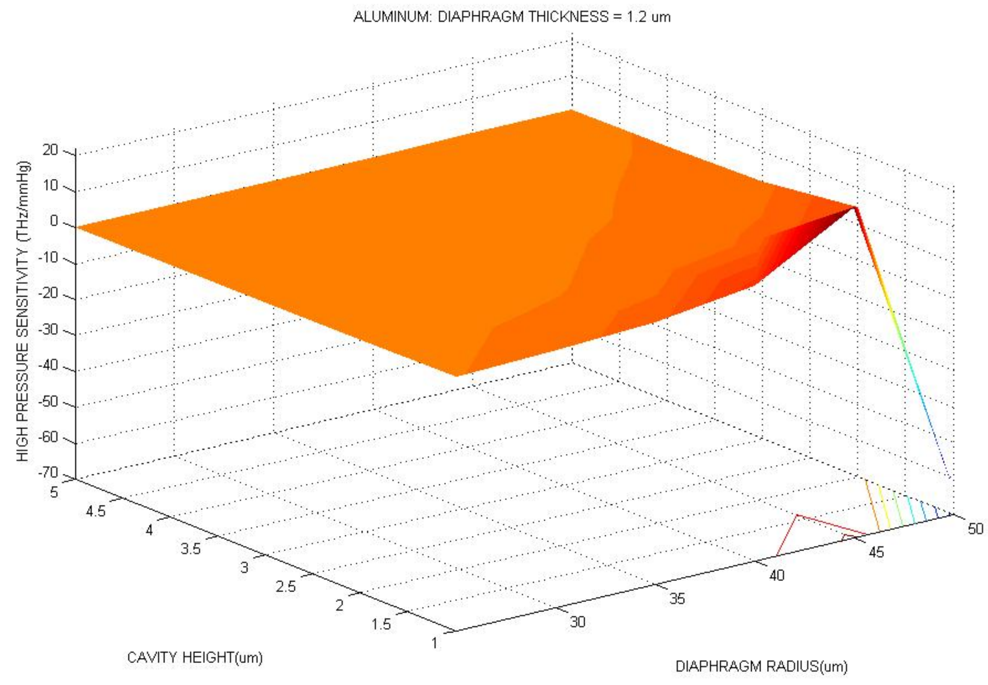

Figure A. 11 High Pressure sensitivity of an Aluminum diaphragm of thickness 1.2μm.

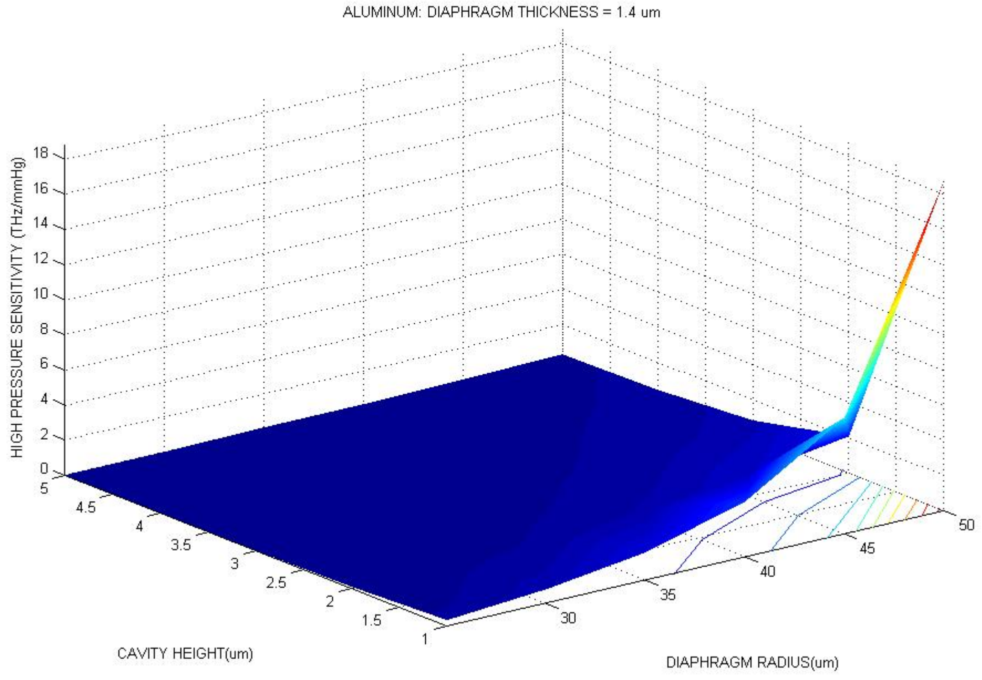

Figure A. 12 High Pressure sensitivity of an Aluminum diaphragm of thickness 1.4μm.

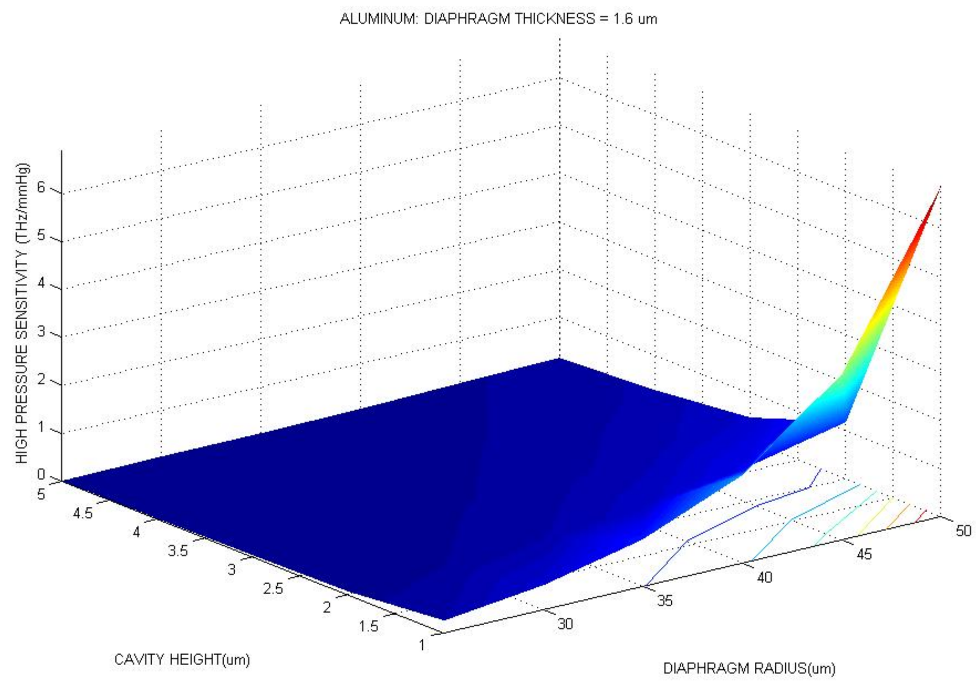

Figure A. 13 High Pressure sensitivity of an Aluminum diaphragm of thickness 1.6μm.

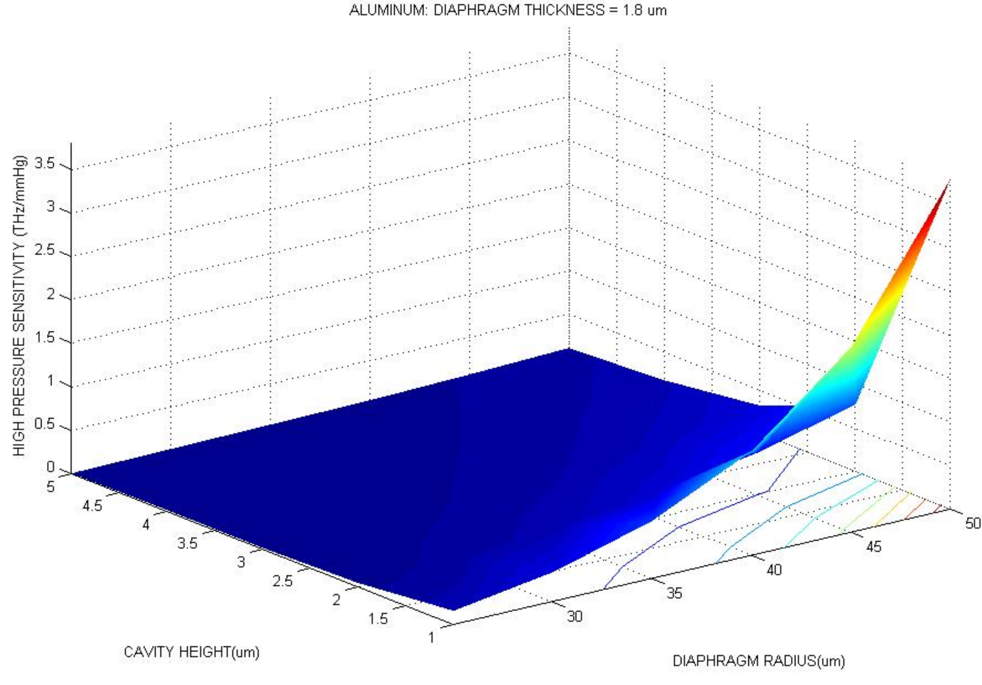

Figure A. 14 High Pressure sensitivity of an Aluminum diaphragm of thickness 1.8μm.

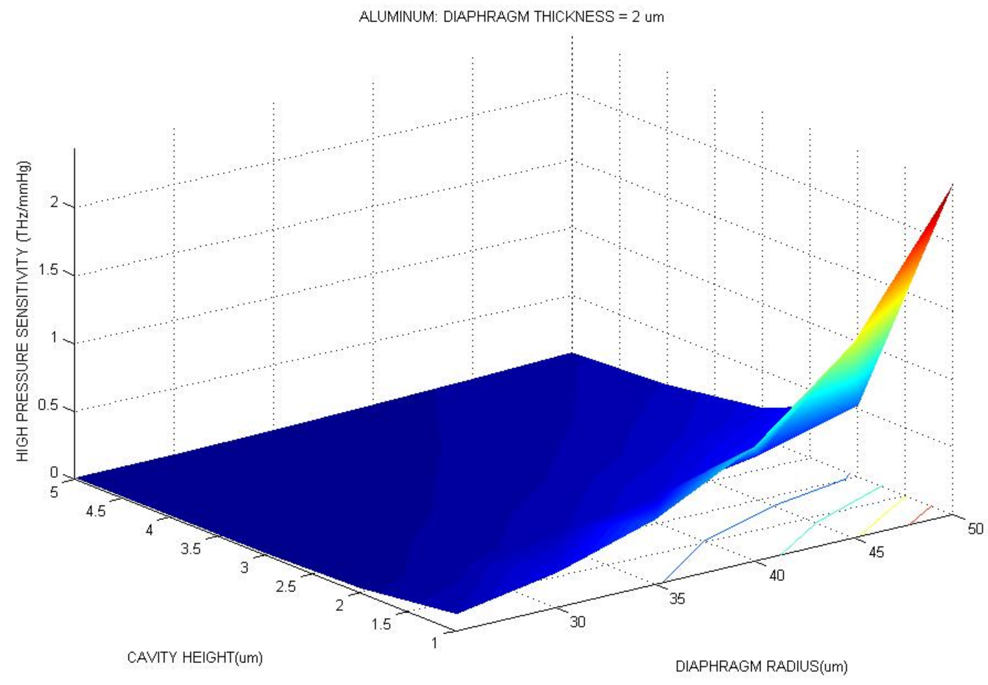

Figure A. 15 High Pressure sensitivity of an Aluminum diaphragm of thickness 2μm.

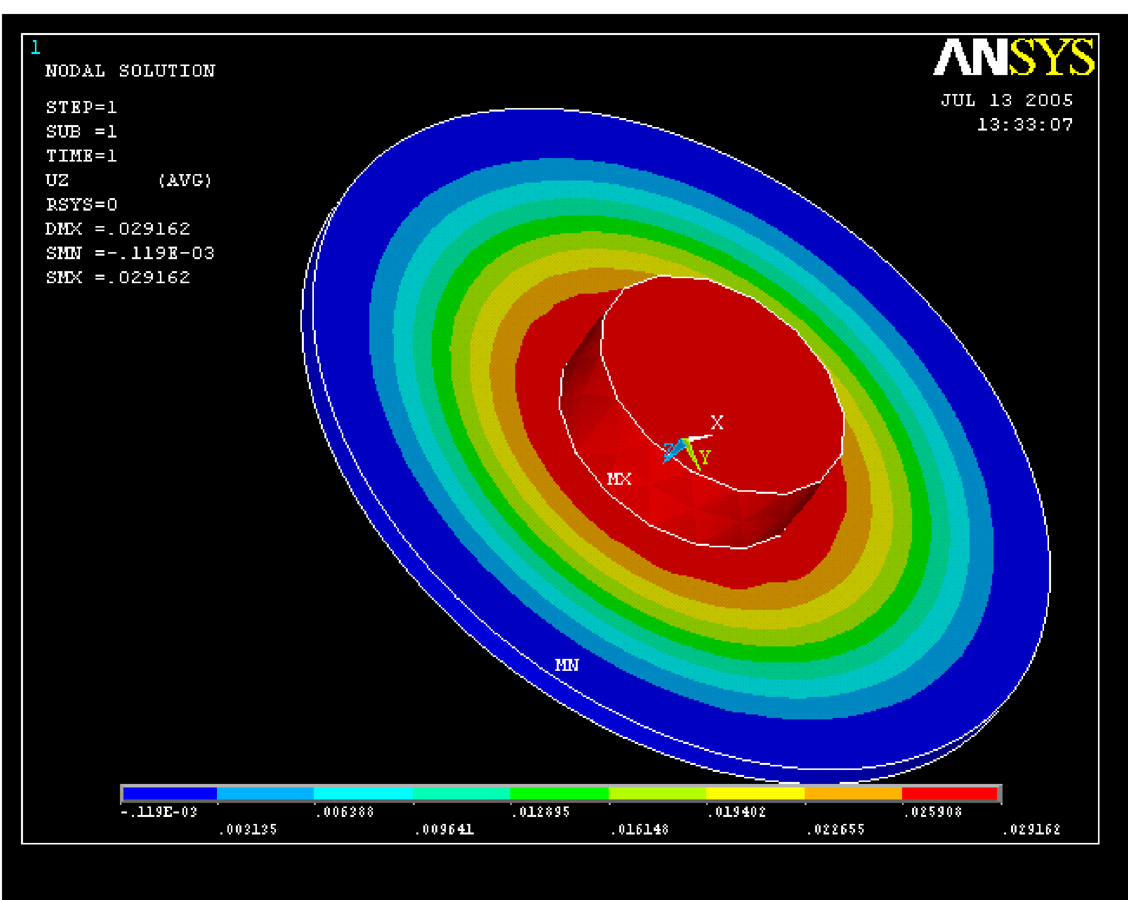

Figure A. 16 Bossed membrane structure on a hollow-cylinder support for a 1.8µm thickness, 50µm radius and 1µm height cavity.

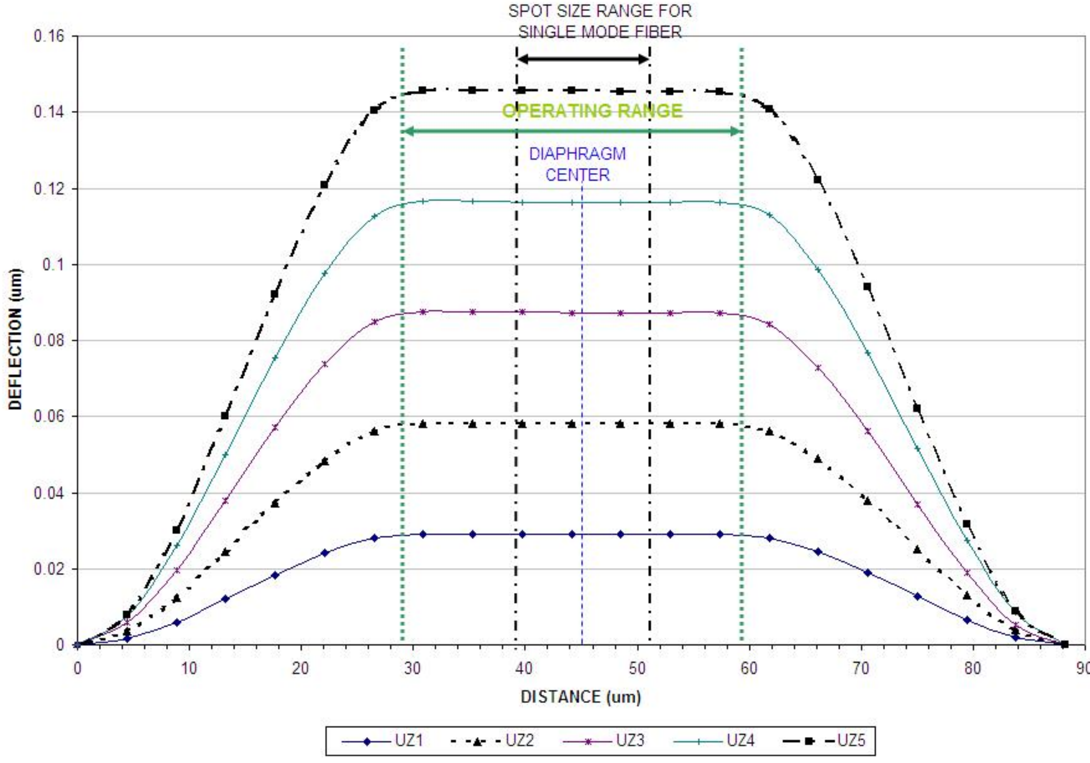

Figure A. 17 Bossed membrane on a hollow-cylinder support – deflection profile. UZ indicates different pressures applied, UZ1<UZ2 and so on.

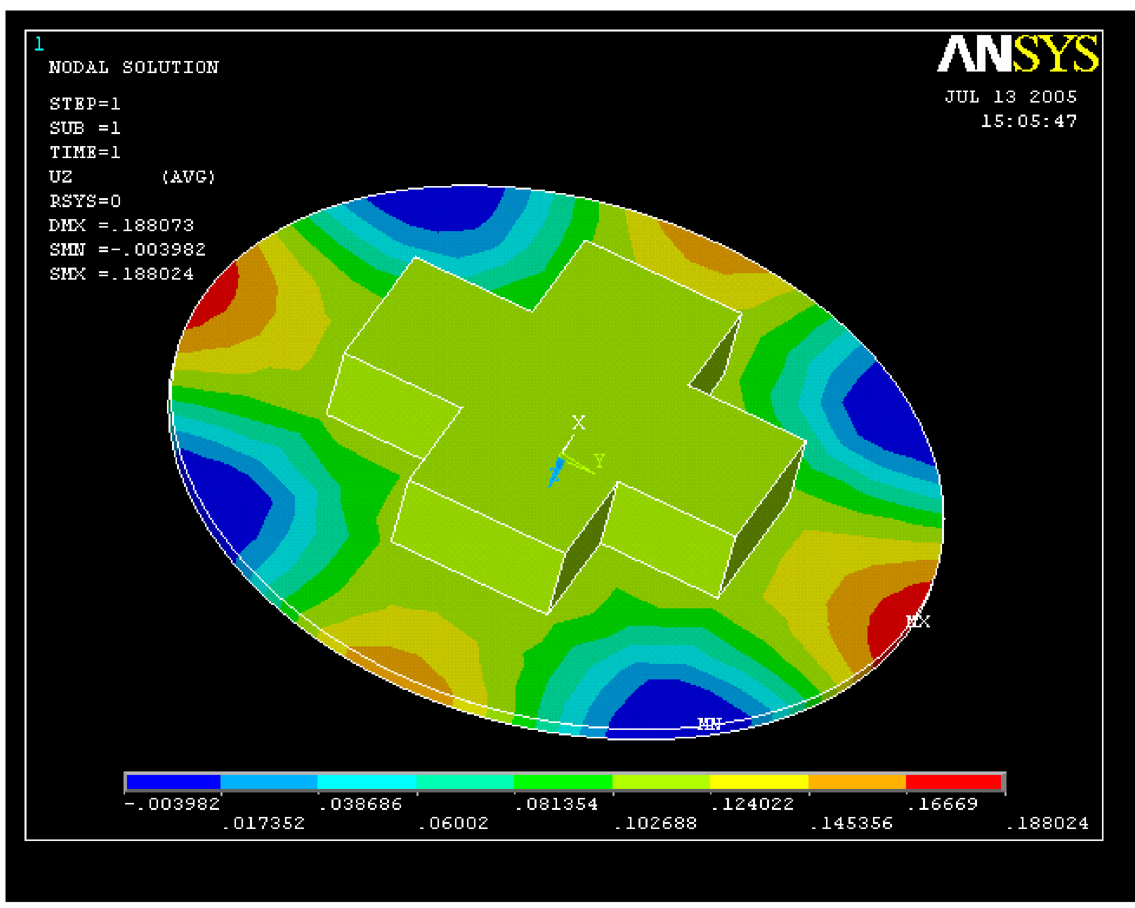

Figure A. 18 Bossed membrane on a four-pillar support structure for a 1.8µm thickness, 50µm radius and 1µm height cavity.

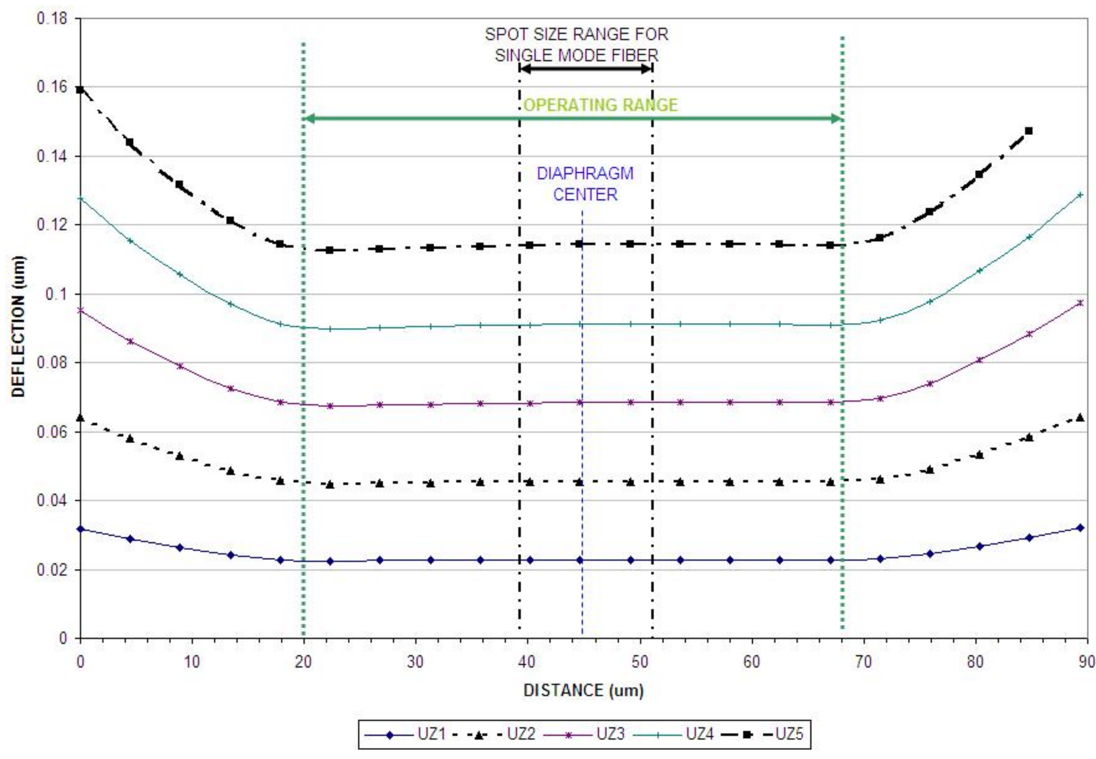

Figure A. 19 Deflection profile of a bossed membrane on a four-pillar support structure. UZ indicates different pressures applied, UZ1<UZ2 and so on.

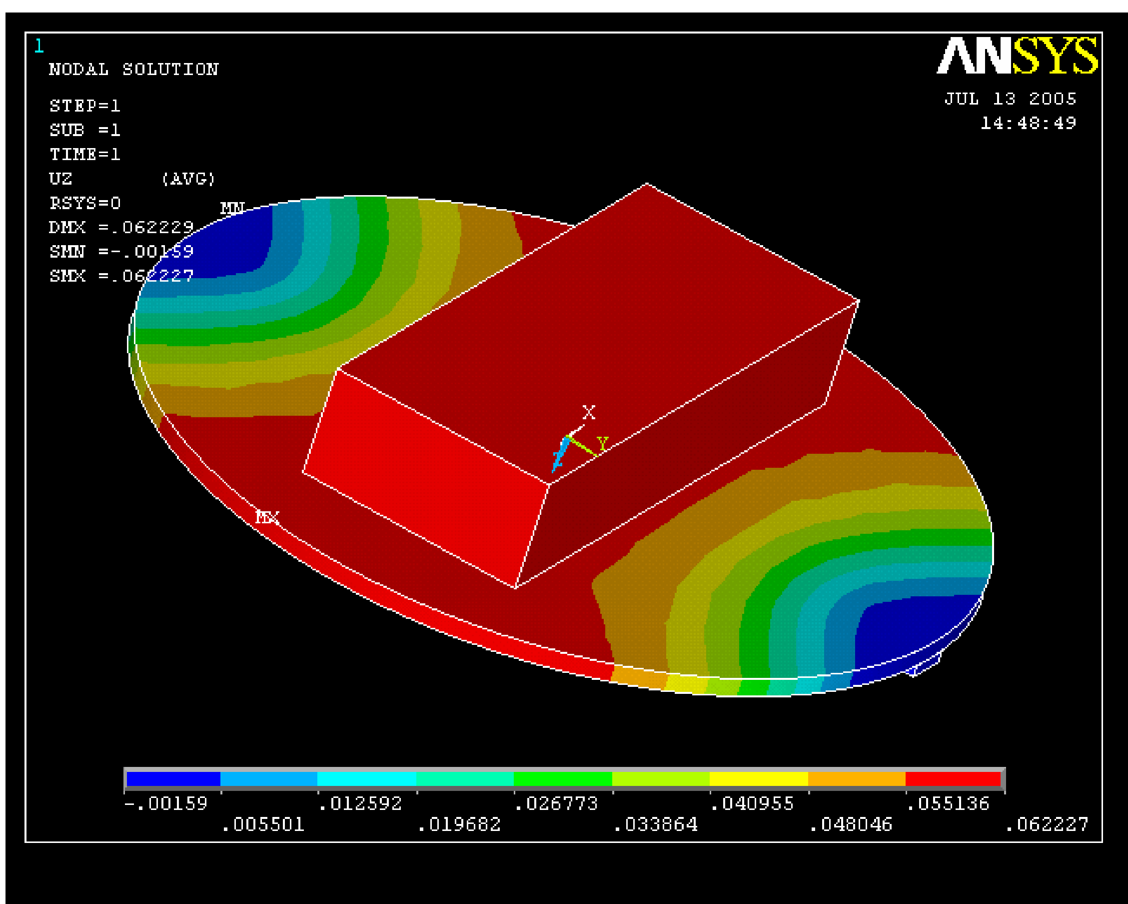

Figure A. 20 Two-pillar support structure with a bossed membrane. Dimensions of sensor – 35μm radius, 1.8μm thickness, 1μm cavity height, dimensions of the bossed structure – 50μm in length (along x direction) and 20μm in width (perpendicular to x direction) and 9.6μm in height.

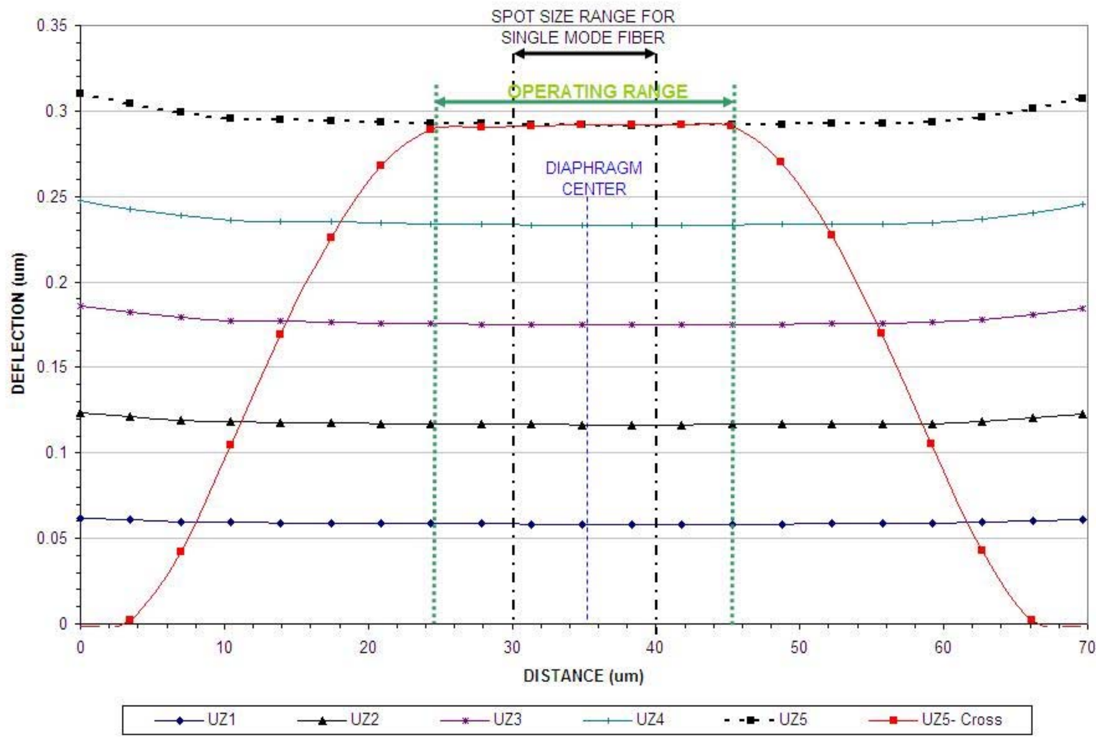

Figure A. 21 Deflection profile for a bossed membrane on a two-pillar support structure. UZ indicates different pressures applied, UZ1<UZ2 and so on. UZ5 – cross is deflection profile along the support structure.

Table A.2 Summary of the Sensor and Boss structure for a sensor made of Aluminum.

Type of Support	Best Dimensions	Deflection Profile of the diaphragm
Hollow-cylinder	Sensor: Diaphragm radius –50µm Diaphragm thickness – 1.8µm Cavity height – 1µm Emboss: Shape: Solid cylinder Radius – 15µm Thickness – 9.6µm	1. Remains flat but the operating range is less than the desired spot size 2. Magnitude of deflection is small 3. Sensitivity is low
Four-Pillar	Sensor: Diaphragm radius –50µm Diaphragm thickness – 1.8µm Cavity height – 1µm Emboss: Shape: two cuboids at right angles to each other Length – 50µm Width – 20µm Thickness – 9.6µm	1. Remains flat with operating range equal to the desired spot size 2. Magnitude of deflection is small 3. Sensitivity is low
Two-Pillar	Sensor: Diaphragm radius – 35µm Diaphragm thickness – 1.8µm Cavity height – 1µm Emboss: Shape: two cuboids at right angles to each other Length – 50µm Width – 20µm Thickness – 9.6µm	1. Remains flat but the operating range is less than the desired spot size 2. Magnitude of deflection is large 3. Sensitivity is high

APPENDIX B

DESIGNING THE PRESSURE SENSOR USING NICKEL AS A MATERIAL

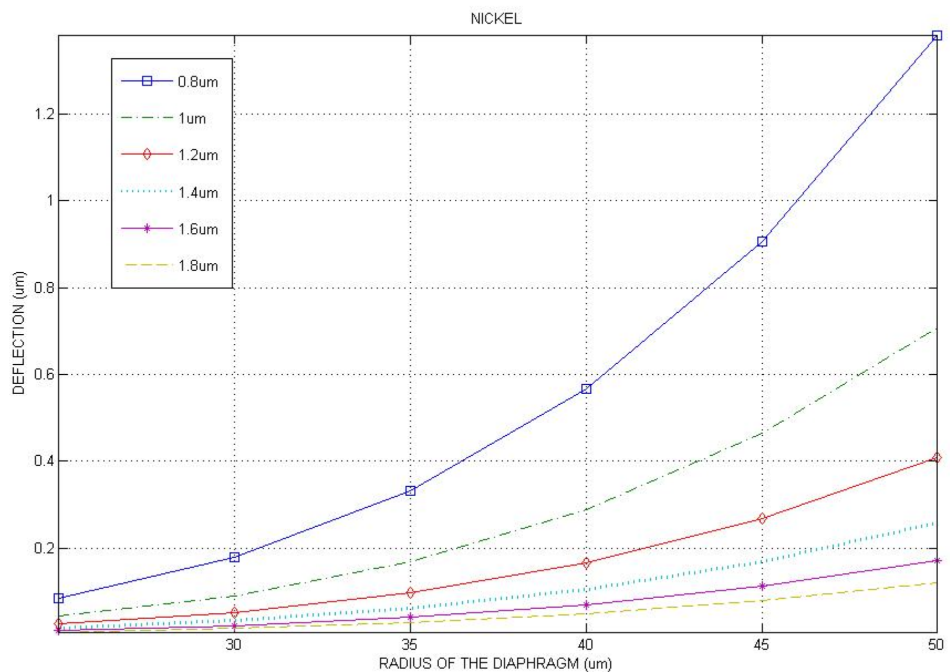

Figure B. 1 Deflection vs. diaphragm Radius for different thickness of a Nickel diaphragm.

Table B.1 One-fifth rule applied to Nickel diaphragms.

Thickness	Maximum deflection	Radius satisfying one-fifth rule
0.8μm	0.16μm	25μm
1μm	0.2μm	35μm
1.2μm	0.24μm	40μm
1.4μm	0.28μm	50μm
1.6μm	0.32μm	50μm

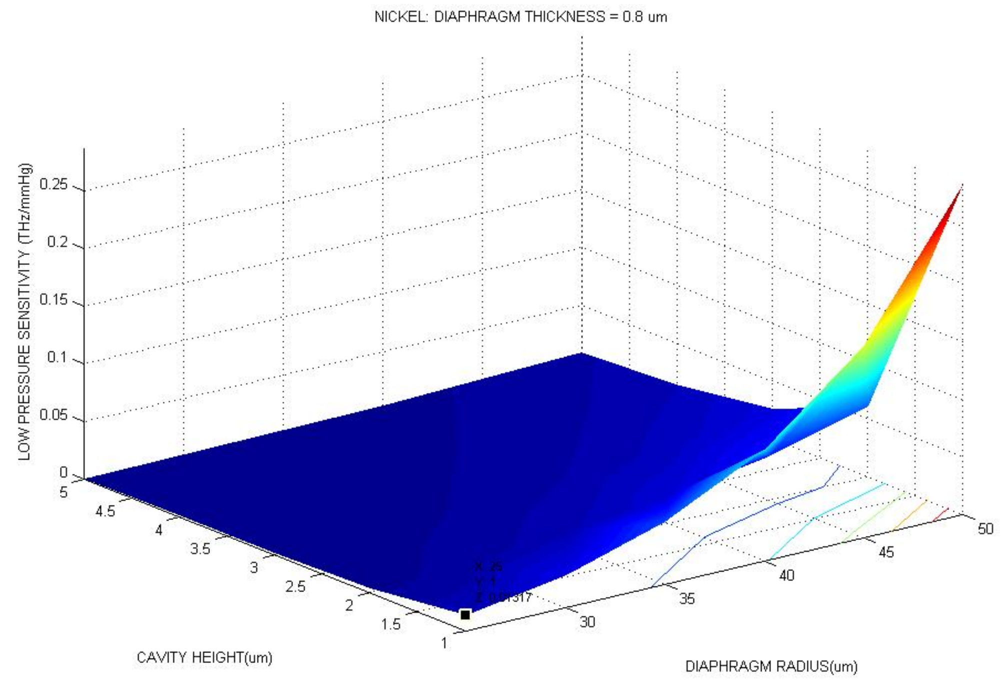

Figure B. 2 Low Pressure sensitivity of a Nickel diaphragm of thickness 0.8μm.

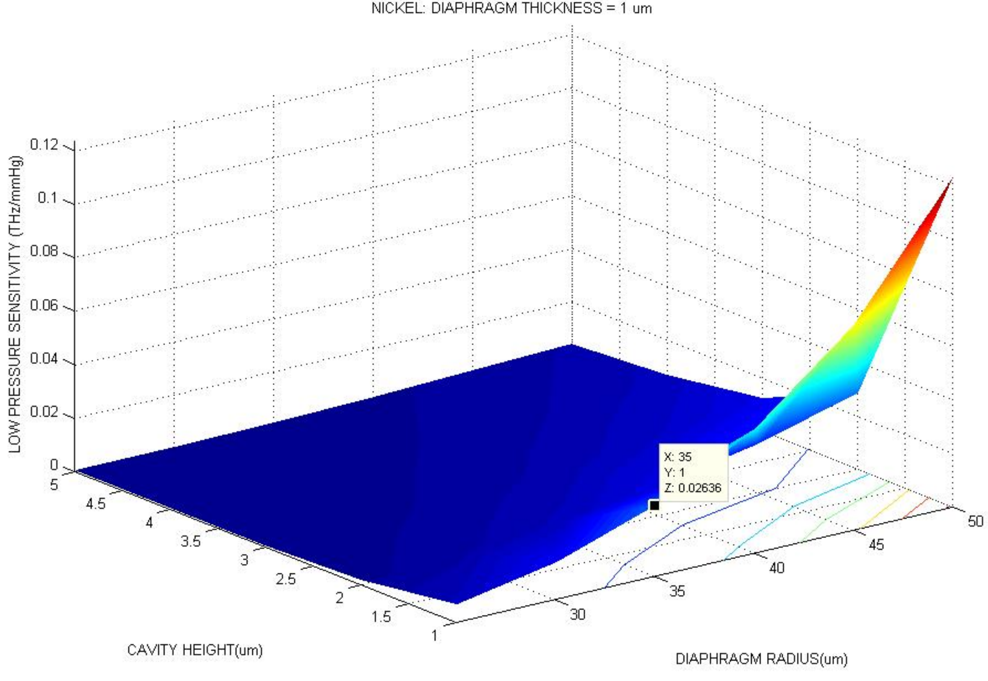

Figure B. 3 Low Pressure sensitivity of a Nickel diaphragm of thickness 1μm.

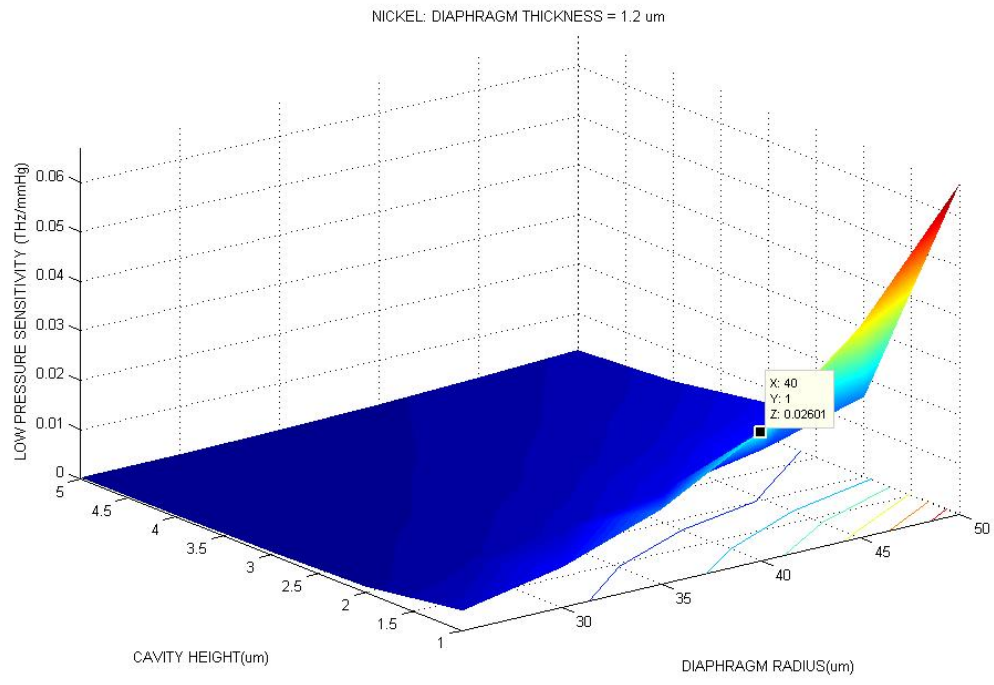

Figure B. 4 Low Pressure sensitivity of a Nickel diaphragm of thickness 1.2μm.

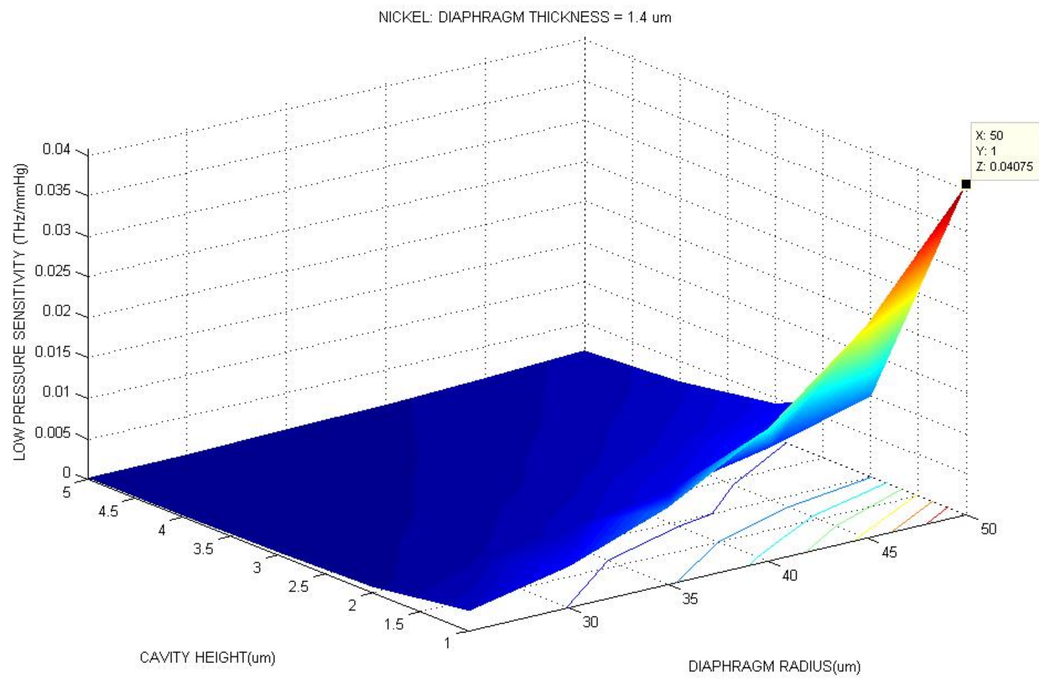

Figure B. 5 Low Pressure sensitivity of a Nickel diaphragm of thickness 1.4μm.

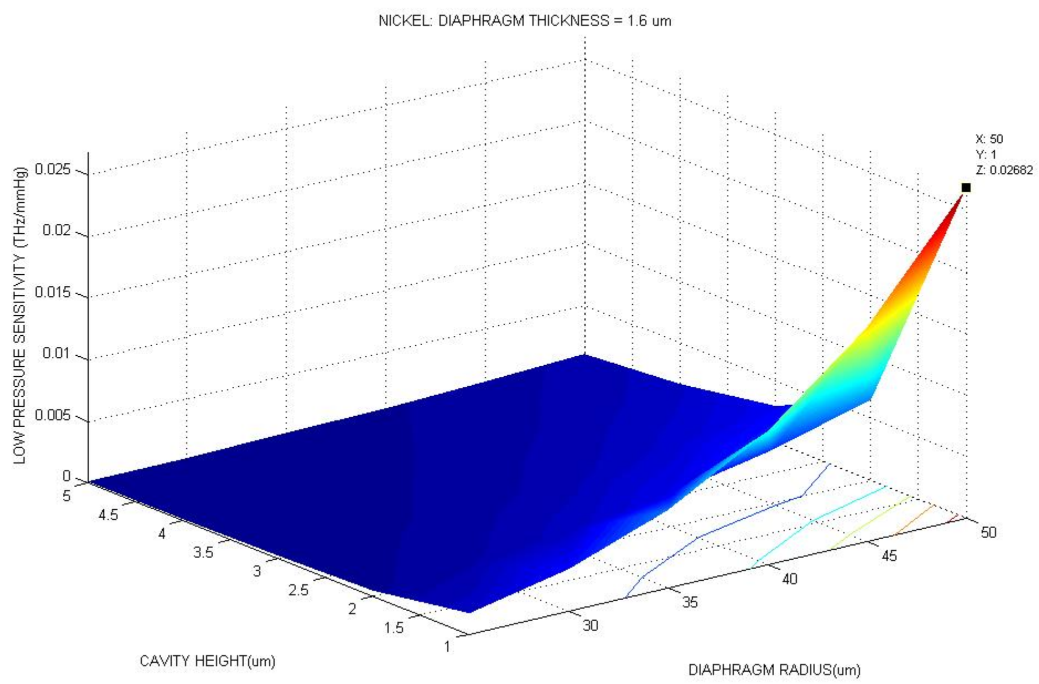

Figure B. 6 Low Pressure sensitivity of a Nickel diaphragm of thickness 1.6μm.

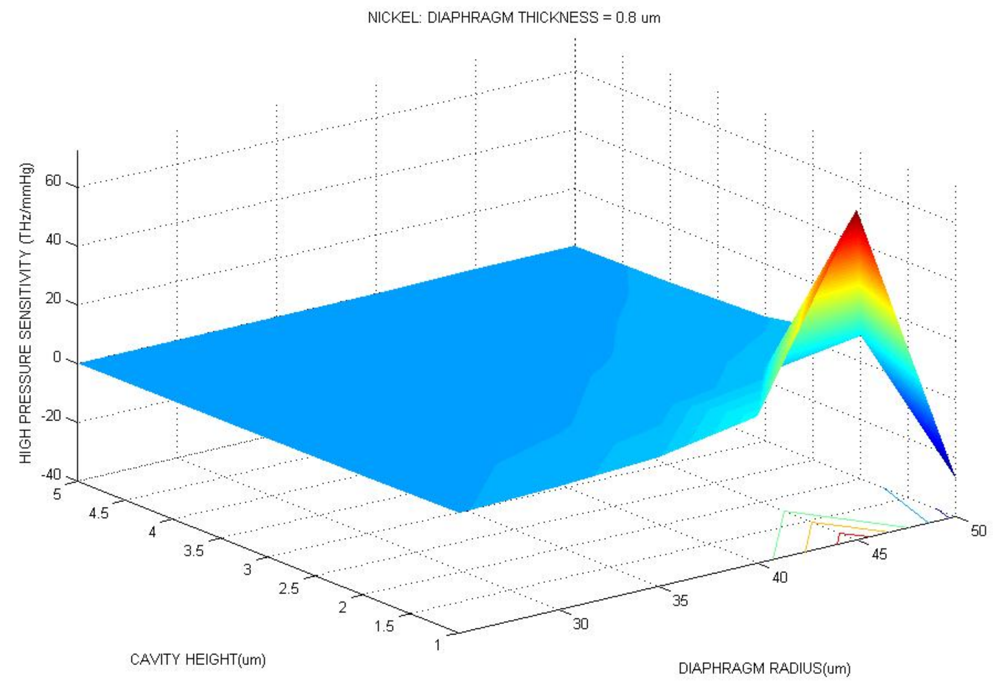

Figure B. 7 High Pressure sensitivity of a Nickel diaphragm of thickness 0.8µm.

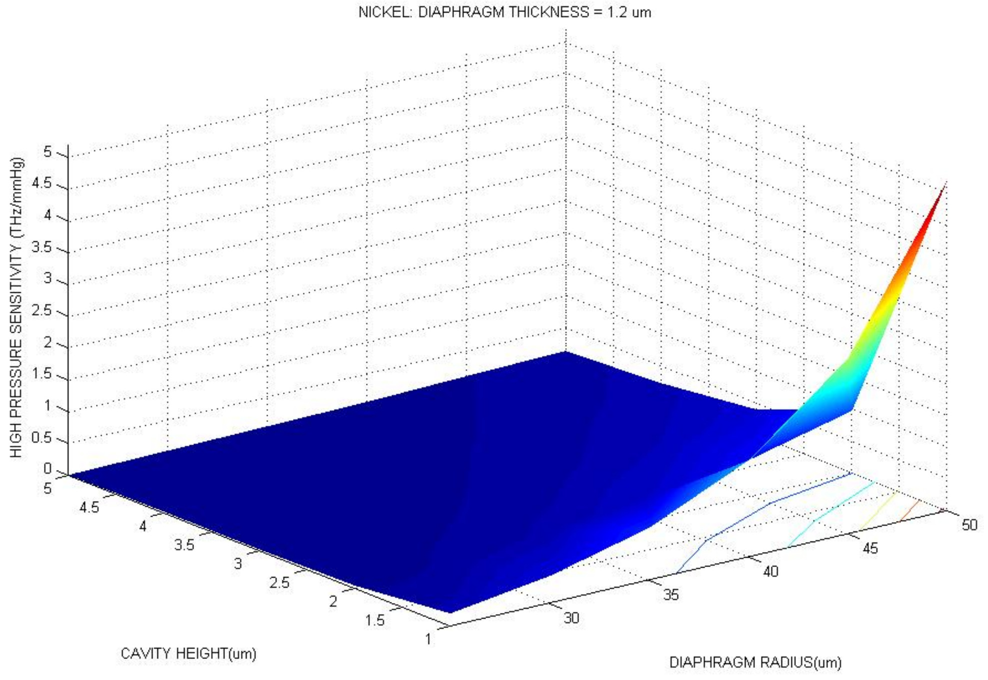

Figure B. 8 High Pressure sensitivity of a Nickel diaphragm of thickness 1µm.

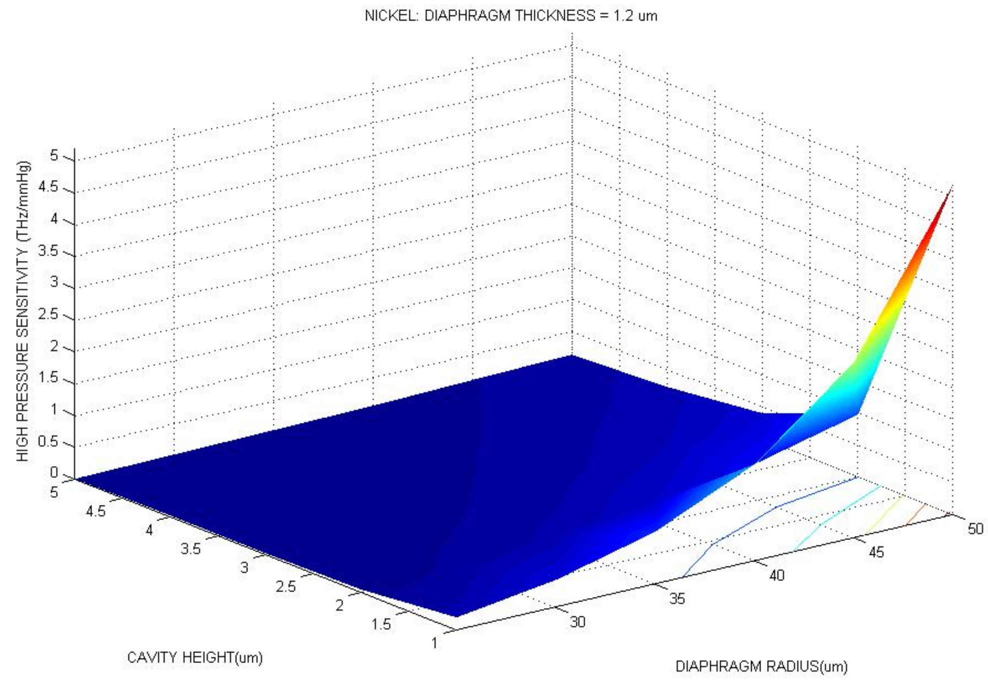

Figure B. 9 High Pressure sensitivity of a Nickel diaphragm of thickness 1.2µm.

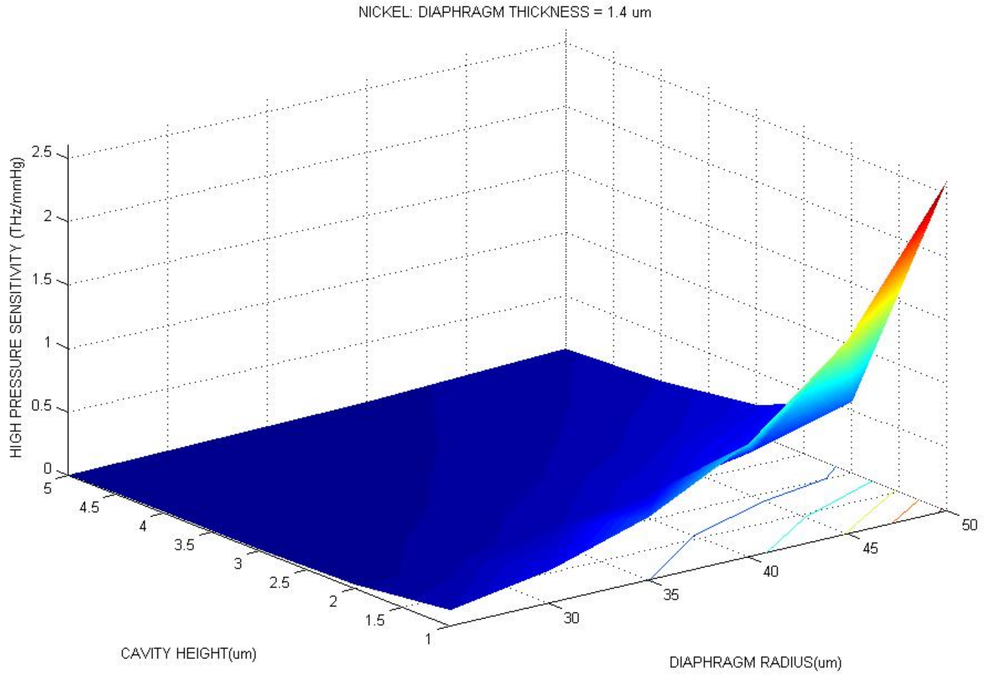

Figure B. 10 High Pressure sensitivity of a Nickel diaphragm of thickness of 1.4µm.

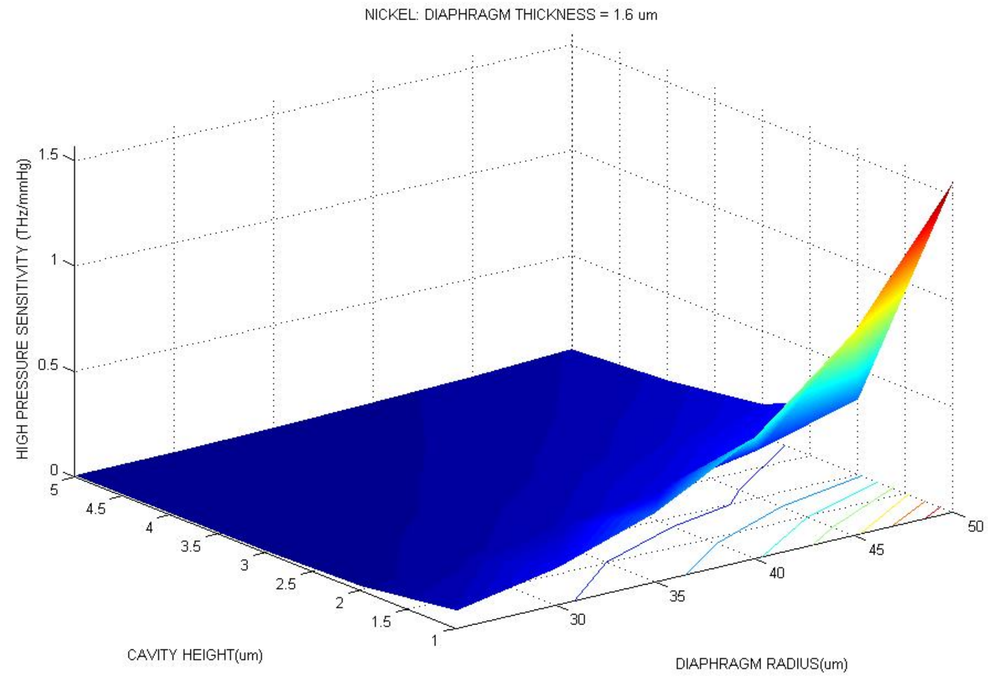

Figure B. 11 High Pressure sensitivity of a Nickel diaphragm of thickness of 1.6μm.

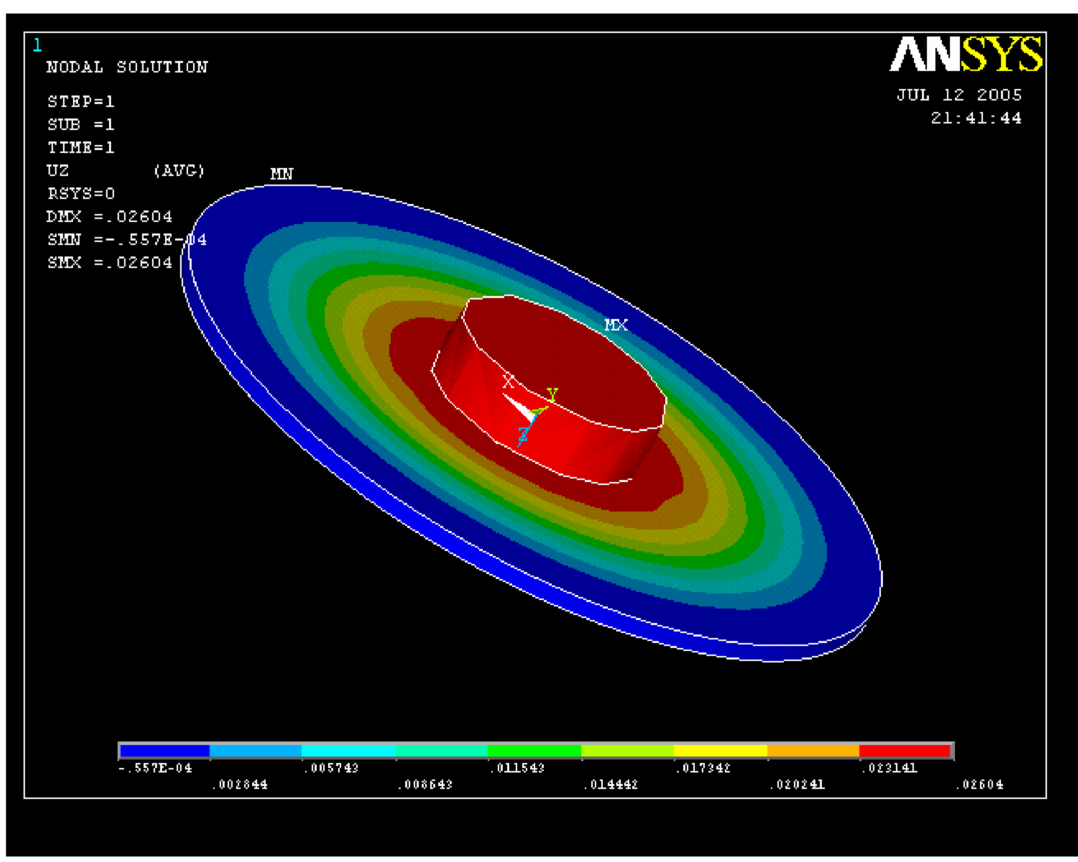

Figure B. 12 Bossed membrane structure on a hollow-cylinder support for a 1.4µm thickness, 50µm radius and 1µm height cavity.

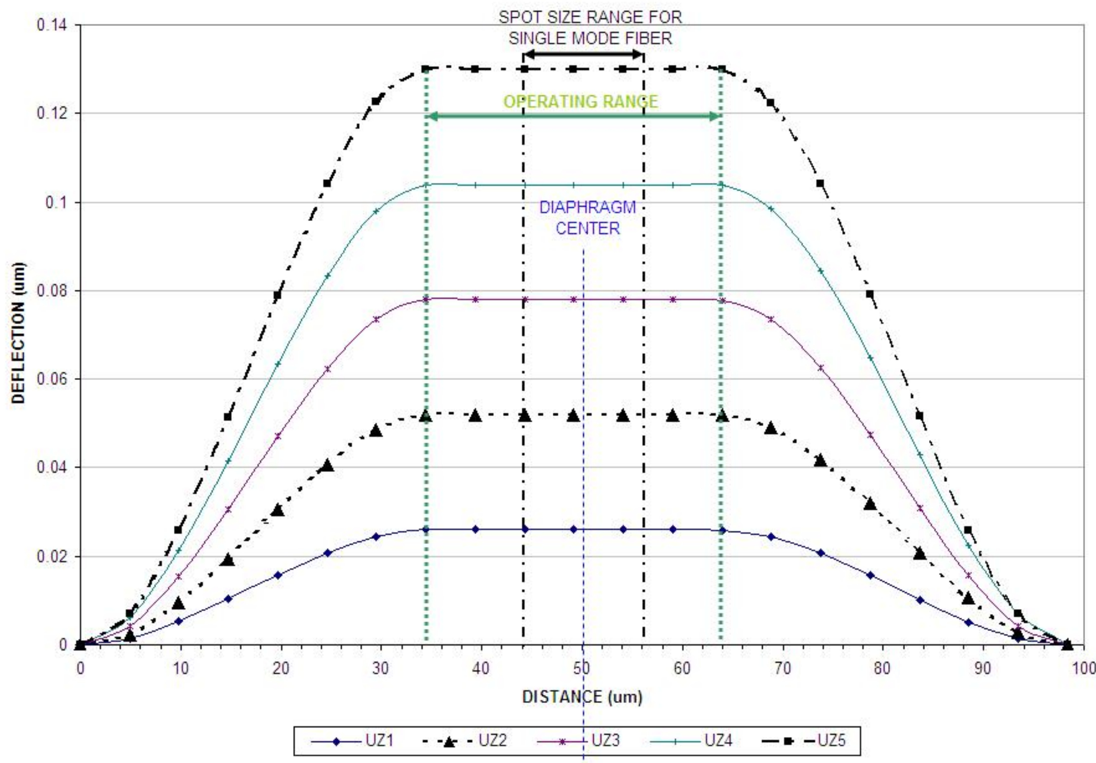

Figure B. 13 Bossed membrane on a hollow-cylinder support – deflection profile. UZ indicates different pressures applied, UZ1<UZ2 and so on.

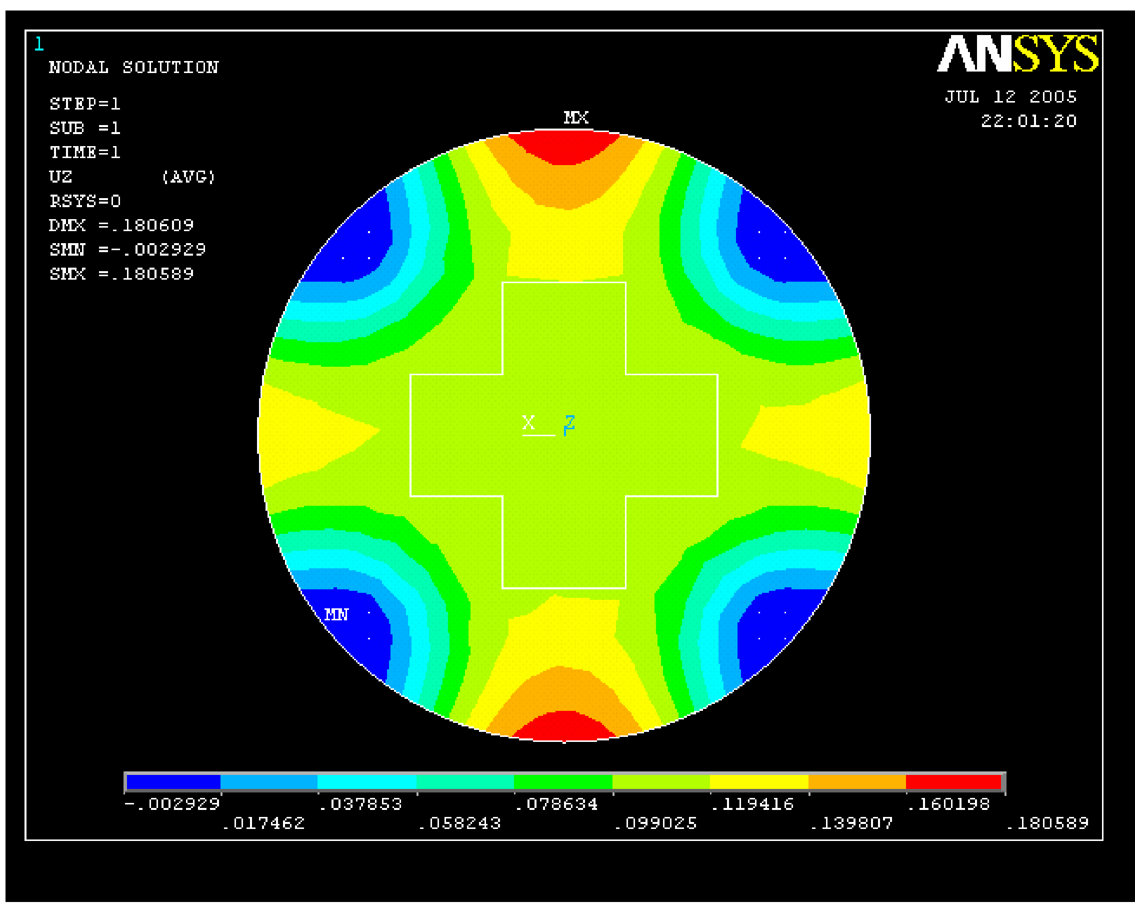

Figure B. 14 Bossed membrane on a four-pillar support structure for a 1.4µm thickness, 50µm radius and 1µm height cavity.

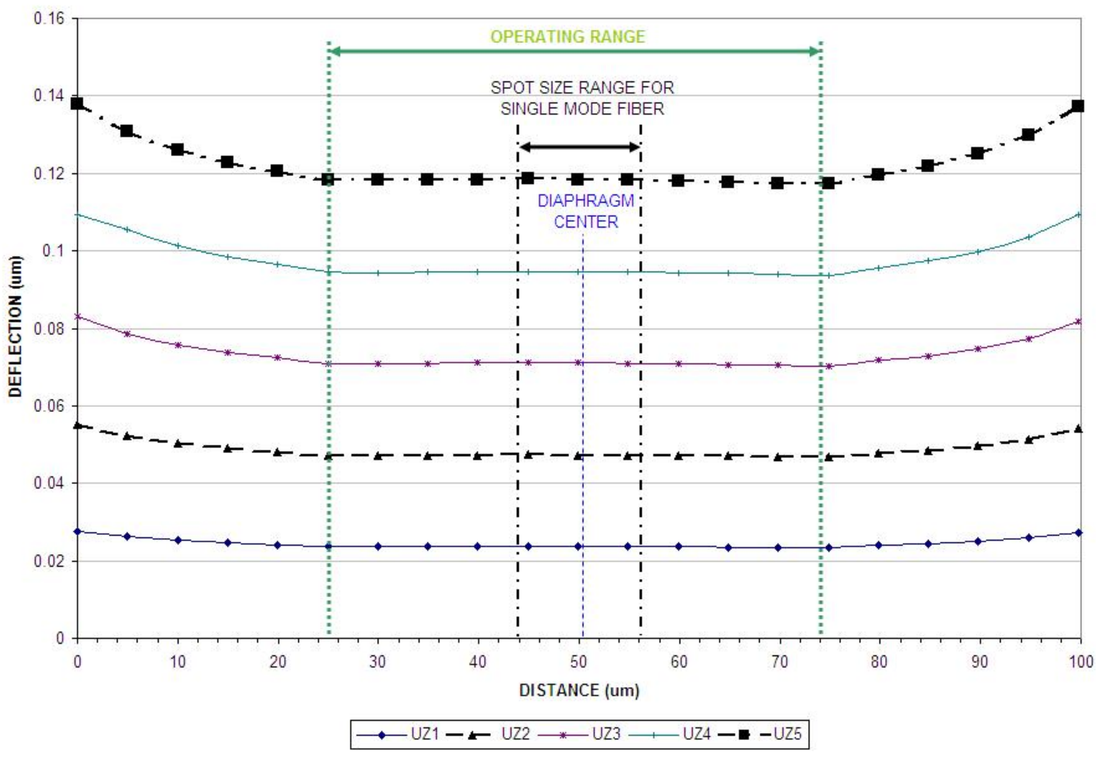

Figure B. 15 Deflection profile of a bossed membrane on a four-pillar support structure, UZ indicates different pressures applied, UZ1<UZ2 and so on.

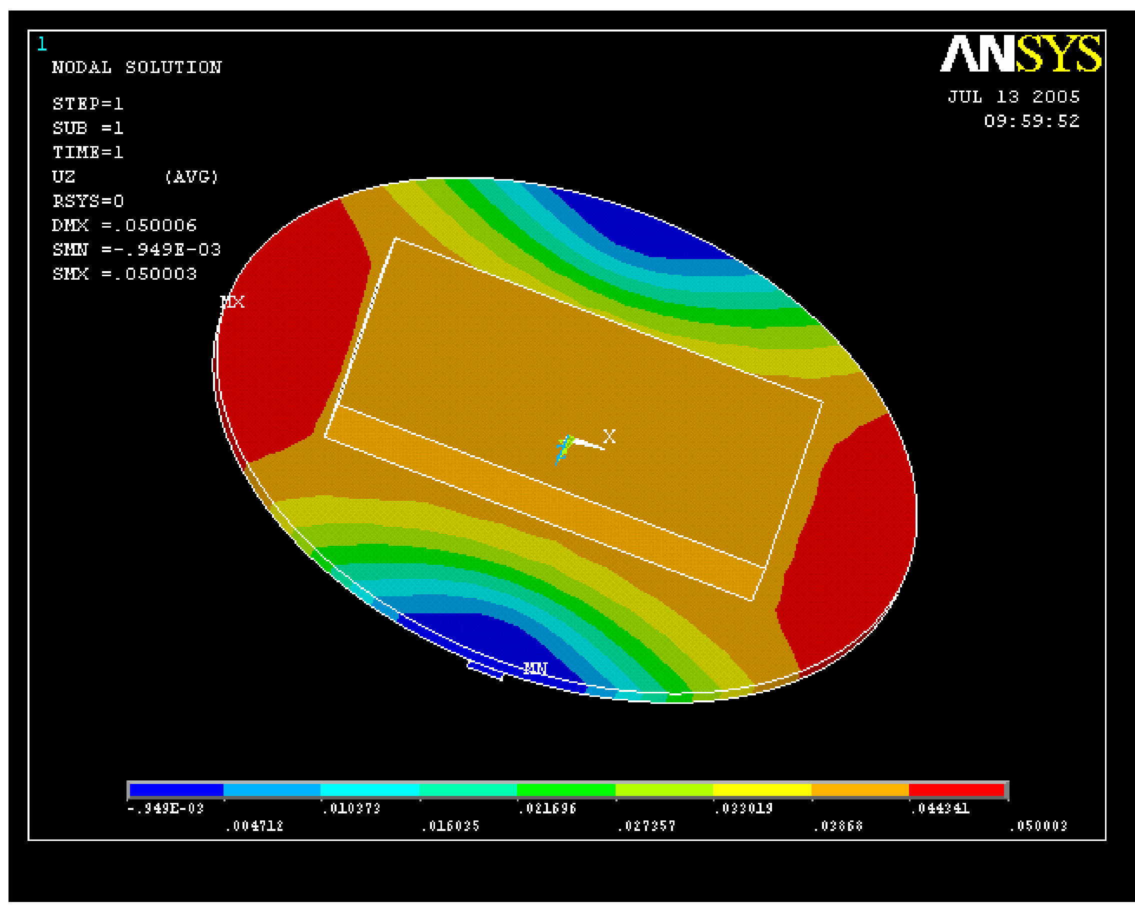

Figure B. 16 Two-pillar support structure with a bossed membrane. Dimensions of sensor – 40µm radius, 1.4µm thickness, 1µm cavity height, dimensions of the bossed structure – 50µm in length (along x direction) and 30µm in width (perpendicular to x direction) and 5µm in height.

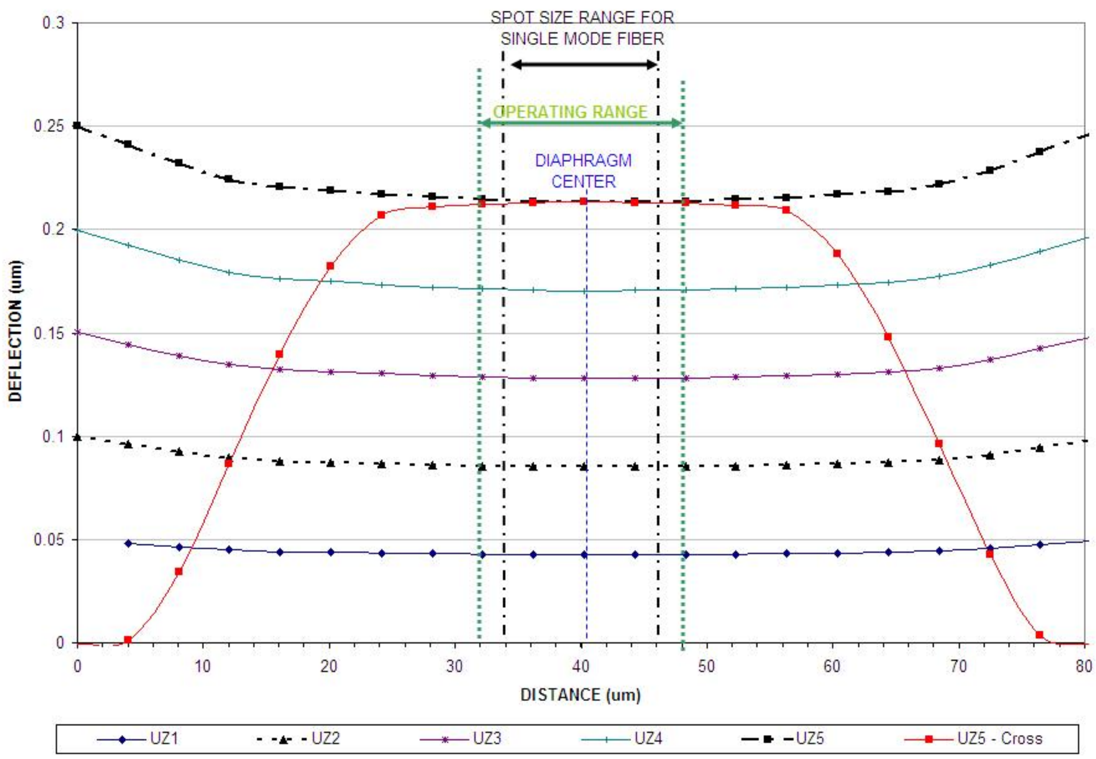

Figure B. 17 Deflection profile for a bossed membrane on a two-pillar support structure, UZ indicates different pressures applied, UZ1<UZ2 and so on. UZ5 –cross is deflection profile along the support structure.

Table B.2 Summary of the Sensor and Boss structure for a sensor made of Nickel.

Type of Support	Best Dimensions	Deflection Profile of the diaphragm
Hollow-cylinder	Sensor: Diaphragm radius – 50µm Diaphragm thickness – 1.4µm Cavity height – 1µm Emboss: Shape: Solid cylinder Radius – 15µm Thickness – 8.4µm	1. Remains flat but the operating range is less than the desired spot size 2. Magnitude of deflection is small 3. Sensitivity is low
Four-Pillar	Sensor: Diaphragm radius – 50µm Diaphragm thickness – 1.4µm Cavity height – 1µm Emboss: Shape: two cuboids at right angles to each other Length – 50µm Width – 20µm Thickness – 8.4µm	1. Remains flat with operating range equal to the desired spot size 2. Magnitude of deflection is small 3. Sensitivity is low
Two-Pillar	Sensor: Diaphragm radius – 40µm Diaphragm thickness – 1.4µm Cavity height – 1µm Emboss: Shape: one cuboid at the center of the diaphragm Length – 50µm Width – 30µm Thickness – 5µm	1. Remains flat but the operating range is less than the desired spot size 2. Magnitude of deflection is large 3. Sensitivity is high

APPENDIX C

DESIGNING THE PRESSURE SENSOR USING SILICON NITRIDE AS A MATERIAL

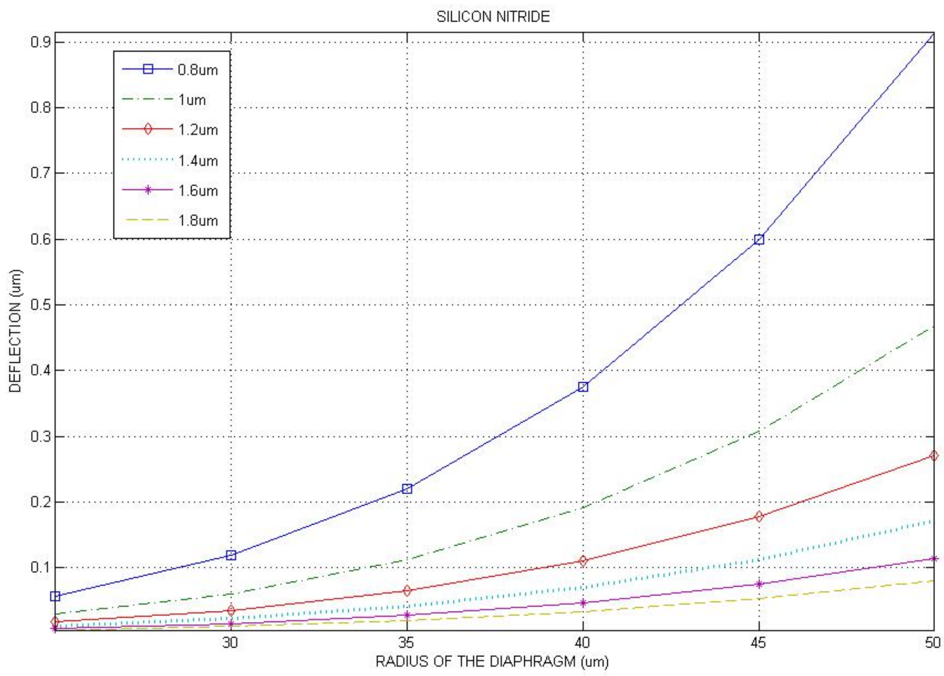

Figure C. 1 Deflection vs. diaphragm Radius for different thickness of a Silicon Nitride diaphragm.

Table C.1 One-fifth rule applied to Silicon Nitride diaphragms.

Thickness	Maximum deflection	Radius satisfying one-fifth rule
0.8μm	0.16μm	30μm
1μm	0.2μm	40μm
1.2μm	0.24μm	45μm
1.4μm	0.28μm	50μm

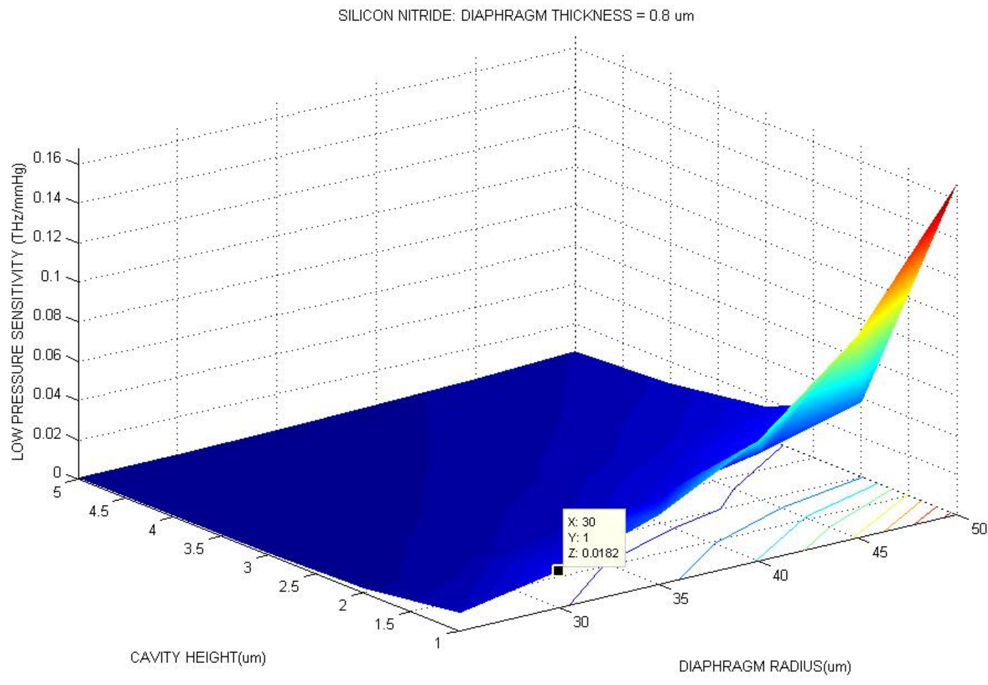

Figure C. 2 Low Pressure sensitivity of a Silicon Nitride diaphragm of thickness 0.8μm.

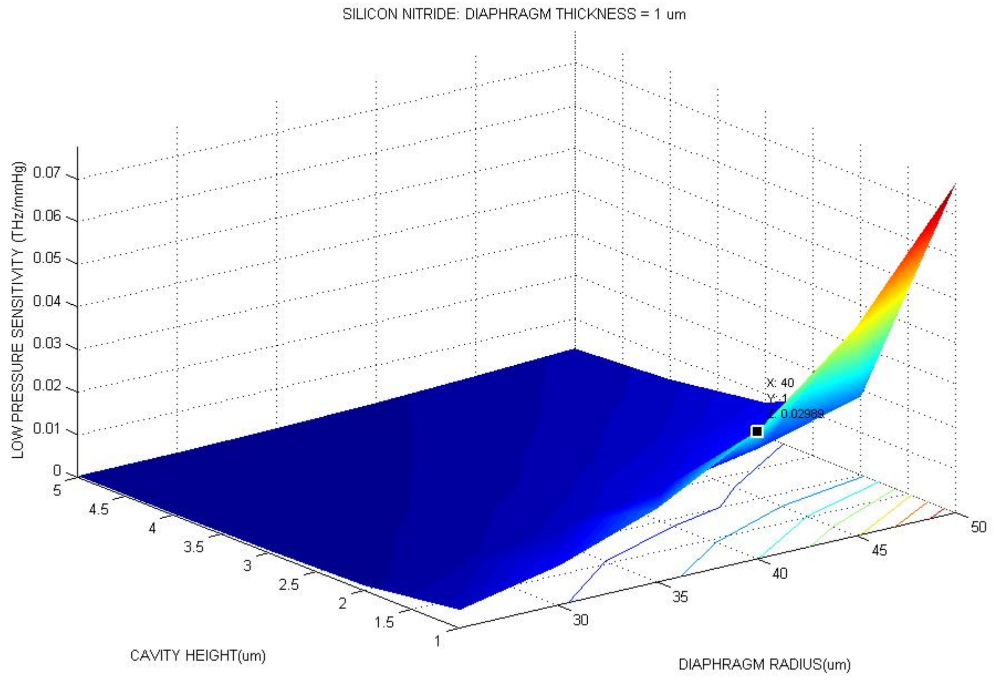

Figure C. 3 Low Pressure sensitivity of a Silicon Nitride diaphragm of thickness 1μm.

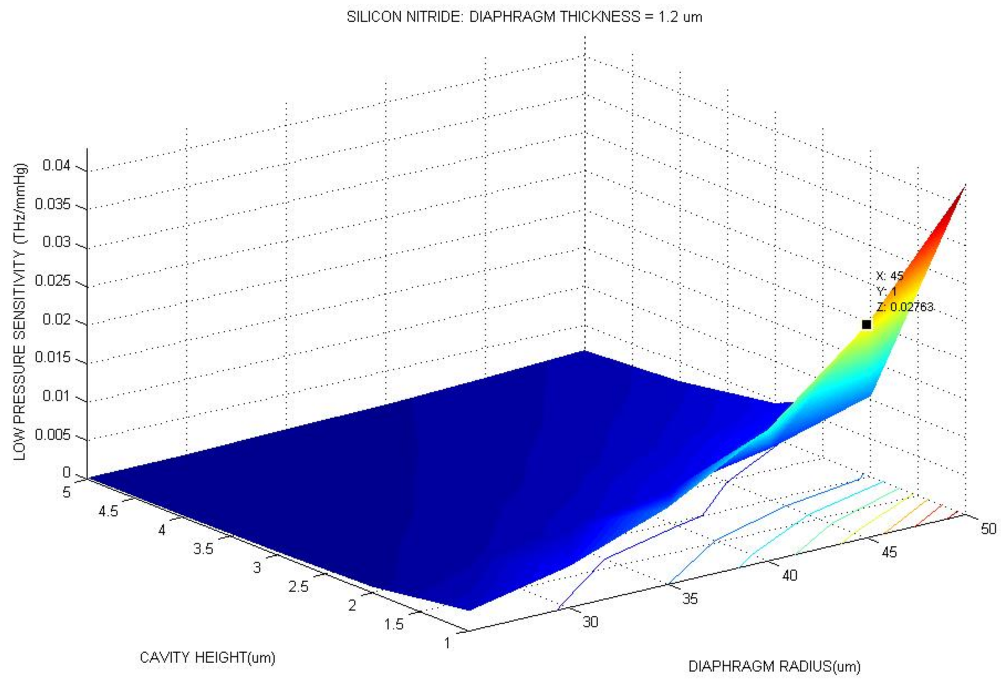

Figure C. 4 Low Pressure sensitivity of a Silicon Nitride diaphragm of thickness 1.2µm.

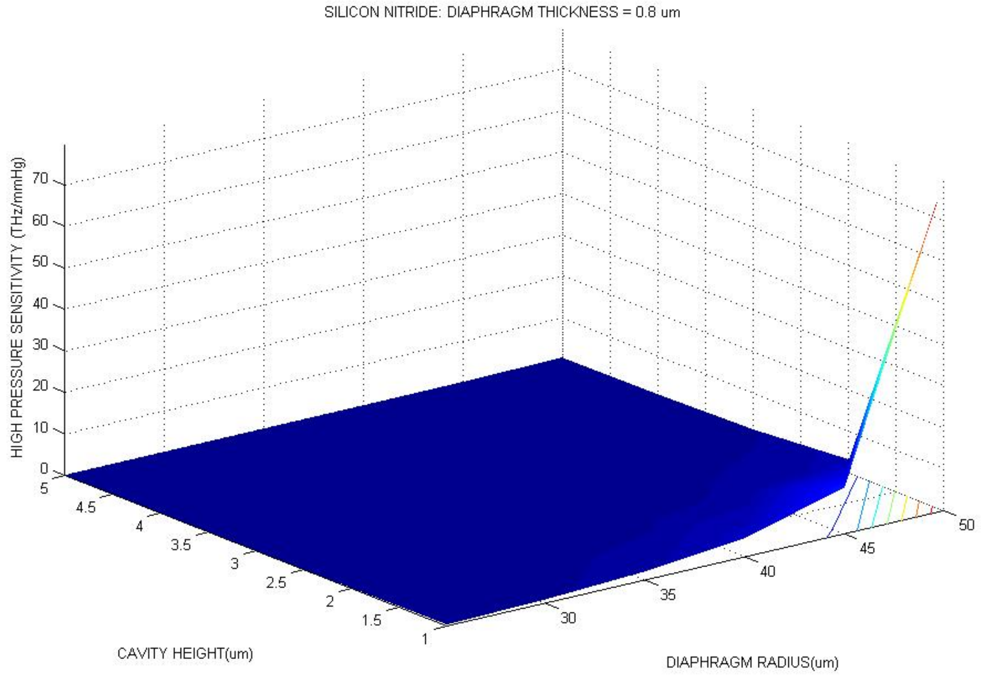

Figure C. 5 High Pressure sensitivity of a Silicon Nitride diaphragm of thickness 0.8µm.

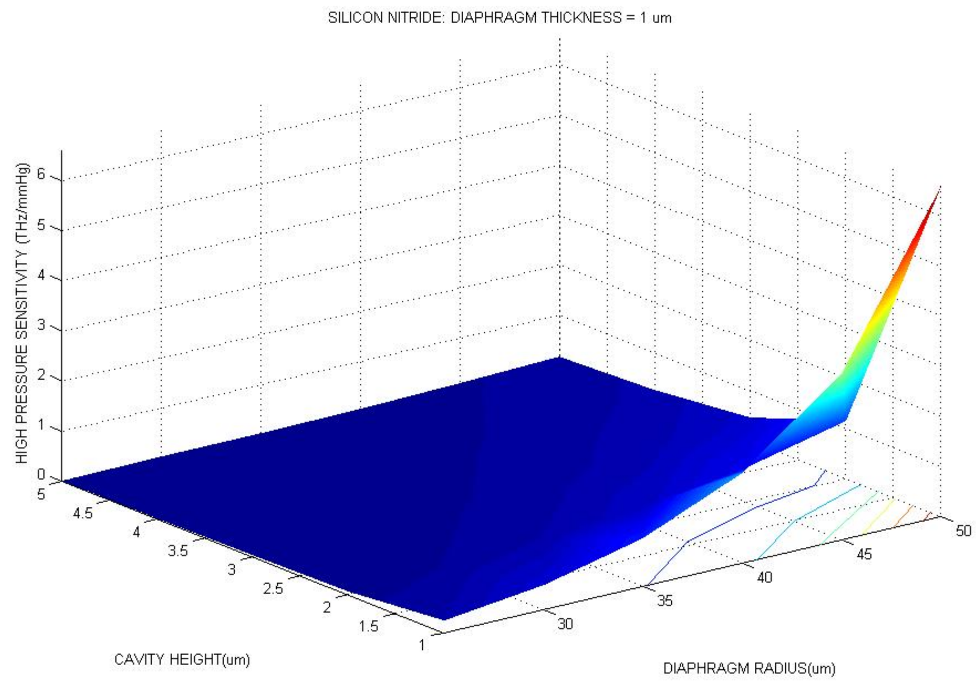

Figure C. 6 High Pressure sensitivity of a Silicon Nitride diaphragm of thickness 1μm.

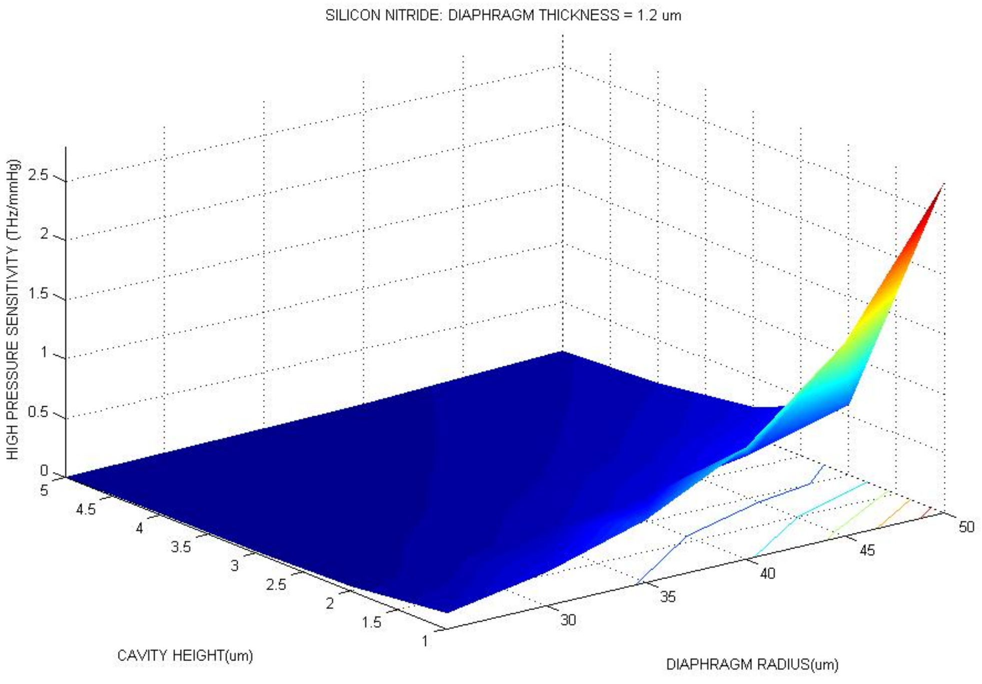

Figure C. 7 High Pressure sensitivity of a Silicon Nitride diaphragm of thickness 1.2μm.

BOSSED MEMBRANE

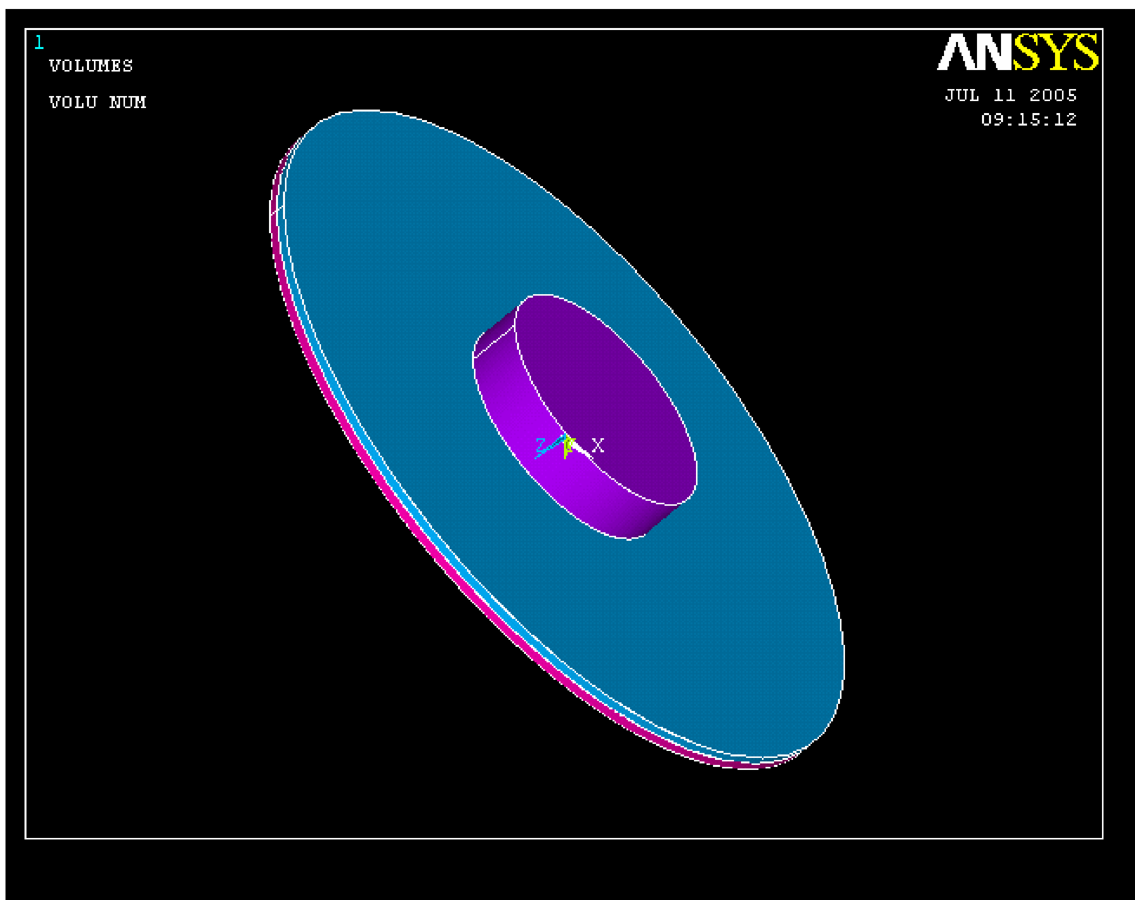

Figure C. 8 Bossed membrane structure on a hollow-cylinder support for a 1μm thickness, 40μm radius and 1μm height cavity.

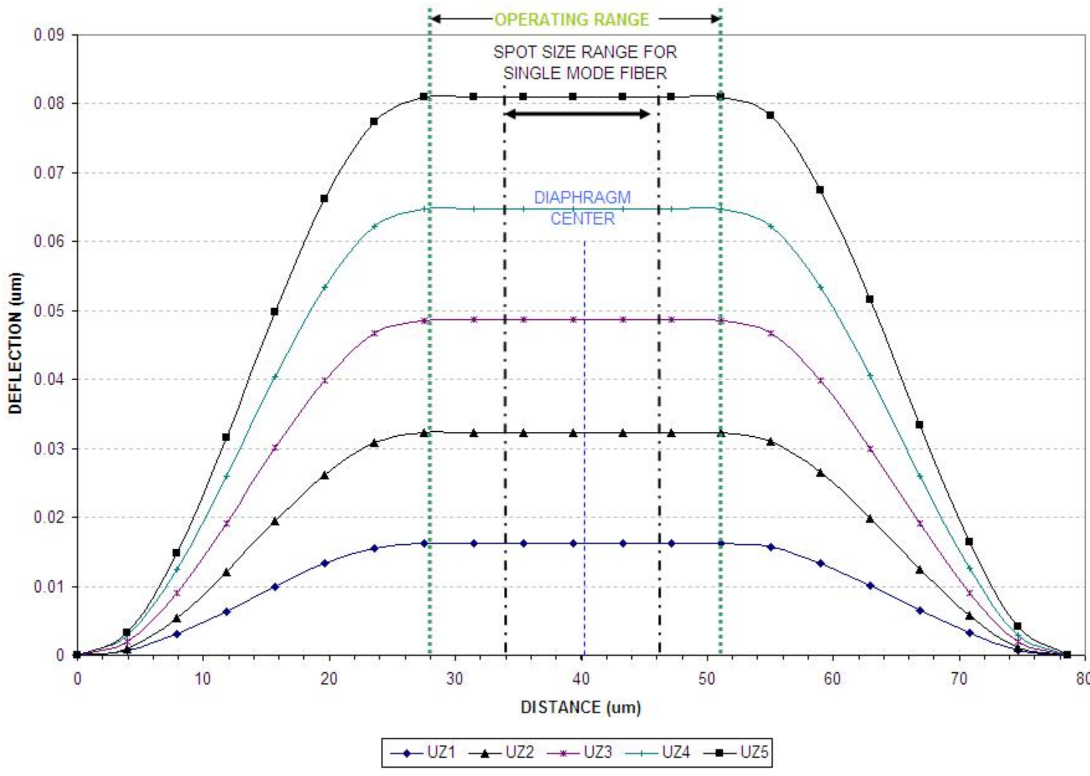

Figure C. 9 Bossed membrane on a hollow-cylinder support – deflection profile. UZ indicates different pressures applied, UZ1<UZ2 and so on.

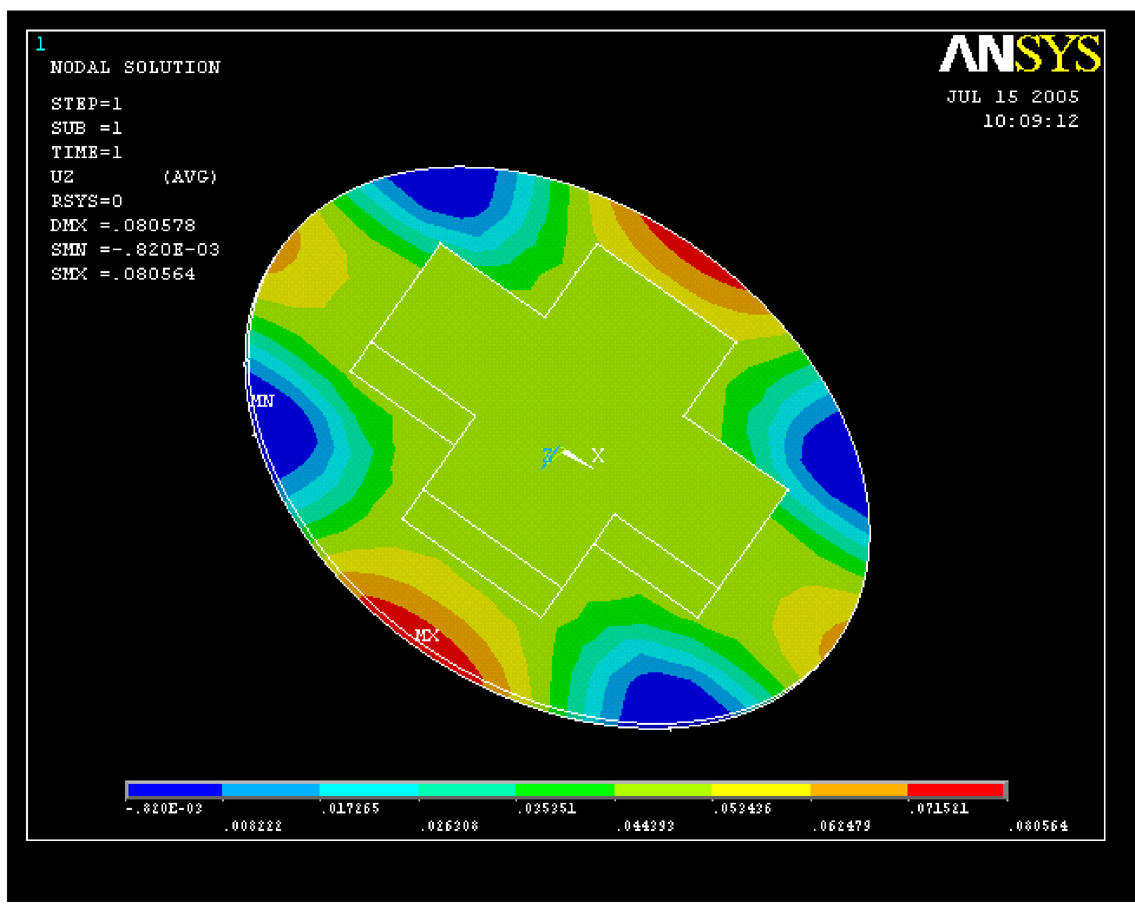

Figure C. 10 Bossed membrane on a four-pillar support structure for a 1μm thickness, 40μm radius and 1μm height cavity.

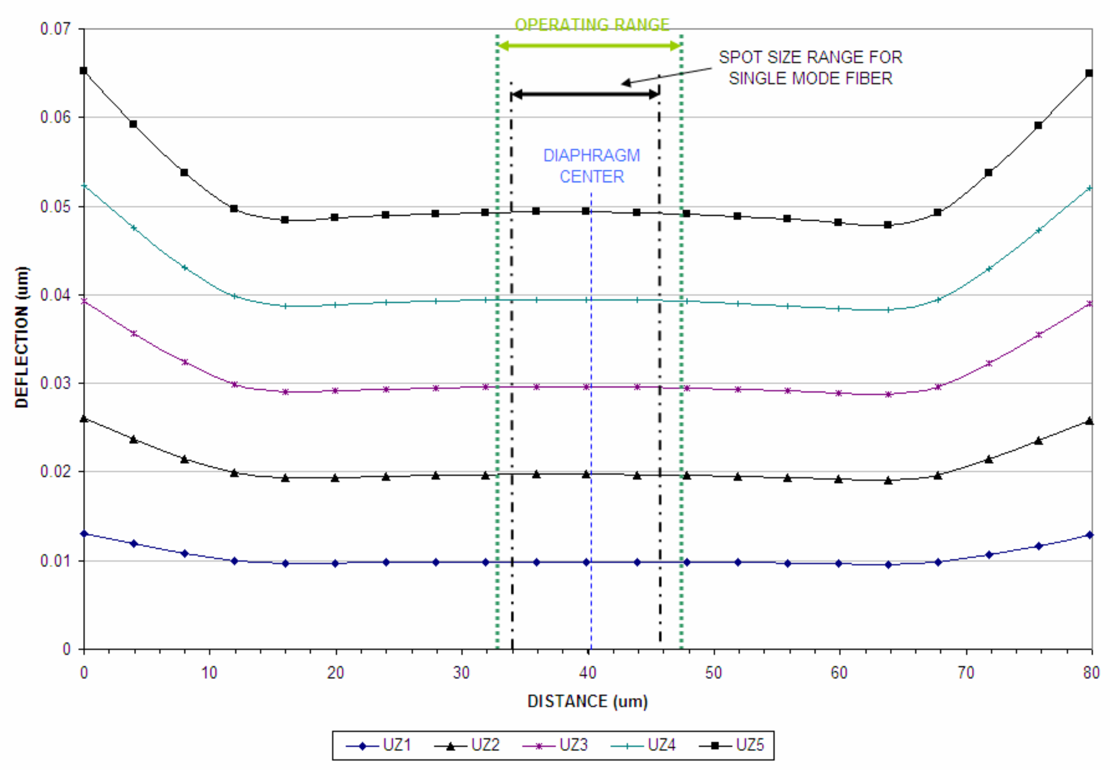

Figure C. 11 Deflection profile of a bossed membrane on a four-pillar support structure. UZ indicates different pressures applied, UZ1<UZ2 and so on.

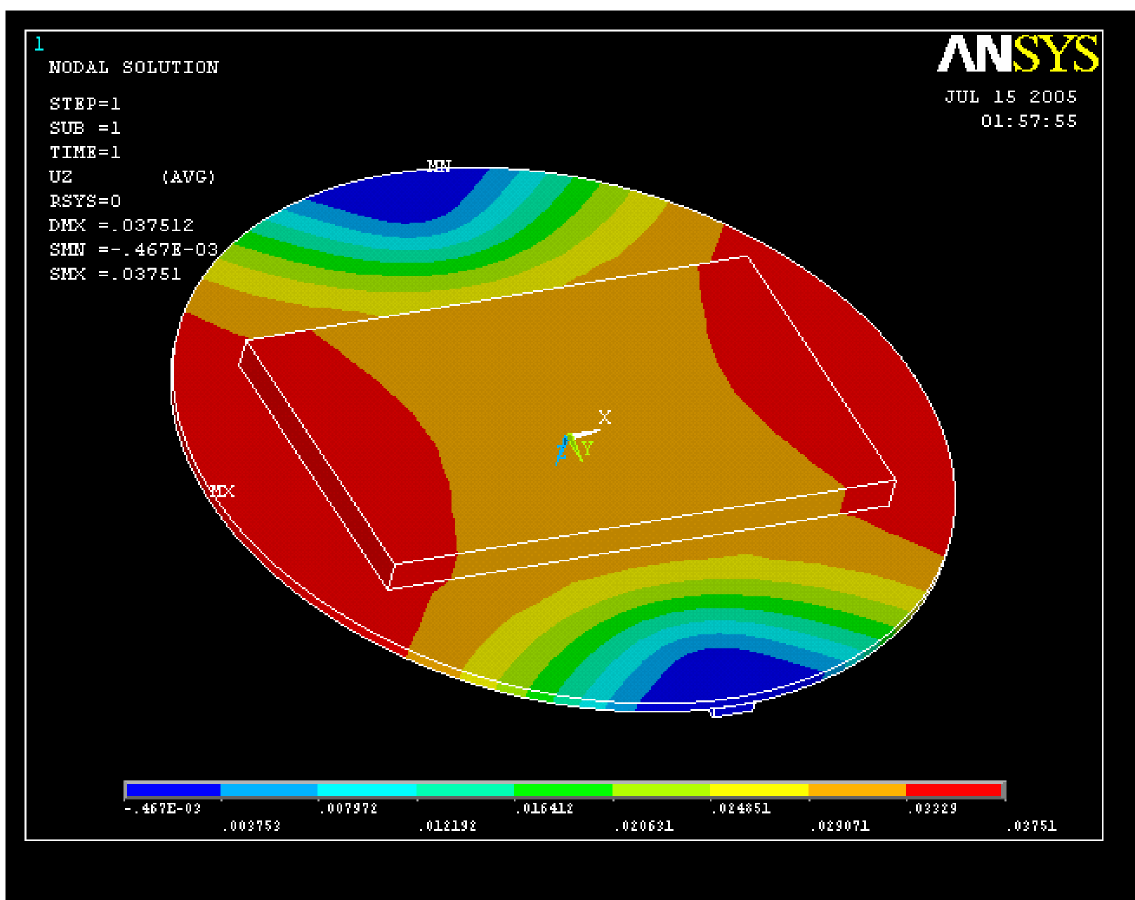

Figure C. 12 Two-pillar support structure with a bossed membrane. Dimensions of sensor – 35µm radius, 1µm thickness, 1µm cavity height, dimensions of the bossed structure – 50µm in length (along x direction) and 30µm in width (perpendicular to x direction) and 3µm in height.

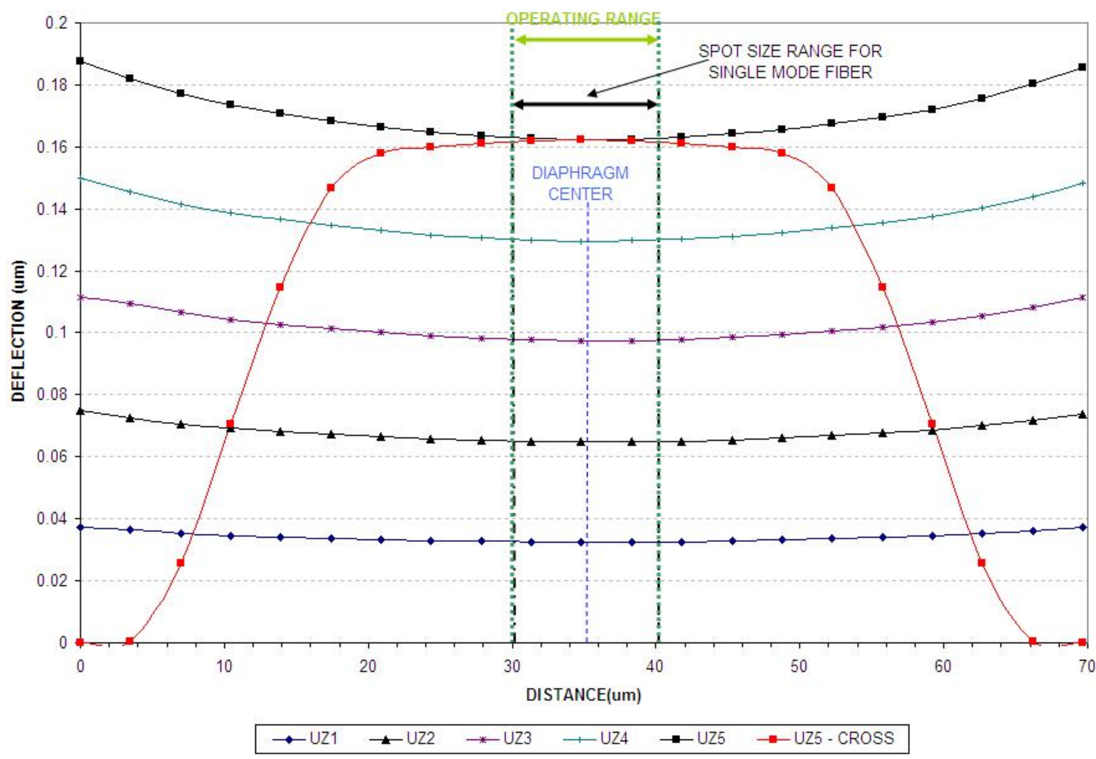

Figure C. 13 Deflection profile for a bossed membrane on a two-pillar support structure, UZ indicates different pressures applied, UZ1<UZ2 and so on. UZ5 – cross is deflection profile along the support structure.

Table C.2 Summary of the Sensor and Boss structure for a sensor made of Silicon Nitride.

Type of Support	Best Dimensions	Deflection Profile of the diaphragm
Hollow-cylinder	Sensor: Diaphragm radius – 40µm Diaphragm thickness – 1µm Cavity height – 1µm Emboss: Shape: Solid cylinder Radius – 13µm Thickness – 6µm	1. Remains flat but the operating range is more than the desired spot size 2. Magnitude of deflection is small 3. Sensitivity is low
Four-Pillar	Sensor: Diaphragm radius – 40µm Diaphragm thickness – 1µm Cavity height – 1µm Emboss: Shape: two cuboids at right angles to each other Length – 50µm Width – 20µm Thickness – 8µm	1. Remains flat with operating range slightly more than the desired spot size 2. Magnitude of deflection is small 3. Sensitivity is low
Two-Pillar	Sensor: Diaphragm radius – 35µm Diaphragm thickness – 1µm Cavity height – 1µm Emboss: Shape: one cuboid at the center of the diaphragm Length – 50µm Width – 30µm Thickness – 3µm	1. Remains flat but the operating range is equal to the desired spot size 2. Magnitude of deflection is large 3. Sensitivity is high

REFERENCES

[1] The MEMS handbook (2002), Boca Raton, FL CRC Press,

[2] Carr J J, Brown J M, Sensor Terminology, Introduction to Biomedical Equipment Technology, Third Edition, Prentice Hall.

[3] Carr JJ, Sensors and Circuits, Prentice-Hall.

[4] Rao S M N, Miniature fiber optical pressure sensor for biomedical applications, Theses, University of Texas at Arlington, May 2004.

[5] Pandojirao-Sunkojirao P, Fabrication of a novel optical pressure sensor using Fabry-Perot interferometry, Theses, University of Texas at Arlington, May 2004.

[6] Hecht, Eugene, Optics, Reading, Mass.: Addison-Wesley, c1998

[7] Agarwal G P (2002), Fiber-Optic Communication systems, Third Edition, New York: John-Wiley and Sons Inc.

[8] FOP MIV – product datasheet, FISO Technologies

[9] Totsu K, Haga Y and Esashi M (2005), Ultra-miniature fiber-optic pressure sensor using white light interferometry, J. Micromech. Microeng. 15 71-75

[10] Han J and Neikirk D P (1996), Deflection behavior of Fabry-Perot pressure sensors having planar and corrugated membrane, SPIE's Micromachining and Microfabrication '96 Symposium: Micromachined Devices and Components II, R. Roop and K. Chau, Proc. SPIE 2882, Austin, Texas, USA, 79-90.

[11] Nemeth N N, Palko J L, Jadaan O, Mitchell J S and Zorman C A (2001), Structural modeling and probabilistic characterization of MEMS pressure sensor membranes, Proceedings of MEMS: Mechanics and Measurements symposium, Portland, Oregon, 46-51.

[12] Su Y H, Chen K S, Roberts D C and Spearing S M (2001), Large deflection analysis of a pre-stressed annular plate with a rigid boss under axisymmetric loading, J. Micromech. Microeng. 11, 645-653.

[13] Komaragiri U, Begley M R, and Simmonds J G (March 2005), The Mechanical Response of Freestanding Circular Elastic Films Under Point and Pressure Loads, Journal of Applied Mechanics, Volume 72, Issue 2, 203-212.

[14] Timoshenko S and Woinosky-Krieger S (1987), Theory of Plates and Shells, McGraw Hill Classic Textbook Reissue.

[15] Eaton W P, Bitsie F, Smith J H and Plummer D W, A New Analytical Solution for Diaphragm Deflection and its Application to a Surface-Micromachined Pressure Sensor , Sandia National Laboratories

[16] Schellin R, Hess G, Kühnel W, Thielemann C, Trost D, Wacker J and Steinmann R (April 1994), Measurements of the mechanical behavior of micromachined silicon and silicon-nitride membranes for microphones, pressure sensors and gas flow meters, Sensors and Actuators A: Physical, Volume 41, Issues 1-3, 1, 287-292.

[17] Kondziela J, Laser Spectral Analysis Made Easy, Application Note, Product Line Manager, EXFO Burleigh Products Group.

[18] Chiao J C, EE5365 - Fiber optics and theory, Lecture Notes, University of Texas at Arlington, Spring 2005.

[19] Paulo S. F. de Matos1, Niklaus U. Wetter2, and Gess´e E. C. Nogueira (March 2003), Single Frequency Oscillation in a Coupled Cavity ND:GYLF Laser by Interferometric Control of the Cavity's Length, Revista de F´ısica Aplicada e Instrumentac¸˜ao, vol. 16, no. 1,.

[20] Ansys Inc., Structural analysis online tutorial, Help document available with Ansys, version 8.1.

[21] Cook R (1989), Concepts and Applications of Finite Element Analysis, John Wiley & Sons.

[22] Pan J Y, Lin P, Maseeh F & Senturia S D, Verification of FEM analysis of load-deflection methods for measuring mechanical properties of thin films, IEEE Solid-State Sensors and Actuators Workshop (Hilton Head Island, SC, 1990) technical digest, 70–3

[23] Luo C, Schneider T W, White R C, Currie J and Paranjape M (2003), A simple deflection-testing method to determine Poisson's ratio for MEMS applications, J. Micromech. Microengineering 13, 129–133

[24] Kazinczi R., Mollinger J. and Bossche A., 3-D Resonator Bridges as Sensing Elements, Proceedings of SeSens November 30, 2001, Veldhoven, the Netherlands, 803-808

[25] Cherobrier N (2003), MEMS: A Nickel for your thoughts, Application Note, Circuits assembly.

[26] Eaton W P, Bitsie F, Smith J H & Plummer D W (99), A new analytical solution for diaphragm deflection and its application to a surface-micromachined pressure sensor, International conference on Modeling and Simulation of Microsystems (MSM).

[27] Katsumata T, Haga Y, Minami K and Esashi M (1997), Micromachined 125μm diameter ultra miniature fiber optic pressure sensor for catheter, Technical digest of International Conference on Optical MEMS and their applications, Japan, 141-146.

[28] Totsu K, Haga Y and Esashi M (2003), Vacuum sealed ultra miniature fiber-optic pressure sensor using white light interferometry, The 12th International conference on Solid State Sensors, Actuators and Microsystems, Boston.

[29] Giovanni MD (1982), Flat and corrugated diaphragm design handbook, Marcel Dekker.

[30] Gillella S R (May 2004), Micro-viscosity effect and characterization of mems based micropumps with flat and bossed membranes, Theses, University of Texas at Arlington.

BIOGRAPHICAL INFORMATION

Shruthika Prasanna received her bachelor's degree in Electrical Engineering from the Vishveswarya Technological University, Karnataka, India in the year 2002. She worked as a Systems Engineering for Tata Consultancy Services, Mumbai, India for duration of 1 year. She pursued her master's in Electrical Engineering at University of Texas at Arlington majoring in both VLSI and MEMS and graduated in August 2005.